Design of a colorless transmitter based on Fabry-Perot cavity for applications in WDM-PON systems

Jhon Anderson Lopera Cortés

Tesis de maestría presentada para al título de Magíster en Ingeniería de Telecomunicaciones

Directores
Jhon James Granada Torres, Doctor(PhD) Ingeniería Electrónica
Juan Diego Zapata Caro, Doctor(PhD) Ingeniería Electrónica

Universidad de Antioquia
Facultad de Ingeniería
Maestría en Ingeniería de Telecomunicaciones
Medellín, Antioquia, Colombia
2022

Design of a colorless transmitter based on Fabry-Perot cavity for applications in WDM-PON systems

Research work for obtaining the Master of Science degree in Telecommunication engineering

Jhon Anderson Lopera Cortés

Advisor: PhD. Jhon James Granada Torres

Co-advisor: PhD. Juan Diego Zapata Caro

Facultad de Ingeniería

Departamento de Ingeniería Electrónica y Telecomunicaciones

Universidad de Antioquia

Acknowledgement

First, I would like to thank the project OPTOPUS (CODI 2017-16369) from the University of Antioquia, because without their funding it would not have been possible to complete my master's studies and this project could not have reached its goal.

Moreover, this work would not have been possible without the help of many people. I am very grateful to my advisors Professor Jhon James Granada, Professor Juan Diego Zapata and Professor Ana María Cárdenas for providing guidance and feedback throughout the project. I also want to thank my friends and colleagues in the GITA research group, our discussions about science were always a fundamental part of the learning process in this master's degree: I learned a lot from all of them, and I am very grateful for their support in different areas of my professional and personal life. Finally, to my personal friends and family, I thank you very much for your support, for always being with me and for encouraging me to keep going forward.

Last but not least, I want to thank myself. I want to thank myself for believing in me. I want to thank myself for doing all this hard work. I want to thank myself for not having days off. I want to thank myself for always being a giver and trying to give more than I receive. I want to thank myself for never having given up. Lastly, I want to thank myself for always being me.

Abstract

In order to satisfy the exponential increase of data traffic demand in access networks (fixed or mobile), mainly due to the increasing of broadband services (as high-quality video applications), Passive-Optical-Networks (PON) based on Wavelength-Division-Multiplexing (WDM) techniques has been considered as a promising solution. However, the lack of low-cost optical sources represents a high implementation cost of WDM-PON systems in access networks. Hence, the WDM-PON systems have been proposed using a kind of optical sources, known as colorless transmitters, which act as tunable lasers with an emission wavelength controlled by external mechanisms (usually located in the central office side). The main idea of colorless technology is to reduce the inventory, operation, and maintenance cost by the implementation of universal transmitter devices, mainly at the end-user side. Currently, there are several approaches for implementing a colorless transmitter according to the network requirements (speed, distance range, and spectrum usage efficiency), however, the most common approaches can be classified according to the following 4 categories: (1) Based on Tunable Laser diodes (TLD), (2) Based on Reflective Semiconductor Optical Amplifiers (RSOA), (3) Based on Electro-Absorption Modulators (EAM), and (4) Based on Fabry-Perot Laser Diodes (FPLD). Nevertheless, even considering the recent advances, the colorless transmitter based on TLDs or EAMs are still considering high-cost solutions to be implemented in optical access networks. Besides, although the RSOA case is considered one of the best solutions for the deployment of low-cost and spectral efficient WDM networks, devices to ensure this low-cost condition have not been commercialized yet. Finally, the FPLDs are low-cost devices (usually two digits) that are available in the market and although their emission spectra are limited by the longitudinal modes in the cavity, these can be customized to be useful for applications in optical communications, making them a suitable option to deploy low-cost colorless WDM-PON systems.

Thereby, in this work, we propose and numerically analyze a colorless transmitter based on a Fabry-Perot Laser Diode (FPLD) with an emission wavelength that is externally tuned using an ASE optical carrier. The Fabry-Perot based colorless transmitter is designed to support 100 GHz spaced longitudinal modes with a central wavelength of 1552.525 nm. Furthermore, we analyze the cavity's end-facets reflectivity, to determine a FPLD's configuration that allows a good trade-off between the injection power requirement for seeding the emission wavelength with at least 30 dB Side Mode Suppression Ratio (SMSR) and the source chirp. Finally, we analyze the transmission performance of the colorless transmitter in a PON with the following configuration: Transmission distances up to 100 km, seeding carrier with a 3 dB bandwidth of 12.5 GHz, 25 GHz, and 50 GHz, and two optical channels spaced each other 400 GHz: (1) 1552.525 nm (central mode), and (2) 1550.125 nm. Moreover, for all cases was used a Return to Zero (NRZ) modulation format at 2.5 Gbps

bit rate. The results show that reflectivities of 10 % and 90 % for the front-facet and end-facet, respectively, allows a good trade-off between the injection power requirement and the transmission performance, achieving SMSR above 30 dB for injection powers below to 300 μW and error-free transmissions (BER 10^{-9}) for distances over 25 km. These results can only be achieved if the optical carrier used to seed the FPLD has a 3-dB bandwidth that is a fraction of the longitudinal mode spacing and the bias current is below 60 mA. Thus, in our case, for longitudinal modes spaced 100 GHz, the 3-dB bandwidth of this optical carrier must be less than 25 GHz. Furthermore, a comparison between the performance of the designed colorless transmitter and a commercial FPLD showed that our laser allows tuning at least 8 longitudinal modes with an SMSR of 30 dB, using one third of the power required by a commercial FPLD. Moreover, if we use a 300 μW seeding carrier to tune the commercial FPLD, it is not possible to achieve error-free transmission for the longitudinal modes far from the central.

Hence, the proposed colorless source can be a suitable low-cost solution to implement optical access networks. Furthermore, if the bias current is set at a value between 35 mA (above the threshold current) and 60 mA, it is possible to guarantee an SMSR of 30 dB for at least 13 longitudinal modes, i.e., it is possible to obtain a WDM-PON system with at least 13 optical carriers.

Additionally, in order to improve the colorless transmitter performance, coherent type-sources such as Laser Diodes can be used as seeding source not only to reduce the ASE noise in the resulting optical carrier, but also to transmit information in a carrier reuse scheme. However, laser diodes typically present a narrow bandwidth spectrum, therefore it would be necessary to have a different laser diode for each longitudinal mode to be tuned in the FPLD. Therefore, to use Ultra Short Pulsed Lasers (USPL) as seeding sources in colorless WDM-PON system can a suitable option not only for its wide spectrum, but also due to its high stability and coherence. Hence, we experimentally design a USPL based on optical fiber a graphene saturable absorber that emits in the spectral region around 1558 nm, and presents a 3-dB bandwidth up to 21 nm, which is adequate for WDM applications. Furthermore, using experimental data from the USPL spectrum and introducing them into a simulated network using the software VPItransmissionMaker^{TM}, we demonstrate that it is possible to use the USPL as a multi-wavelength source, for transmitting information in a WDM-PON system. Therefore, we propose as a future work the use of a USPL as a seeding source in colorless WDM-PON system with and without carrier reuse.

Contents

Chapter 1

Introduction

1.1 Context and motivation

In the last 25 years, the data traffic on the networks has presented an exponential growth which in terms of capacity, it has been a constant challenge for the telecommunications industry [1]. It is considered that there are two main causes of this increase in data traffic: 1) the increase in broadband services, such as high-definition video transmission, and 2) the growing number of users and devices connected to the Internet (driven by the Internet of Things and the development of G5 technologies). In addition, according to the CISCO global forecast, the number of devices connected to the Internet is expected to increase to about 29.3 billion by 2023 (more than three times the world's population) [2]. Therefore, adapting and expanding current communication systems or investigating new communication plans, in which user devices support and adapt to large amounts of traffic, is an imminent necessity if the network capacity demands of future technologies are to be fulfilled.

Thus, In order to satisfy the exponential increase of data traffic demand, the implementation of Passive-Optical-Network (PON) in an access level has been considered as a promising solution mainly due to its high bandwidth [3, 4]. Thus, PONs are telecommunication technologies for point-to-multipoint broadband access over an optical network infrastructure characterized to have low power consumption, a low implementation cost, and a coverage range of several tens of kilometers [5].The operation of a PON-system can summarize as follows: (1) An Optical Line Terminal (OLT) located at the operator's central office transmits the DownStream (DS) data to multiple Optical Network Units (ONUs) at the customer's premises through an optical distribution network consisting only of passive elements such as beam splitters, circulators, dispersion compensation fiber and attenuators. The user's ONU sends the UpStream (US) information to the OLT side using the media access technique imposed by the operator. In addition, these media access techniques, in general terms, are defined according to the speed requirements of the network and the operating window, i.e., the wavelength range in which the network operates.

Thus, the Table 1.1 summarized the evolution of the international standards in Passive Optical Networks (PON) along the time in terms of transmission rate and the wavelength allocation [6–10]. In this table is evidenced two important facts: (1) The demand on network capacity is growing every year, not only for the DS channel, but also for US, noting the necessity of symmetrical configuration in the optical access network. (2) There are several approaches to the implementation of a PON system which, from a commercial approach, can

Table 1.1. International standards for Passive Optical networks over the time

Standard	Year	Media Access	DS [Gbps]	US [Gbps]	Wavelegths [nm]	
					DS	US
BPON	2001	TDM -Based	0.625	0.155	1490 - 1500	1300 - 1310
EPON	2004	TDM -Based	1.25	1.25	1490 - 1500	1260 - 1360
GPON	2004	TDM -Based	2.5	1.25	1490 - 1500	1260 - 1360
XG-PON	2009	TDM -Based	10	2.5	1260 - 1280	1575 - 1580
NG-PON2	2015	TDM-WDM	40 (4 λ)	10	1524 - 1544	1596 - 1603
		PtP WDM	40 (8 λ)	10	1524 - 1624	524 - 1624
XGS-PON	2016	TDM-based	10	10	1260 - 1280	1570 - 1580

be classified into two general groups according to the media access control technique used in the network deployment. These are, (i) Time-Division-Multiplexing (TDM) Passive Optical Networks (which includes Asynchronous TDM and statistical TDM), and (ii) Wavelength Division Multiplexing (WMD) Passive Optical Networks [7, 11, 12].

1.1.1 TDM-based PONs

The Figure 1.1 shows a general operation scheme of TDM-based PON. In this type of optical network, the OLT broadcasts the DownString data over the user's ONU using a single optical carrier λ, usually in a spectral region with zero or low dispersion, and different time slots T_n for each user. Then, using a different wavelength regarding the DS data, each ONU transmit the UpString signal in the assigned time slot [6, 11]. In addition, to ensure that no time slot is wasted in case a user does not transmit information on its assigned slot, TDM-based systems propose statistical multiplexing, which provides improved link utilization by avoiding fixed allocation of time slots for data transmission and introducing asynchronicity in communication.

TDM-PON is the most widely deployed architecture for optical access networks worldwide [6, 13] due to its several advantages such as the statistical multiplexing gain, low-latency and simplicity [6, 13]. However, considering the capacity demand of the incoming technologies as 5G, TDM-based optical networks present several drawbacks, mainly when working with noncoherent sensing optical systems: the bit rate is limited by the switching speed of the

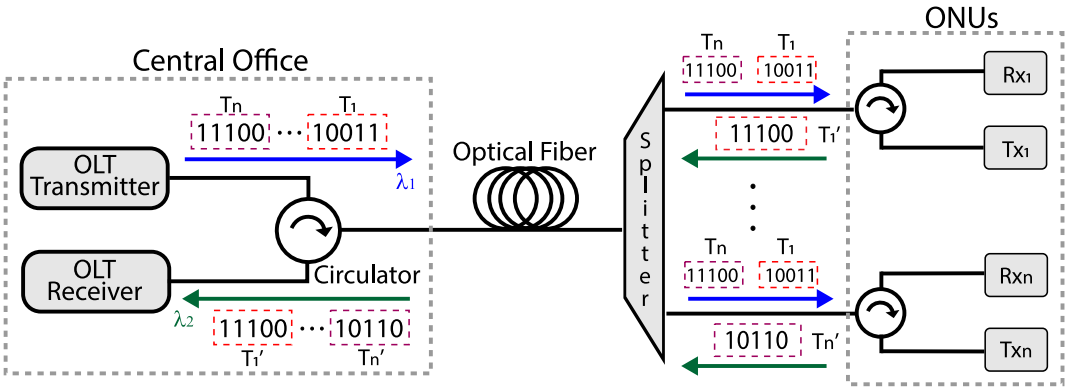

Figure 1.1. TDM-PON operation scheme

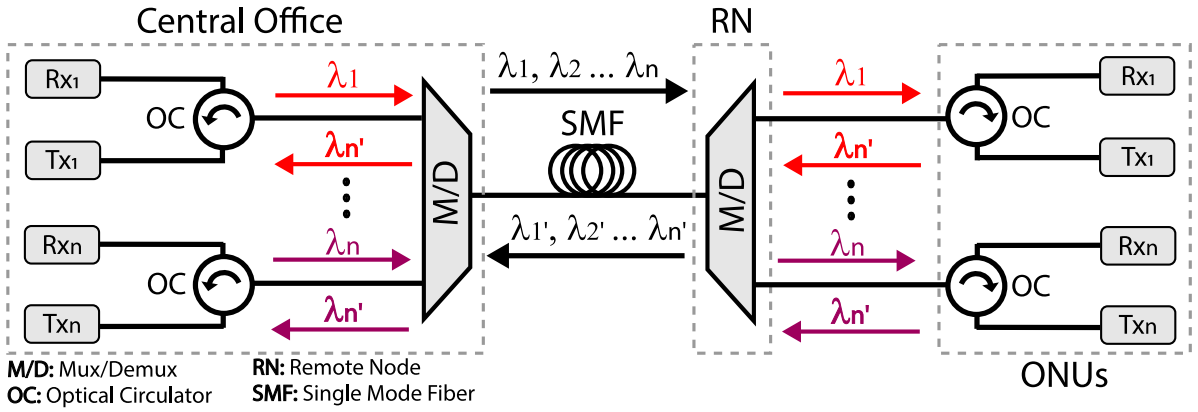

Figure 1.2. WMD-PON operation scheme

electronic devices modulating the optical carrier, which reaches its limit around 40 GHz [14]. In addition, because TDM systems propose to use a single optical carrier for all customers, optical fiber dispersion effects and polarization mode dispersion (PMD) will penalize the network performance proportionally to the increase of the system's modulation rate [15]

These drawbacks make the TDM-PON architecture not very attractive, especially when considering that access networks must be scalable in capacity. Thus, although it is possible to overcome the capacity limitations of TDM architecture by using multilevel modulation formats, it would be increasing the cost of operation because the reception schemes become more complex.

1.1.2 WDM-based PONs

In the case of WDM-PON, the information channels are separated using optical carriers with different wavelengths: Each ONU is assigned its own dedicated wavelength channel, forming a logical point-to-point system as is showed in the Figure 1.2 [16]. In order to share the same physical medium (optical fiber), an optical multiplexer/demultiplexer (MUX/DEMUX) device used to direct the information from all transmitters to the same Single Mode Fiber (SMF). Then, in the Remote Node (RN), an optical MUX/DEMUX is assigned to separate the wavelengths that travel together along the fiber, and send them to their respective optical receivers.

In contrast to TDM systems operating around 1310 nm, where fiber dispersion is very low, WDM-PON was designed to operate in the range between 1535 nm and 1565 nm (c -band), where the optical losses are low (¡0.5 db/km) but dispersion presents a considerable value: 16 ps/nm.km. Thereby, due to in PON networks no device is used to perform a type of signal processing to compensate the signal's distortion introduced in the light propagation along the optical fiber, the range of a PON-PON system is limited to 2 factors: (1) the power losses (attenuation in the fiber + insertion losses), and (2) dispersive phenomena associated with light propagation in optical fibers, such as group delay, polarization mode dispersion, chirp, etc.

In the first case, it is possible to know the distance limitations imposed by power loss by calculating a power budget. In the case of a PON-WDM system, three parameters need to be taken into account for the power budget: (i) The attenuation factor of an optical fiber in

the spectral region around 1550 nm. (ii) The insertion losses due to passive elements such as connector, beam splitters and MUX/DEMUX. (iii) The minimum power requirement of an optical receiver needs to operate reliably with a Bit Error Rate (BER) below a specified value, which is proportional to the square bit rate B [15]. Thus, the general idea is that the power of the optical transmitter exceeds the sum of the optical losses considered below. This power requirement is expressed in logarithmic scale in the equation 1.1, where, P_{Tx} is the output power of the optical transmitter, $P_{Rx}(B)$ is the power requirement of the optical receiver for a target BER, $\alpha(\lambda)$ represent the f attenuation factor of the optical fiber a wavelength function, L is the fiber length, and IL is a factor that considers all insertion losses in the link.

$$P_{Tx} \geq P_{Rx}(B) + \alpha(\lambda)L + IL \tag{1.1}$$

In the second case, there are several dispersive effects that can reduce the network transmission performance. However, one that should always be considered when operating in a spectral band around 1550 nm is the Group Velocity Dispersion (GVD), This phenomenon occurs because the spectral frequencies that make up an optical pulse travel at different speeds through the optical fiber. Thus, ω spectral component arrives at the fiber's output with a time delay $T = L/V_g$, where L is the fiber length and V_g is the group velocity. which is defined as $V_g = (d\beta/d\omega)^{-1}$.

Since the propagation constant β is a frequency-dependent parameter, so V_g will also be a frequency-dependent function, and this frequency dependence leads to pulse broadening simply because different spectral components of the pulse disperse during propagation and do not arrive simultaneously at the fiber output [15]. Thereby, for a spectral width of the pulse $\Delta\omega$, the extent of pulse broadening along the fiber length L, is given by the equation 1.2. Where $\beta_2 = d^2\beta/d\omega^2$ is known as the GVD parameter.

$$\Delta T = \frac{dT}{d\omega}\Delta\omega = \frac{d}{\delta\omega}\left(\frac{L}{V_g}\right)\Delta\omega = L\frac{d^2\beta}{d\omega^2}\Delta\omega = L\beta_2\Delta\omega, \tag{1.2}$$

In order to express ΔT in terms of the range of wavelengths $\Delta\lambda$ emitted by the optical source, we use $\omega = 2\pi c/\lambda$ and $\Delta\omega = -(2\pi c/\lambda^2)\Delta\lambda$, so the equation 1.2 can be written as:

$$\Delta T = L\frac{d}{\delta\lambda}\left(\frac{L}{V_g}\right) = DL\Delta\lambda, \tag{1.3}$$

Where, D is the known dispersion parameter, which takes into account two different dispersive phenomena: Material scattering and waveguide scattering. Material dispersion occurs because of the refractive index of silica (the material used to build up the optical fiber) changes with the optical frequency ω. On the other hand, the waveguide dispersion is related to the difference of refractive index between the core and cladding of the optical fiber. As an optical pulse does not propagate only in the fiber core: a fraction of the pulse goes out to the cladding (evanescent field), different parts of the optical pulse will travel with a different phase velocity, which will modify the group velocity of the pulse resulting in chromatic dispersion [17]. The dispersion parameter D can be calculated using the equation 1.4 and usually is present in units $ps/nm - km$. Additionally, a Standard Single Mode Fiber (SSMF) present a dispersion parameter about 16 ps/nm-km for a wavelength of 1550 nm.

$$D = \frac{d}{\delta\lambda}\left(\frac{L}{V_g}\right) = -\frac{2\pi c}{\lambda^2}\beta_2, \tag{1.4}$$

Up to this point, it is clear that the dependence of group velocity and emission frequency causes a broadening of the optical pulses traveling along the fiber, mainly in the case where the bandwidth of the source $\Delta\lambda$ is wide. Thereby, the effect of dispersion on the bit rate B can be the time-bandwidth $B\Delta T$product as follows:

$$BL|D|\Delta\lambda < A \tag{1.5}$$

The Equation 1.5 relates the maximum length L that the optical fiber can have when using a laser with spectral width $\delta\lambda$ modulated at a bit rate B, in a medium with a dispersion parameter $D(\lambda)$ that depends on the wavelength. According to this equation, the product of these 4 quantities must be less than a constant factor A, which indicates how much a pulse stays within its bit time as it scatters along the optical fiber [15]. Generally A takes values between 0.25 and 1, where 1 is the limit value at which two pulses start to interfere at a distance L.

Moreover, there are other factors that can produce temporal broadening in the pulses and penalize the network performance, such as: (1) PMD, which occurs due to fiber birefringence causing two orthogonality polarized components to travel with different group velocities. (2) Time dependence of the instantaneous frequency of an optical pulse (chirp) that affects the pulse shape at the fiber output due to it induces a spectral broadening, which according to equation 1.2, increases the pulse width. This phenomenon is mainly considerable when direct modulation is applied to an optical source, and is due to the instantaneous changes in the refractive index that occur from varying the carrier density (varying the electric current modifies the carrier density) [15].

However, due to it is possible to mitigate these dispersive effects at least for the distances established by international standards (< 25 km), to operate in a spectral region with nonzero dispersion is not the main drawback for WDM-Based access optical networks. The main problem is that the implementation cost of an optical system, where each user has an optical transmitter with different wavelengths, is very high to be considered in the access level [4]. Thereby, although WDM-based system has been considered as a promising solution for the high capacity demand expected in the next generation networks, the lack of low-cost optical sources and fixed wavelength assignment (which increasing the inventory cost and the network's deployment complexity), make this solution unfeasible in terms of cost-benefit [18].

1.2 Colorless Networks

To overcome the problem associated with the high cost of implementation of WDM-PON systems, it has been proposed to use colorless sources as optical transmitters. Mostly, the colorless transmitters are devices that act as tunable lasers whose emission wavelength is externally tuned, either by a control signal which indicates the laser's emission frequency, or by an external carrier that induces a mode-locking in a laser's optical cavity [19]. Thus, the main idea of the colorless technology is to reduce the inventory, operation, and maintenance

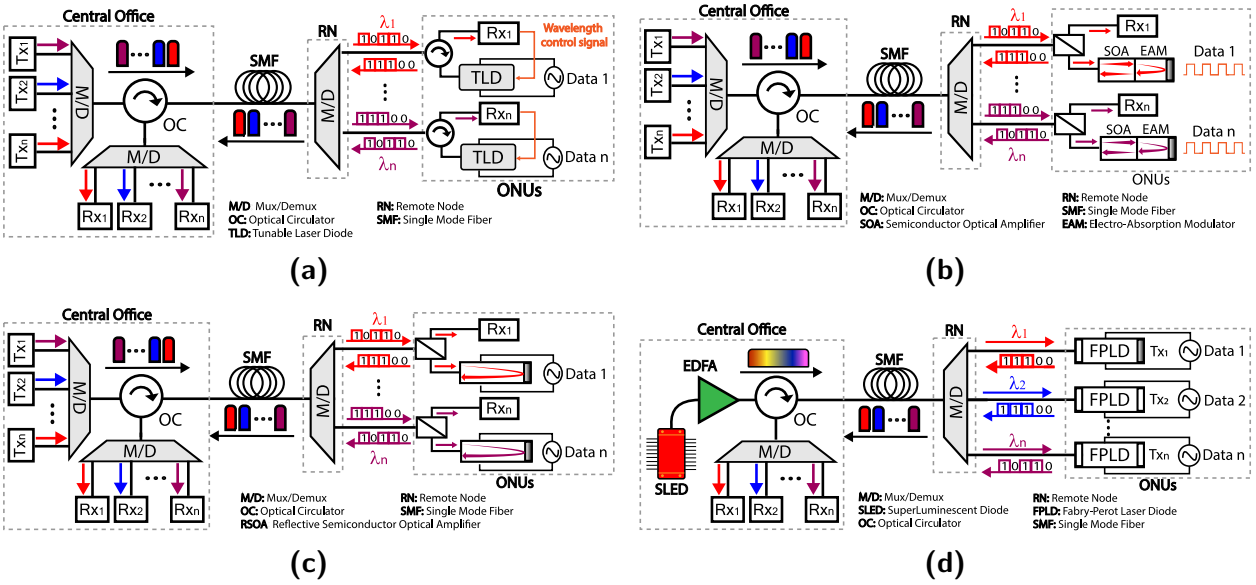

Figure 1.3. Colorless WDM-PON based on: a) TLD. b) EAM. c) RSOA. d) FPLD (Only Up-stream link).

cost in WDM-based networks by the implementation of universal transmitter devices (mainly at the end-user side) with flexible wavelength assignment [18].

1.3 State Of The Art

There are different approaches to implement colorless-WDM-PON, which can be categorized according to the optical device used to deploy the colorless transmitter[19, 20]. The most commonly approaches are the Colorless networks based on: (1) Tunable Laser diodes (TLD) [21–23], (2) Reflective Semiconductor Optical Amplifier (RSOA) [24–26], (3) Electro-Absorption Modulator (EAM) [19, 27, 28], and (4) Fabry-Perot Laser Diodes (FPLD) [18, 29, 30].

The figure 1.3a shows a Colorless-WDM-PON system based on TLD. TLDs can be considered the best option in terms of capacity and spectral efficiency due to the fact that, in general, TLDs allow large modulation bandwidths (typically around of 10 GHz) and almost free wavelength tuning (limited by the tuning technique) in a wide spectral range: around to 80 nm. However, even taking into account the recent tunable vertical surface cavity lasers, TLDs are still a very high-cost solution and their application in access networks is not cost-effective [21, 25]. The EAM-based colorless approach uses a carrier remodulation scheme to achieve a colorless performance, i.e., its emission wavelength is seeded by the optical transmitter in the central office side as is shown in the figure 1.3b [27, 28]. However, even the EAM has a large modulation bandwidth (>10 GHz), this device is still high cost, and because the remodulation process is usually done with less than 20 % of the received power, it needs to be combined with an optical amplifier, which increases the network's deployment cost. On the other hand, As is shown in the figure 1.3c, RSOA-based Colorless networks can also work using a remodulation scheme, but in this case no external optical amplifier is needed: The RSOA itself works as a low-cost optical amplifier which gain that can be modulated by the

information signal. Thus, even the RSOAs presents a relative low modulation bandwidth in comparison with the TLDs and EAMs (Typically around of 2 GHz), it can be considered as one of the best solutions for the deployment of low-cost and spectral efficient WDM-based networks. Nevertheless, devices to ensure this low-cost condition imposed by the WDM-PON system have not been commercialized yet [19]. Finally, the FPLDs are devices with a relatively low modulation bandwidth (typically of 2 GHz) that can be externally tuned using an optical carrier generated by an Amplified Spontaneous Emitting (ASE) source (See the figure 1.3d), do not need external amplification and are commercially available low-cost devices. The main drawbacks of the FPLD-based co FPLD emission spectrum are limited by the periodic losses in the resonant cavity: Only a certain wavelength, usually knows as longitudinal modes, can be emitted. However, longitudinal modes in a Fabry-Perot type cavity can be customized for applications in optical communications according to ITU-T G.694.1 standard for WDM grid, making the FPLDs a suitable option to deploy colorless WDM-PON systems.

Research question

What type of optical parameters should be optimized in the design of a Fabry-Perot Laser Diode Cavity, in order to achieve a Side Mode Suppression Ratio (SMSR) of 30 dB o highest, and improve its performance as a colorless transmitter in access optical networks standardized according to the ITU-T G.694.1?

1.4 Goals

General Goal

Design in simulation, based on a Fabry-Perot Laser Diode cavity, an optical colorless transmitter for applications in WDM-PON Access networks

Specific Goals

- Design a Fabry-Perot Laser Diode Cavity with longitudinal modes spaced according to the ITU-T G.694.1 standard for WDM grids
- Validate in simulation the behavior of the designed Fabry-Perot using an external wavelength seeding approach, and verify its performance as colorless based on the SMSR measurements
- Numerically analyze the transmission performance of the designed Colorless transmitter and Fabry-Perot with commercial features, comparing the BER achieved for both cases as a function of optical link parameters, such as: link length, number of channels and transmission rate.

1.5 Research Impact

This research discusses key issues for the development of future telecommunication networks. First, a recent paradigm known as colorless optical networks, which emerges as a proposal

to overcome the exponential increase in the demand for data traffic, is addressed. The introduction of colorless networks will allow the standardization of flex-grid and gridless, which in comparison with the current standard for WDM (fixed grids), it allows an efficient spectrum usage. Thus, not only reduces the cost of WDM-based networks by introducing universal transmitters, but also increases capacity due to better spectrum utilization, without significantly increasing power consumption. Furthermore, the implementation of colorless networks can contribute to the development of new telecommunications services that benefit society, increasing the reach and capacity of access networks (greater coverage and better quality of service for the user).

On the other hand, from a methodological approach, this project proposes a colorless font design based on FPLD, through the specialized use of VPITransmissionMaker software. Additionally, the studies that will be conducted about the design of Fabry-Perot cavities, may be useful to determine those fundamental elements that can improve the performance of the colorless transmitter based on FPLD.

Finally, we design and experimentally validate an Ultra Short Pulsed laser (USPL) based on optical fiber and graphene, which could be used to perform the external wavelength seeding even in carrier reuse colorless systems. These types of sources are not only more stable and more coherent than ASE sources, but they also improve the coupling to fiber systems, specialized rooms for manufacturing (i.e. clean rooms), so, their manufacturing might be simple. It should be noted that the design of this source is opening a new possibility both for improving the performance of colorless WDM-PON systems in terms of transmission, as well as in the implementation of low-cost WDM networks. Because of this, focusing our future efforts on the experimental implementation of a multiwavelength source in a colorless WDM-PON system would be worthwhile.

Chapter 2

Fabry-Perot Laser Diode

This section describes the Fabry-Perot cavity design considerations to implement it as a low-cost colorless transmitter in a WDM-PON system standardized according to ITU-T G.694.1, as well as the theoretical background used to model and simulate light propagation in the FPLD resonant cavity.

2.1 Fabry-Perot Laser as colorless transmitter

An FPLD is a multi-wavelength source composed of a gain medium, such as a semiconductor hetero-structure, embedded in a resonant cavity of length L and end-facet reflectivities R_1 and R_2, as shown in Fig. 2.1a. This type of structure has boundary conditions that allow the emission only for wavelengths that correspond to a round-trip phase shift inside the cavity. These emission wavelengths, usually known as longitudinal modes, are not emitted at the same time inside the cavity when the FPLD is in typical operation regime: the laser exhibits sudden jumps of optical frequency, which are associated with transitions between different modes of its resonant [31]. This is an undesirable feature for an optical transmitter because the same signal will be able to travel in the different frequencies of the longitudinal modes, causing 2 main drawbacks: (1) Dispersion-induced distortions due to the same time-domain signal traveling in several wavelengths. (2) Signal deformations due to the optical filters used to select the channel in the remote node of a WDM system can spectrally suppress part of the signal.

We can avoid this limitation imposed by the FPLD emission spectrum, since it is possible

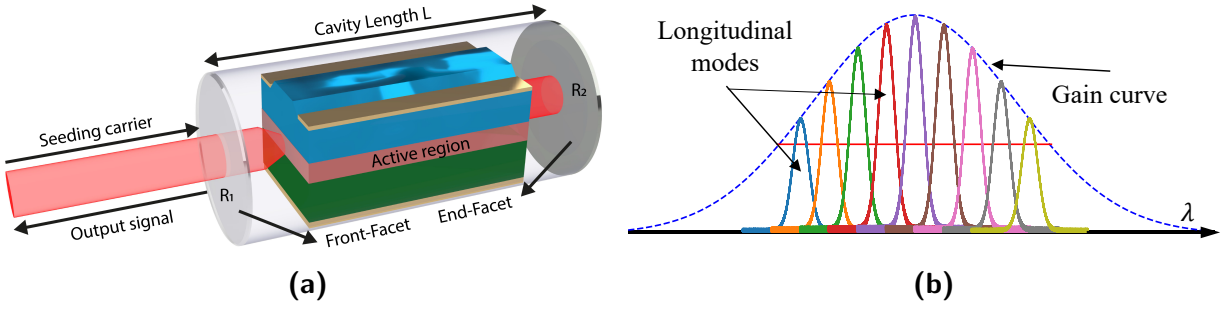

Figure 2.1. Semiconductor Fabry-Perot Laser Diode. a) Cavity Structure. b) Emission spectrum (ideal parabolic shape)

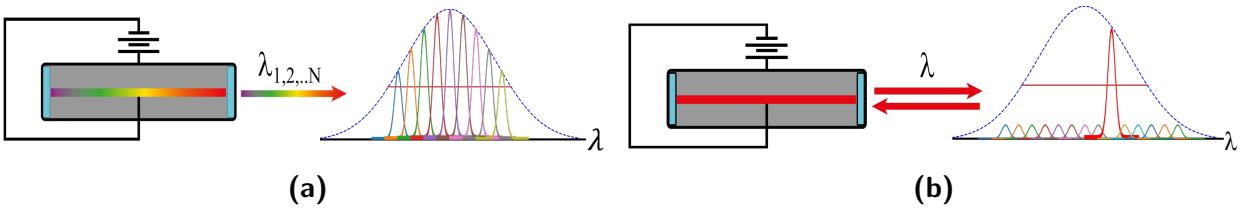

Figure 2.2. Longitudinal Modes in a FPLD. a) Free-runing operation. b) Tuning a longitudinal mode using an external optical carrier.

to tune a single longitudinal mode using an external optical carrier. In this process, known as carrier seeding or mode locking (depending on the accuracy), the FPLD (the slave source) acts as an amplifier for an optical carrier generate in the seeding source [32, 33]. If the optical frequency of the seeded light is close enough to the resonant frequency of a particular longitudinal mode in the FPLD's cativity, that mode can start oscillating with a much higher power than all competing modes, and thus can strongly dominate in the output pulse, as is showed in the 2.2b [33]. In this way, the emission bandwidth is considerable reduced regarding unseeded (free-running) FPLD. Additionally, the temporal profile of the pulse can be smoother, because mode beating is avoided. Besides, other conditions must be fulfilled to perform a correct wavelength tuning in the Fabry-Perot cavity, i.e., to achieve an extinction ratio between the tuned mode and the lateral modes, such that these can be considered noise. The most important conditions (in addition to the wavelength match between the longitudinal mode and the external carrier), are mentioned below: 1) The bandwidth of this optical carrier must not exceed a fraction of the mode spacing, and 2) the power of this injected carrier must be high enough to overcome the spontaneous emission into the laser's cavity [33].

2.1.1 Longitudinal modes spacing and linewidth

Before to fulfill the conditions mentioned above, it is necessary to adjust the longitudinal modes spacing to match the ITU-T G.694.1 recommendations for the channel spacing in PONs. However, For this, it is first necessary to understand how the longitudinal modes are formed into the FPLD cavity.

A simple way to understand the longitudinal modes formation into a FPLD is to consider the evolution of a plane-wave propagating along the resonant cavity during a round trip. It should be kept in mind that laser modes are never plane waves; spatial variations must be taken into account in a more realistic model. However, this approach is a practical way to understand the essential physics of the lasing process [31]. First, consider a plane wave propagating in the positive z direction of a medium (The FPLD) that are conveniently described by a refraction index n and an absorption coefficient $\alpha(\lambda)$ (includes free-carrier absorption, scattering, and other possible mechanisms) as is showed in the equation 2.1. Where E_0 is constant amplitude and $k(n, \lambda) = 2\pi n/\lambda$ is wave number.

$$E = E_0 e^{(ik(n,\lambda)-\alpha(\lambda))z} \tag{2.1}$$

On the other hand, a necessary condition for laser operation is that the gain medium of the FPLD is dominated by stimulated emission. When this condition is fulfilled, the active

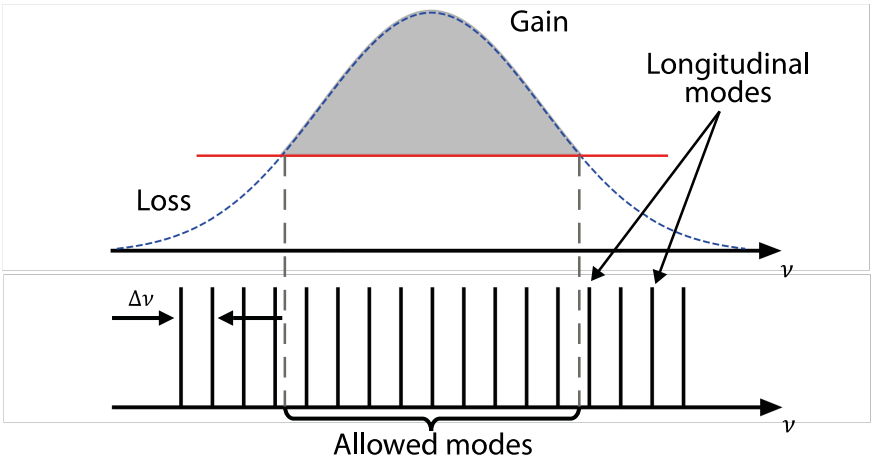

Figure 2.3. Longitudinal modes formation in a Fabry-Perot Laser Diode

media exhibit an optical gain, and therefore an input signal propagating inside the active layer would then amplify as e^{gz}, where g as usually known as the gain coefficient. However, the optical gain alone it is not enough to guarantee the laser operation: it is necessary to introduce an optical feedback that converts the amplifier behavior of the gain medium in an optical oscillator. This feedback is usually achieved placing the gain medium between mirrors (external o or only the cleaved end-facets). Additionally, It is necessary to note, that g is not the material gain g_m. Since the optical mode extends beyond the active layer while the gain exists only inside it, the gain coefficient becomes $g = \Gamma g_m$, where Γ is the confinement factor of the active region and represents the fraction of the mode energy contained in the active region.

Consequently, if we consider a resonant-cavity of length L, and end-facets with reflectivity R_1 and R_2, during each round-trip in the cavity, the photon-flux density is increased by a factor of exp((g/2) (2L), reduced in $\sqrt{R_1 R_2}$ exp$(-\alpha(\lambda)/2(2L))$ and the phase changes by $2kL$ [15]. Moreover, in order to build up the photon population and obtain a laser operation, it is necessary that the optical field described in the equation 2.1 reproduce itself after each round trip under steady-state operation conditions (a Continuous Wave regimen). This behavior occurs when the pumping current reaches a certain threshold where the photon population causes the cavity gain to be higher than the cavity losses. Thereby, this threshold condition can be expressed as follows [15, 31]:

$$E_0 e^{gL} \sqrt{R_1 R_2} e^{-\alpha_{int}(\lambda)L} e^{2ik(n,\lambda)L} = E_0 \tag{2.2}$$

Taking $k = 2\pi n\nu/c$, where ν is the emission frequency, and by equating the phase and the amplitude on two sides:

$$2kL = 2m\pi \quad or \quad \nu = \nu_m = mc/2nL \tag{2.3}$$

$$gL - \alpha_{int}(\lambda)L + \ln(\sqrt{R_1 R_2}) = 0 \tag{2.4}$$

The phase condition in equation 2.3 shows that an FPLD cannot emit freely in all regions of the spectrum, as is showed in the Figure 2.3; the laser frequency ν must match one

frequency of the set ν_m, where m is an integer number. It is therefore understood that longitudinal modes spacing $\Delta\nu$ can be calculated as a function of the optical length, nL such that $\Delta\nu = (\nu_m - \nu_{m-1}) = c/2nL$ [15]. However, this equation would only be correct if there were no dependence between refractive index and frequency. This dependence on frequency can be taken into account by using the group index n_g instead of the refractive index alone, whereby the expression for calculating the mode spacing becomes as follows:

$$\Delta\nu(n_g, L) = \frac{c}{2n_g L} \qquad n_g = n + \omega(\frac{dn}{d\omega}) \tag{2.5}$$

To calculate the cavity length first it is necessary to consider the material to be used as a gain medium. For applications in optical networks, Indium gallium Arsenide phosphide (InGaAsP) can be considered a useful option for two reasons: (1) It presents a direct band-gap that allows an electronic inter-band transition without the need to interact with the crystal lattice (via phonons). (2) The energy of the band-gab determines the wavelengths of laser emission, and calculating this value as a function of the amount of each component is well known for this material [31]. For example, at emission wavelengths around the center of C-Band for optical communications such as 1552.525 nm, the band gap energy of $In_xGa_{1-x}As_yP_{1-y}$ lattice matched to InP can be calculated according to the equation 2.6 [31].

$$E_g = 1.35 - 072y + 0.12y^2. \tag{2.6}$$

Here, The fractions x and y selected arbitrary, but are related by $x/y = 0.45$ to ensure matching of the lattice constant. In this way, for an Arsenic (As) fraction y = 0.9, the band gap energy take a value of 0.8 eV, a suitable choice for a Laser diode with an emission around 1552 nm. additionally, the group index of this material is about of 3.7 in $\lambda = 1552.525$ nm. hence, if we consider a WDM-PON system with channels spacing at 100 GHz and use as gain medium InGaAsP with the conditions mentioned above, the cavity of the FPLD must be 405.125 μ m length.

On the other hand, the cavity length not only determines the channel spacing of the WDM system, but also affects the line-width of the longitudinal modes, and therefore imposes a threshold for the 3-dB bandwidth of the wavelength seeding carrier to achieve a target SMSR. This behavior can be evidenced from the *Finesse* of an optical resonator, which is defined as the free spectral range $\Delta\nu$ divided by the 3-dB bandwidth of the resonances of an optical resonator $\delta\nu$ [17]. Besides, *Finesse* is a consequence of the periodical losses that the material's absorption and the cavity's end facets induces of each round trip in the optical resonator, and its value depends on these losses. Thus, if the cavity's losses remains an almost fixed value, it can be noted from the equation 2.7 that the 3-dB line-width of each mode is proportional to $\Delta\nu$. Thus, the smaller the separation between the longitudinal modes, the smaller the line-width of the modes will have to be in order to be emitted without overlapping.

$$Finesse = \frac{\Delta\nu(n, L)}{\delta\nu} \qquad \delta\nu = \frac{\Delta\nu(n, L)}{Finesse} \tag{2.7}$$

2.1.2 End facets reflectivity

Other important feature for taking into account in the design of the FPLD-based colorless transmitter is the reflectivity value of cavity end-facets. This reflectivity vale have direct impact in the strength of the feedback process, in the photon density, and therefore in the amplification level of the longitudinal modes into the resonant-cavity [34].

A simple approximation to understand the reflecitivy impact over the FPLD, it is to consider the amplitude side of the equation 2.2. This equation allow us to obtain the laser threshold condition in terms of the absorption parameter $\alpha(\lambda)$, the cavity length L and the reflectivity of the cavity's end-facets R_1 and R_2, such that:

$$g(\lambda, R_1, R_2, L) = \alpha_{int}(\lambda) + \frac{1}{2L}\ln(\frac{1}{R_1 R_2}) \tag{2.8}$$

Thereby, from the equation 2.8 it can be seen that variations in the reflectivity of one end-facet of the cavity induce changes in the gain threshold. Thus, due to the losses of the active laser medium are function of frequency, high reflectivity values will cause that, in a steady state operation, the emission of the longitudinal modes located around the peak gain of the material will predominate while the other modes will be extinguished due to them gain do not exceed the cavity losses. However, for a colorless approach, an emission spectrum limited only to this high-gain modes is an undesirable feature: few emission modes imply a narrower injection-locking range, which would limit the number of possibles optical carriers and therefore the network's scalability. Thus, for solving this problem, a colorless transmitter that uses a Fabry-Perot resonant cavity with a low-reflective front-facet was proposed [18, 35–37]. In this configuration, not only the FPLD emission spectrum is broadened due to the weak-resonant condition, improving the flexibility in the mode selection, but also the power requirement to start the mode-locking is decreased.

The main drawback of these propose is that decreasing the reflectivity of the cavity may cause a decrease in laser coherence, an increase in temporal frequency fluctuations (chirp), and therefore a penalty in transmission performance due to the pulse broadening induces by this phenomenon. Thus, it is necessary to study a cavity configuration that provides an adequate trade-off between injection power requirement and transmission performance, which is penalized by the dispersives phenomena such as chirp. A simulation scenario is proposed in chapter 4 with the objective of determining a suitable trade-off between transmission performance and injection power requirement.

2.1.3 Confinement Factor

The confinement factor has an important role in cavity design since its value not only affects the laser threshold condition, but also affects the density of photons carrier density in the active layer[38]. Thus, due to the introduction of variations in photon density changes the carrier population, the mode refractive index is also affected, so the central emission wavelength will undergo a shift depending on the direction of change (carrier enhancement or carrier depletion)[15].

As mentioned in 2.1.2, the confinement factor of the active region represents the fraction of the mode energy contained in the active region. This means that the heterostructure of a semiconductor laser exhibits waveguide behavior, where the doped materials sandwiching

the active layer act as the waveguide cladding. Whereby, to calculate the confinement factor it is necessary to considers the transverse and lateral modes specifying the field distribution in the direction perpendicular and parallel to the junction plane of the semiconductor laser, respectively [15, 17]. This mechanism is often referred to as index guiding, since the refractive-index discontinuity between the active and cladding layers is responsible for the mode confinement through the total internal reflection occurring at the interface. However, field confinement in the lateral direction, which is parallel to the junction plane, is not always due to index guiding. Semiconductor lasers can be classified as gain-guided or index-guided, depending on whether it is the lateral variation of the optical gain or the refractive index that confines the mode [15, 17]. Thus, it is possible to define a confinement factor for the transverse modes Γ_T , and a second one for the longitudinal modes Γ_L, so that the confinement factor Γ can be calculated as:

$$\Gamma = \Gamma_T \Gamma_L \tag{2.9}$$

The confinement factor for the transverse modes Γ_T can be calculated, according to the equation 2.10, as a function of the active layer thickness d, the refractive index of the active layer $n1$, the refractive index of the waveguide cladding, and the emission wavelength.

$$\Gamma_T \cong D^2/(2 + D^2) \tag{2.10}$$

Where D is the normalized waveguide thickness, and can be calculated as follows:

$$D = k_0 d\sqrt{(n_2^2 - n_1^2)} \qquad k_0 = 2\pi/\lambda \tag{2.11}$$

It should be noted that this expression is only valid when the fundamental mode is propagating. However, it is possible to fulfill this condition if the cavity thickness is chosen such that:

$$d < \frac{\lambda}{2}(n_2^2 - n_1^2)^{-1/2} \tag{2.12}$$

The Figure 2.4 shows the confinement factor Γ_T as a function of the active region thickness d. Besides, to calculate Γ_T InGaAsP with different doping percentages were considered for the active layer and Indium Phosphide (InP) with refractive index $n_1 = 3.1646$ were considered for the waveguide cladding. Finally, 1552.525 nm was considered as emission wavelength.

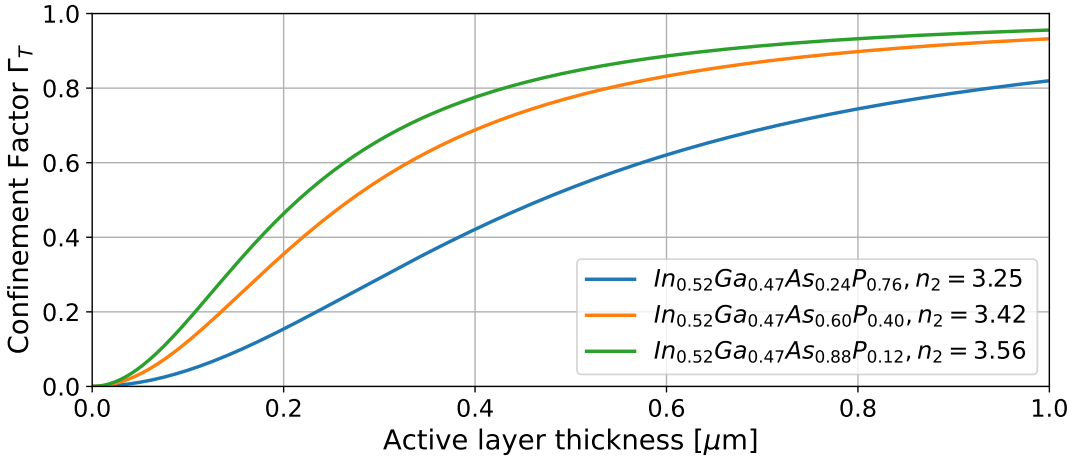

Figure 2.4. Transverse confinement factor for the fundamental TE mode.

On the other hand, The confinement factor for the longitudinal modes Γ_T can be calculated as a function of the active layer width w, the effective index $n_e(x)$, and the emission wavelength λ. Nevertheless, The lateral-mode behavior in semiconductor lasers is different depending on whether gain guiding or index guiding is used to confine the lateral modes. In a gain-guided device, $n_e(x)$ is a constant given by [31]:

$$n_e \cong n_1^2 + \Gamma_T((n_2^2 - n_1^2)) \tag{2.13}$$

By contrast, in an index-guided device, structural lateral variations are used to make $n_e(x)$ larger in a central region of width w. In these cases $n_e(x)$ can be expressed in two separated regions width refractive index n_e^{in} and n_e^{out} such that:

$$n_e(x) = \begin{cases} n_e^{in} & \text{if } |x| < w/2. \\ n_e^{out} & \text{otherwise.} \end{cases} \tag{2.14}$$

For this analysis, we are going to consider a strongly-guide-index device, in which the refractive index is a function of position along the active layer width w. Thus, the lateral confinement factor can be calculated as follows:

$$\Gamma_T \cong W^2/(2 + W^2) \tag{2.15}$$

where W is the normalized waveguide width, defined in the equation 2.16 as follows

$$W = k_0 w \sqrt{(n_e^{in})^2 - (n_e^{out})^2)} \tag{2.16}$$

As in the case of the transverse mode, the equation, 2.15, is only valid for the propagation of the lowest order lateral mode. Hence, to ensure that only the fundamental mode propagates in the laser cavity, the waveguide width must be calculated according to the equation 2.17. Where $\bar{n_e}$ and $\Delta n_L = n_e^{in} - n_e^{out}$ the average effective index and the lateral effective index, respectively.

$$w \leq \lambda/(8\bar{n_e}\Delta n_L)^{1/2} \tag{2.17}$$

Finally, For typically used values $w \cong 2\mu$m, $\Gamma_L \cong 1$, therefore Γ_T can be used for confinement factor Γ.

2.2 Numerical Methods

This section describes the theoretical models used to simulate the light propagation inside a resonant cavity such as a Fabry-Perot Laser Diode, and numerically analyze the injection seeding process taking into account several phenomena as cavity reflectivity, the carriers' dynamics (rate equations), photon's dynamics, stimulated emission, spontaneous emission, and electro-absorption.

2.2.1 Photonic Transmission-Line Model

The Photonic Transmission-Line Model (TLM) is an approach used for simulations of multi-section semiconductor devices with a built-in optical waveguide made from either a bulk or multiquantum well active medium. This Photonics TLM approach is based on the transmission-line matrix/modeling method, originally developed by P.B. Johns and R.L. Beurle for the analysis of resonances in microwave cavities and then applied to a multitude of other problems [39, 40]. However, in this work are considered enhancement of this TLM model proposed in [39]. This new approach, known as Photonics TLM, is an extension of the Transmission-Line Laser Model (TLLM) that has been developed since 1985 by A.J. Lowery and his colleagues [38, 41–47]. Additionally, all the models mentioned below have been included in the VPIPhotonics Desing Suite ©simulation software, making it a viable option to numerically analyze the behavior of the FPLD.

The TLM method exposed in [39], considers that both, space and time are discretized with a timestep δt and a spatial step $\Delta z = \Delta t v$, where v is the group velocity of signal propagation in the modeled medium. The nodes obtained after such spatial discretization are considered as lumped "scattering nodes" interconnected by"transmission lines" without losses. This way, all transmission lines present a signal delay of one timestep, which allows performing calculations at each scattering node independently of each other, just using information coming from of adjacent nodes (in the previous iteration).

On the other hand, in the Photonic TLM approach, the spatial discretization is confined to only the dimension along the built-in waveguide of the modeled semiconductor device. In this case, the semiconductor device is divided in k section according to the parts that constitute it (active, passive o electrical controlled). As shown in the Figure 2.5 Each device section k is divided in a group of small TLM sections with size $\Delta z = c\Delta t/n_k$, where c is the speed of light in vacuum and n_k is the group refractive index of the modeled device section. Thus, each TLM section contains a scattering node representing the gain (stimulated emission), loss (scattering and absorption), noise (spontaneous emission) and grating-induced reflection that optical waves experience while passing through the section. The information calculated in each TLM section (the output) is used as an input field in the adjacent TLM section. This information is transmitted through the transmission lines, which also take into account the propagation delay of the waveguide. However, this information is not generated in a single direction: During the "scattering" step, the Photonics TLM method generates outgoing forward and backward propagating optical wave $E_{F,m}$ and $E_{B,m}$ respectively. Then, at each "scattering node" (TLM section) are used to calculate the corresponding outgoing

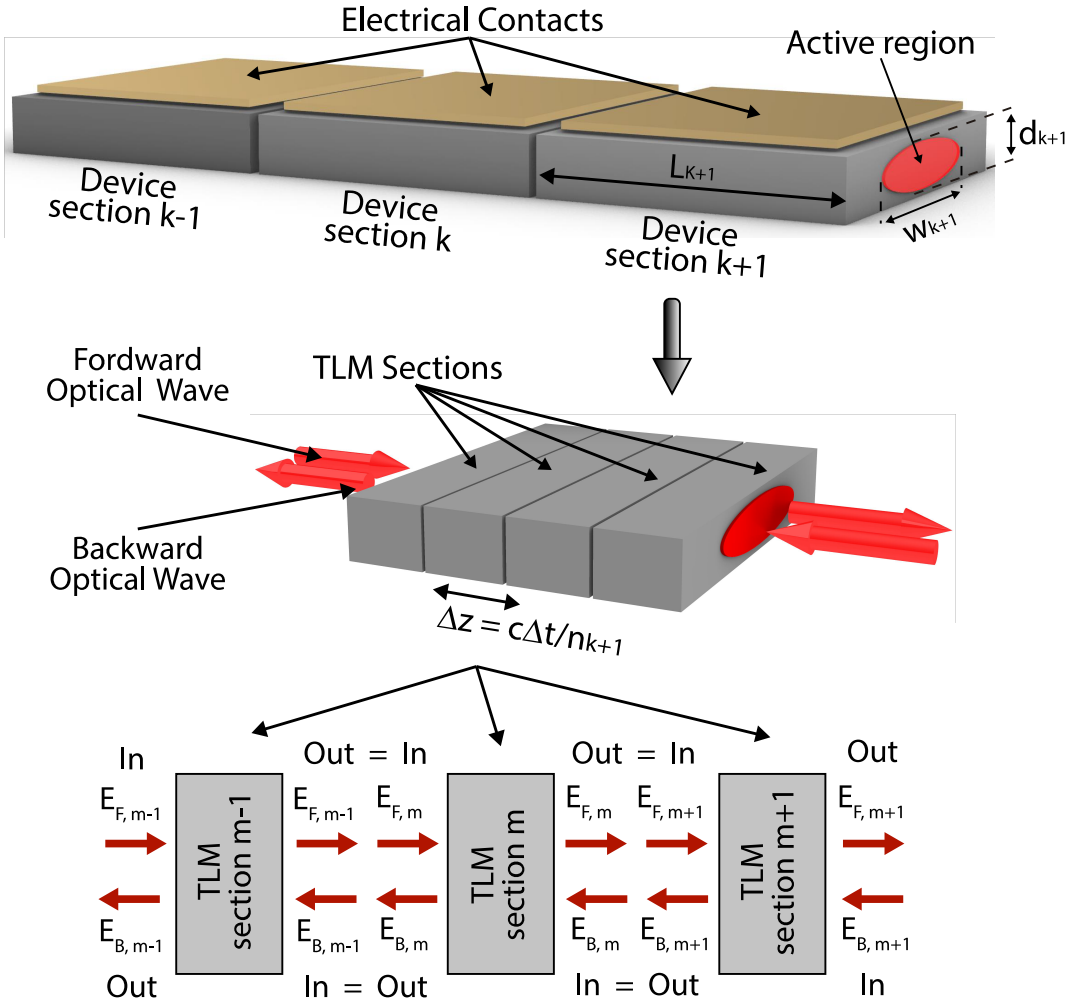

Figure 2.5. Transmission-Line Model for a semiconductor laser.Note that each semiconductor device can comprise several device sections (indexed by k), each of which is composed of many small TLM sections (indexed by m) [48]

forward and backward propagating optical waves, at the same node (See bottom section in the Figure 2.5). For these calculations, it is necessary to use the scatting matrix approach: operation detailed in [49].

2.2.2 Traveling-Wave Equations

The electric field $\vec{E}(r,t)$ inside the active region of the modeled TLM sections can be represented as a superposition of slowly-varying time-complexed envelope amplitudes $A(z,t)$ and $B(z,t)$ for the forward and backward-traveling optical fields, as shown the equation 2.18

$$\vec{E}(r,t) = e^{j2\pi f_c t}[\vec{F}(r,t)A(z,t) + \vec{F}(r,t)^* B(z,t)] + c.c \tag{2.18}$$

Where f_c is the central wavelength of the simulated emission spectrum, $\vec{F}(r,t)$ describes the electric field profile of the fundamental mode(s) in the cross-section area and $c.c$ conjugate complex of the first term. Moreover, due to the envelopes $A(z,t)$ and $B(z,t)$ are still rapidly

oscillating along z, it is convenient to define complex-valued amplitudes with a slow variation on both, t and z:

$$a(z,t) = e^{j\beta_0 z} A(z,t) \tag{2.19}$$

$$b(z,t) = e^{-j\beta_0 z} B(z,t) \tag{2.20}$$

Where β_0 is the propagation constant of the fundamental mode(s) with the effective index $n_{eff}(fc)$, and is defined as:

$$\beta_0 = \frac{2\pi f_C}{c} n_{eff}(f_0) \tag{2.21}$$

Thus, the traveling equations for the slowly-varying complex-valued envelopes $a(z,t)$ and $b(z,t)$ of the forward and backward optical fields within the modeled TLM section m of the device section k, can be derived from replace the equations 2.18, 2.19 and 2.20 in the Maxwell equations:

$$\left(\frac{1}{v_{g,k}}\frac{\partial}{\partial t} + \frac{\partial}{\partial z}\right) a = \left(\frac{1}{2}\hat{G}(N_m, S_m) - \frac{1}{2}\hat{\alpha_a}\right) a + Q_a \tag{2.22}$$

$$\left(\frac{1}{v_{g,k}}\frac{\partial}{\partial t} + \frac{\partial}{\partial z}\right) b = \left(\frac{1}{2}\hat{G}(N_m, S_m) - \frac{1}{2}\hat{\alpha_b}\right) b + Q_b \tag{2.23}$$

Here, $v_{g,k} = c/n_g$,k is the group velocity of the optical mode which is determined by the speed of light in a vacuum, c, and the group index, $n_{g,k}$ for a device section k. The optical loss operators $\hat{\alpha_a}$ and $\hat{\alpha_b}$ account for the internal loss, Free-Carrier Absorption (FCA), Two-Photon Absorption (TPA), and electro-absorption (or stimulated absorption) within the cavity. Then, the terms $Q_a = Q_a(z,t)$ and $Q_b = Q_b(z,t)$ are stochastic variables that denote the spontaneous emission into forward and backward traveling waves, respectively.

On the other hand, $G(\hat{N_m}, S_m)$ is the optical gain operator is responsible for the optical gain inside the active region, $N_m(t)$ the carrier density which is assumed to be constant within each modeled TLM section and can be calculated using rate equations (see subsection 2.2.3). $S_m(t)$ is the average photon's density within the modeled TLM section m of length Δz and can be determined from the forward and backward propagating optical fields according to the equation 2.24. Where, E_{ph} is the photon energy at the nominal frequency f_c, and Γ_k is the confinement factor for a device section k.

$$s_m(t) = \frac{\Gamma_k}{E_{ph}} \cdot \frac{1}{w_k d_k \Delta z} \int_{z_m - \Delta z/2}^{z_m + \Delta z/2} |A(z,t) + B(z,t)|^2 \cdot dz \tag{2.24}$$

The software VPIPhotonics Desing Suite^{TM} propose computational scheme employed for solving equations 2.22 and 2.23 within each TLM section that can be classified as a symmetrical fourth-order split-step scheme [50]

2.2.3 Rate Equations

The traveling-wave equations described in the section 2.2.2 should be accompanied by an additional equation that describes the dynamics of carrier density $N_m(t)$ in the modeled TLM section m of the device section k. In this case, the Photonics TLM approach employs a conventional rate equations in the approximation of uniform distribution of carrier density along the active media of each TLM section (Different TLM sections can present different densities).

For this work, we are going to consider a FPLD with a bulk active region. Consequently, for bulk active regions, each TLM section m of a device section k is described by a single electron density $N_m(t)$ inside the conduction band of the active region. We assume charge neutrality in all portions of the active region. That is, the hole density within the valence band is also assumed to be equal to $N_m(t)$. This carrier dynamics is governed by the follow rate equation:

$$\frac{dN_m}{dt} = \frac{\eta_k I_k}{qV_k} - R(N_m) - v_{g,k}\hat{G}(N_m, S_m) \cdot S_m + \frac{\beta_{TPA,k}}{2E_{ph}} \cdot \frac{\langle |E|^4 \rangle}{A_{eff.k}} \tag{2.25}$$

The first term on the right-hand side of the equation 2.25 represents the carrier injection density, and is responsible for the electron-hole pairs within the active region. Here, I_k is the bias current injected into device section k, and $V_k = w_k d_k L_k$ is the volume of the active region in this device section k. The remaining constants q and η_k are the electron charge and the internal quantum efficiency of the current injection (For well-designed lasers, it is close to one).

The second term on the right of the equation 2.25: $R(N_m)$ is the recombination rate of carrier. This term is taking into account the spontaneous and nonradiative recombination of electron-hole pairs, and is given by equation 2.26. Where the A_k, B_k and C_K are the linear, bimolecular, and the Auger, recombination coefficients of the device section k respectively. Note that the linear recombination coefficient is often expressed as $Ak = 1/\tau_k$, where τ_k is the carrier lifetime. The linear recombination is nonradiative which usually occurs when carriers "trap out" in midgap states and recombine without emitting photons. Instead, the bimolecular recombination produces spontaneous emission when electrons and holes recombine without the need for midgap states (Band-to-band radiative recombination). Finally, the nonradiative Auger recombination usually appears when carriers transfer their energy to other carriers, which interact with phonons to return to an equilibrium condition.

$$R(N_m) = A_k N_m + B_k N_m^2 + C_k N_m^3 \tag{2.26}$$

The third term on the right side of the equation 2.25 represents carrier depletion due to the stimulated emission, being responsible for the stimulated absorption and gain processes. Additionally, as was described in the section 2.2.2, the time-dependent variable $Sm(t)$ is the average photon density inside the active region of the TLM section m, and can be calculated using the equation 2.24. Moreover, The operator $\hat{G}(N_m, S_m)$ determines the temporal gain of light inside a TLM section. This term is considered as an operator in the sense that it filters the permanence after photon density S_m, resulting in a form of frequency-dependent gain.

Finally, the last term in the rate equation represents the creation of carriers due to TPA effect. Here, the constants $\beta_{TPA,k}$ and $A_{eff,k}$ characterizes the strength of the TPA process and the effective mode area in the device section k, respectively. Furthermore, $\langle|E|\rangle$ is the average square of photon power which is give by:

$$\langle|E|^4\rangle = \frac{1}{\Delta z}\int_{z_m-\Delta z/2}^{z_m+\Delta z/2} |A(z,t)+B(z,t)|^4 dz \tag{2.27}$$

2.2.4 Gain and Optical Loss Models

To solve the traveling-wave equations and the rate equation for carrier density, it is necessary to take into account the models for stimulated emission, spontaneous emission and optical losses, including internal FCA, TPA and electro-absorption. The following is a brief summary of these parameters and the considerations necessary to include them in the analysis proposed by the Photonics TLM scheme.

Stimulated Emission Models — Gain

As described in the previous section for the carrier dynamic, the temporal gain operator $G(N_m, S_m)$ determines the stimulated emission and/or absorption of light within the TLM section m. In general, this operator can be expressed as:

$$\hat{G}(N_m, S_m) = \Gamma_k \frac{\hat{g}(N_m)}{1+\epsilon S_{R,m}} \tag{2.28}$$

Where Γ_k is the confinement factor for a section k, $S_{R,m}(t)$ is the photon density causing "compression" of the optical gain, and ϵ is the gain compression factor which is used for introducing the nonlinear photon density–dependence of optical. Usually, the photon density $S_{R,m}(t)$ is assumed to be the instantaneous average photon density $S_m(t)$ within the modeled TLM section, so this can be calculated by integrating the photon density within the section assuming a constant gain. Finally, the operator $\hat{g}(N_m)$ determines the spectral properties of the gain operator and its dependence on the carrier density N_m at m-th TLM section. In the frequency domain, this operator can be represented by the function $g(f, N_m)$ with an explicit dependence on the frequency f.

The spectral properties of the gain (the gain curve) can be modeled in different ways: using a flat gain shape model, a parabolic gain shape model or a file that contain the gain profile of a material. In our particular case we are going to consider the parabolic gain profile as is shower in the Figure 2.6 due to the flat model can be inaccurate to model FPLDs [51]. In this case, it is possible to note that the gain depends on both, optical frequency f and carrier density N_m. Thus, If N_m exceeds certain value known as transparency carrier density N_{tr} (where the population inversion is realized and the active region exhibits optical gain), the gain will be zero for frequencies smaller than the so-called gap frequency, f_{gap}. Besides, the optical gain is positive for frequencies in the range $f_{gap} < f < f_{gap} + \Delta f$, where Δf is the gain bandwidth. If the opposite situation occurs when $N_m < N_{0,k}$, the gain is zero for $f < f_{gap}$ and the optical gain becomes negative for higher frequencies.

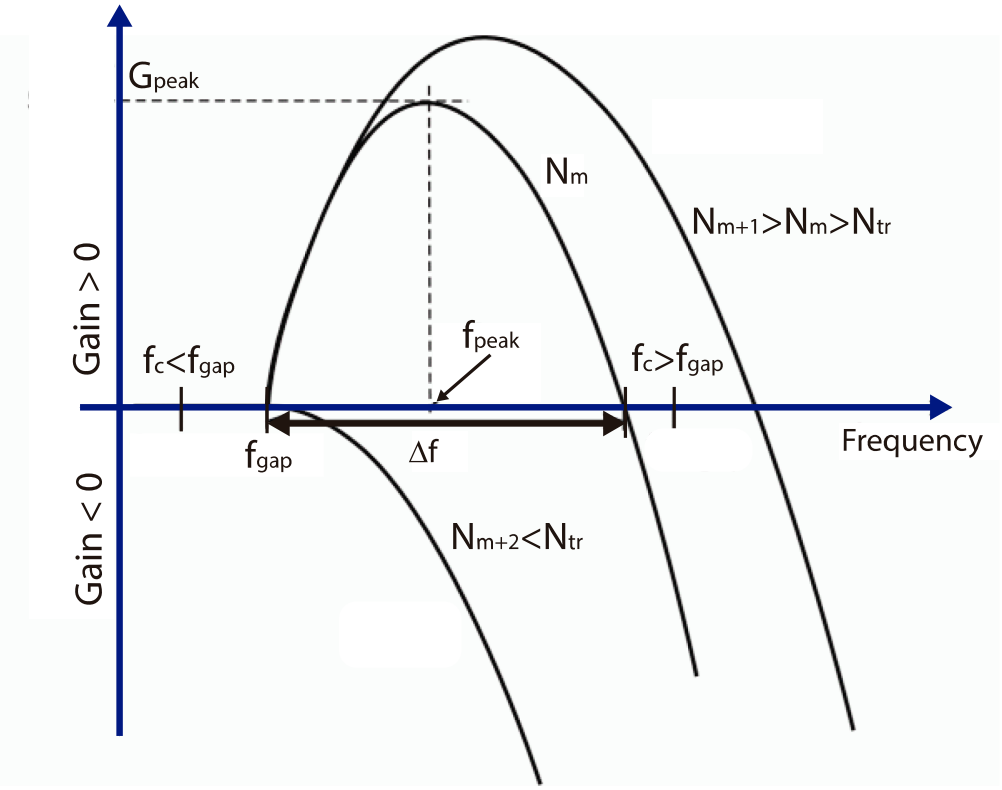

Figure 2.6. Gain shape curves [48].

Thereby, if $N_M > N_{tr}$ the gain shape depicted in the Figure 2.6 will be approximately represented by the equation 2.29,

$$g(f, N_m) = g_{peak}(N_m) \cdot \left(1 - \left[\frac{f - f_{peak}(N_m)}{\Delta f(N_m)/2}\right]^2\right) \tag{2.29}$$

where peak value $g_{peak}(Nm)$ can be represented using a linear gain model or a logarithmic gain model, as showed in the equations 2.30 and 2.31.

$$g_{peak} = a_{linear,k} \cdot (N_m - N_{tr}) \tag{2.30}$$

$$g_{peak} = a_{log,k} \cdot log\left(\frac{N_m}{N_{tr,k}})\right) \tag{2.31}$$

Where $a_{linear,k}$ and $a_{log,k}$ are the linear gain and the logarithmic gain of the material and N_tr, k is the zero gain carrier density (transparency value) for a device section k. It can be noticed that as the carrier density N_m grows, the gain factor for the logarithmic gain model grows slower than for the linear gain model. Therefore, the logarithmic gain model is a more realistic option for taking into account the carrier depletion behavior.

On the other hand, in the case of $N_m < N_{tr,k}$, the gain peak equals zero and the gain frequency dependence will be described as:

$$g(f) = -g_{peak}(N_{ref}, k) \cdot \left(1 - \left[\frac{f - f_{gap}}{\Delta f(N_{ref,k})/2}\right]^2\right) \tag{2.32}$$

In this case, $g_{peak}(N_{ref}, k)$ and $\Delta f(N_{ref,k})$ are the gain peak and the gain bandwidth for some reference carrier density $N_{ref,k}$. The frequency gap can be calculated by the following equations, where $f_{peak}(N_{ref,k})$ gain peak frequency.

$$f_{gap} = f_{peak}(N_{ref,k}) - 1/2\Delta f(N_{ref,k}) \tag{2.33}$$

Finally, the carrier dependence of the gain bandwidth is determined by the expression:

$$\Delta f(N_m) = \Delta f_{ref.k} \cdot \sqrt{\frac{g_{peak(N_m)}}{g_{peak}(N_{ref,k})}} \tag{2.34}$$

Spontaneous Emission Models — Noise

The section 2.2.2 describes the terms $Q_a(z,t)$ and $Q_b(z,t)$, that were introduced to consider the behavior of the spontaneous emission in the traveling equation. The spontaneous emission is the process in which electrons travel from the conduction band to the valence band in the active region, releasing the difference in energy between these two bands as new photons. However, in contrast to the stimulated emission, such new photons are uncorrelated — they have random phases, frequency, wave vectors, and polarization. Hence, only a few of these photons are coupled into the guided mode.

The Photonic TLS approach models the spontaneous emission in terms of $Q_a(z,t)$ and $Q_b(z,t)$ for each TLM section m of a device section k, using Longeving noise sources as follows [52]

$$Q(z,t) = \sqrt{\frac{1}{2}P_{sp}(N_m) \cdot (X(z,y) + jY(z,t))} \tag{2.35}$$

Where $P_{sp}(N_m)$ is the power of the spontaneous emission and $X(z,t)$ and $jY(z,t)$ are uncorrelated pseudo-random sequences modeled by a Gaussian white noise source. Moreover, this generated noise needs to be injected in to each TLM section in two points for forward waves and in two points for the backward waves (Four points at each side of the scattering matrix) [34, 53].

Thus, the calculations of the spontaneous emission are based on the gain due to stimulated emission and enhanced by the inversion parameter n_{sp}, and although this method is widely used for optical amplifiers but is also applicable to semiconductor lasers [44, 52]. Therefore, according to this method, the power of the spontaneous emission generated at TLM section of the length Δz over the simulation bandwidth $\Delta\nu$ is equal to:

$$p_{sp} = h\nu \cdot n_{sp,k} \cdot \frac{g_{peak}(N_m)\Gamma_k}{g_{peak}(N_m)\Gamma_k - \alpha_i(N_m)} \cdot (G_{net}(N_m) - 1) \cdot \Delta\nu \tag{2.36}$$

Where $h\nu$ is the photon energy, $g_{peak}(N_m)$ is the peak gain (calculated according to 2.30 o 2.31), and α_i is the loss per unit length due to waveguide scattering and free-carrier absorption. Finally, $G_{net}(N_m)$ is the net power amplification per TLM section in linear units, and is calculated according to the equation 2.37

$$G_{net}(N_m) = e^{(\Gamma_k \cdot g_{peak}(N_m) - \alpha_i)\Delta z} \tag{2.37}$$

The inversion parameter $n_{sp,k}$ accounts for the fraction of the stimulated emission that is compensated by stimulated absorption events in an imperfectly inverted medium. Finally, the term $g_{peak}(N_m)\Gamma_k/(g_{peak}(N_m)\Gamma_k) - \alpha_i(N_m)$, accounts for an additional gain over the net gain required to compensate for the losses.

Optical Loss Models

The Photonics TLM model considers several types of optical loss mechanisms. However, these can be divided into two groups: (1) the distributed optical losses inside the modeled device sections and (2) the lumped optical losses at the facets of neighboring device sections.

The distributed losses are proportional to the device section lengths and are modeled by the optical loss operators and introduced in equations 2.22 and 2.23. In a general case, they can be expressed as sums of three carrier-dependent terms that describe the internal loss, the free carrier absorption, two-photon absorption (TPA), and the stimulated absorption loss, which causes the generation of free carriers.

$$\hat{\alpha_a} = \alpha_i(N_m) + \alpha_{TPA,a}(a,b) + \alpha_{EAM}(V_k, N_m) \tag{2.38}$$

$$\hat{\alpha_b} = \alpha_i(N_m) + \alpha_{TPA,b}(a,b) + \alpha_{EAM}(V_k, N_m) \tag{2.39}$$

The internal loss parameter $\alpha_i(N_m)$ is supposed to be linearly dependent on the carrier and can be mathematical represented as follows:

$$\alpha_i(N_m) = \alpha_{i,0} + \alpha_{iN} \cdot N_m \tag{2.40}$$

Where $\alpha_{i,0}$ is a parameter known as internal loss, and describes loss mechanisms such as material loss and the Rayleigh scattering. Furthermore, the constant α_{iN} is the carrier-dependent internal losses, which describes loss mechanisms such as free-carrier intraband absorption. It is necessary to note that although the internal loss is a carrier-depending function, it does not affect the carrier density.

The two-photon absorption terms $\alpha_{TPA,a}$ and $\alpha_{TPA,b}$ are determined by the expressions:

$$\alpha_{TPA,a} = \Gamma_{NL,k}\frac{\beta_{TPA,k}}{A_{eff}} \cdot (|a(z,t)|^2 + |b(z,t)|^2) \tag{2.41}$$

$$\alpha_{TPA,b} = \Gamma_{NL,k}\frac{\beta_{TPA,k}}{A_{eff}} \cdot (2|a(z,t)|^2 + |b(z,t)|^2) \tag{2.42}$$

Here, the constant $\Gamma_{NL,k}$ is the nonlinear optical confinement factor, introducing the contribution of Kerr and TPA nonlinearities. The constant $\beta_{TPA,k}$ characterizes the strength of the TPA process in the device section k. The constant A_{eff} is the effective mode area in the device section k. Finally, the factor two for counter-propagating fields reflects the all-known fact that cross-phase modulation is twice as effective as self-phase modulation for the same signal intensity [54]. It should be noted that the TPA value is an experimental measure and its value depends on the material used as gain medium [55].

The voltage-controlled electroabsorption operator $\alpha_{EAM}(V_k, N_m)$ takes into account the stimulated absorption loss (interband) that causes the generation of free carriers. Moreover,

for active device sections, the stimulated absorption at high frequencies is already taken into account by the optical gain operator $\hat{G}(N_m, S_m)$ in the section 2.2.4. However, the use of the gain operator in the stimulated regime is not recommended to modeling the effects of stimulated absorption. Instead, it is recommended to model stimulated absorption explicitly through the operator $\alpha_{EAM}(V_k, N_m)$. The operator character of this loss means that it is frequency dependent and is therefore modeled using a digital filter (FIR or IIR).

These effects of electroabsorption are described using the following equation:

$$\alpha_{EAM}(f, V_k, N_m) = \frac{\alpha_e(f, V_k)}{1 + N_m/N_{sat,k}} \tag{2.43}$$

where N_m is carrier density in the active region of the modeled TLM section m of the device section k, V_k is applied reverse-bias voltage, f is the optical frequency and $N_{sat,k}$ is the saturation carrier density.

The spectral and voltage dependence of $\alpha_e(f, V_k)$ may be modeled using a Lorentzian shape profile:

$$\alpha_e(f, V_k) = \alpha_p(V_k)\frac{(\Delta f(V_k)/2)^2}{(f - f_p(V_k))^2 + (\Delta f(V_k)/2)^2} \tag{2.44}$$

where $\alpha_p(V_k)$ is the peak absorption magnitude, $f_p(V_k)$ is the peak absorption frequency and $\Delta(V_k)$ is the absorption bandwidth. This reverse-bias voltage-dependent function can be calculated using a third-order polynomial approximation such that:

$$\alpha_p(V_k) = \alpha_{0,k} + \alpha_{1,k} \cdot V_k + \alpha_{2,k} \cdot V_k^2 + \alpha_{3,k} \cdot V_k^3 \tag{2.45}$$

$$f_p(V_k) = f_{0,k} + f_{1,k} \cdot V_k + f_{2,k} \cdot V_k^2 + f_{3,k} \cdot V_k^3 \tag{2.46}$$

$$\Delta f(V_k) = \Delta f_{0,k} + \Delta f_{1,k} \cdot V_k + \Delta f_{2,k} \cdot V_k^2 + \Delta f_{3,k} \cdot V_k^3 \tag{2.47}$$

Here, the constants $\alpha_{n,k}$ with n = 0 to 3 are Absorption Peak, Absorption Peak Linear, Absorption Peak Quadratic, and Absorption Peak Cubic, respectively. The same interpretation can be made for equations 2.46 and 2.47.

2.2.5 End-Facets Reflectivity — TLM representation

The TLM technique has been applied to many types of semiconductor lasers, electroabsorption, and passive devices. Moreover, due to its modularity, it is able to model novel designs without modification [47, 56–59].

The simplest of devices that can be modeled using the Photonic TLM approach are Fabry-Perot lasers that consist of a waveguide with reflective facets at the ends (cavity end-facets or mirrors). In these, the end model sections have transmission lines that have a length of half-time step Δt, and the reflectivity of the facets can be as represented by the resistors across these half-length transmission lines. Besides, these reflectivity values can be controlled by the value of these resistors, as shown in Figure 2.7. Consequently, the optical field samples traveling to the cavity's facets from the end nodes, are reflected back to the

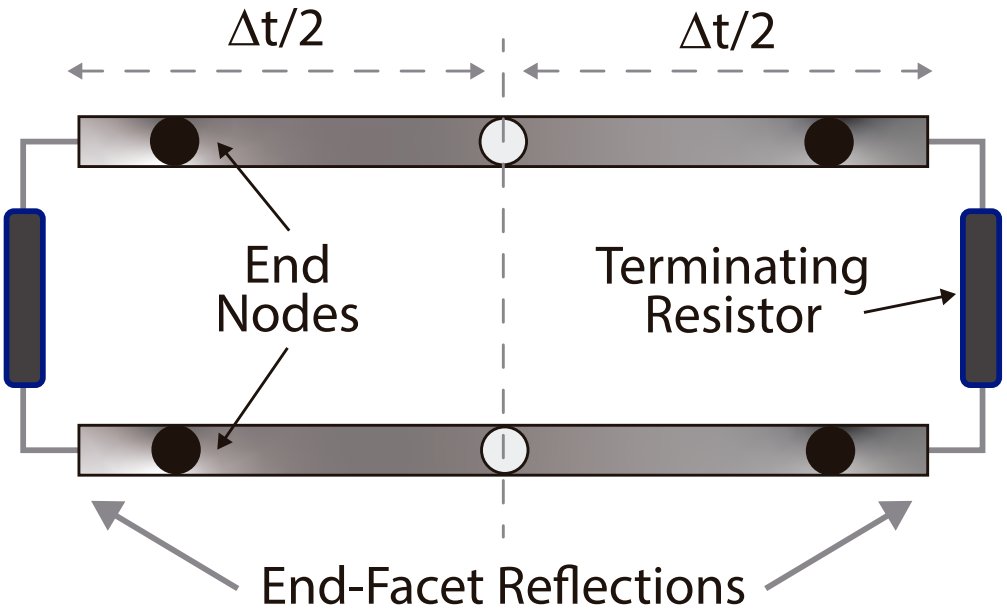

Figure 2.7. TLM representation of the cavity's end-facets reflectivity using terminator resistor [48].

same node. Since the round-trip delay of the final transmission line is one time step, the pulses from the facets arrive in synchrony with the pulses from the nodes toward the center of the laser.

Chapter 3

Colorless Transmitter Design

This chapter summarizes all design considerations used for the implementation of a Fabry-Perot Laser as a colorless transmitter in a WDM network. This chapter includes the basic cavity parameters that allow adequate mode spacing for WDM networks, as well as the simulation schemes proposed to determine the value of the end reflectivity as a function of the required injection power and source chirp. Finally, the simulation setup used to measure the transmission performance of the designed colorless transmitter is also presented in this section.

3.1 Design considerations

As mentioned in2, several features need to be taken into account to design a colorless transmitter based on a FPLD that is suitable for applications in WDM-PON systems.

The first drawback of this colorless transmitter approach is the wavelength emission, that in a FPLD is limited to these wavelengths that correspond to a round-trip phase shift inside the cavity. This mean that we can only tune the emission wavelengths allowed for the Fabry-Perot type structure, i.e., a discrete set of longitudinal modes. However, according to the equation 2.5 it is possible to customize the longitudinal mode spacing selecting the correct cavity length for a material with a well-known refractive index. In this case, InGaAsP lattice matched to Inp can be considered a useful option due to is direct band-gap material that allows an electronic inter-band transition without the need to interact with the crystal lattice (via phonons), and a function to calculate the energy of band-gap to guarantee emission around to 1552.525 nm (optical communications c-band center) can be calculated from equation 2.6.

Thereby, for obtaining a Fabry-Perot laser emitting around 1552.525 nm it is necessary a band-gap energy around of 0.8 ev, which can be achieved by using $In_xGa_{1-x}As_yP_{1-y}$ with arsenic allow fraction y = 0.9. As a result, for this arsenic fraction and maintaining the ratio $x/y = 0.45$ to ensure the matching of the lattice constant, the material group index is of 3.7 [31]. Moreover, to guarantee the propagation of only the fundamental modes, it is necessary to calculate the active region thickness d and the active region width w according to equations 2.10 - 2.17. Thus, in order to confinement Γ be almost equal to the confinement factor of the transverse mode Γ_T, the confinement factor of the longitudinal mode $\Gamma_L \approxeq 1$, therefore the active width W need to be of the order of 2 μ m. On the other hand, de confinement factor of the transverse mode is a parameter that can be calculated a function

of the cavity thickness, e.g, for d= 210 nm, Γ_T takes a value of 0.4. Besides, this confinement factor helps to tune the FPLD central wavelength, due to its value affecting the fraction of energy inside the active media, i.e, is related to the photon's density in the active region and therefore to the refractive index.

The following is a summary of the fixed design parameters for the colorless transmitter based on a FPLD:

- Cavity Length: 405.125 μm
- Material: $In_xGa_{1-x}As_yP_{1-y}$ with y=0.9 and x/y = 0.45
- Group index at 1552.525 nm: 3.7
- Active region thickness: 190 nm
- Active region width: 2.6 μm
- Confinement factor: 0,4
- Active region type: bulk

Finally, regarding the power requirement, the main idea is to achieve 30 dB SMSR using the lowest possible injection power, maintaining a good trade-off with the transmission performance. 30 dB SMSR is necessary to ensure that in a multi-carrier system, adjacent channels do not interfere with each other. In addition, we are going to consider as a low injection power requirement at power values below 300 μW: about 10% of the average transmit power according to the ITU-T G.694.1 recommendations [15]. It is necessary to note that the SMSR is measured as the difference between the peak power of the tuned longitudinal mode and side mode with the highest peak power.

3.2 Simulation setup

In this section, we propose the simulation scenarios used for analyzing the performance of the FPLD as colorless transmitter. Here, the first scenario is used to analyze the impact of the end-facet's reflectivity over the injection power requirement for achieving 30 dB SMSR, the source chirp, how many optical carriers it is possible to tune using a low power requirement (300 μW), and how the optical carrier bandwidth affects SMSR. Then, in the second simulation scenario, the transmission performance of the colorless transmitter over a WDM-PON system is tested. All simulations are performed with the specialized software VPI Photonics Design Suite ©. Besides, for all performance measurements is considered a FPLD with the features mentioned in section 3.1: 405.125 μm length, a group index of 3.7 at 1552.525 nm and longitudinal modes with 100 GHz spacing. Additionally, a general scheme of the simulations and the steps to be followed are described in the figure Figure 3.1.

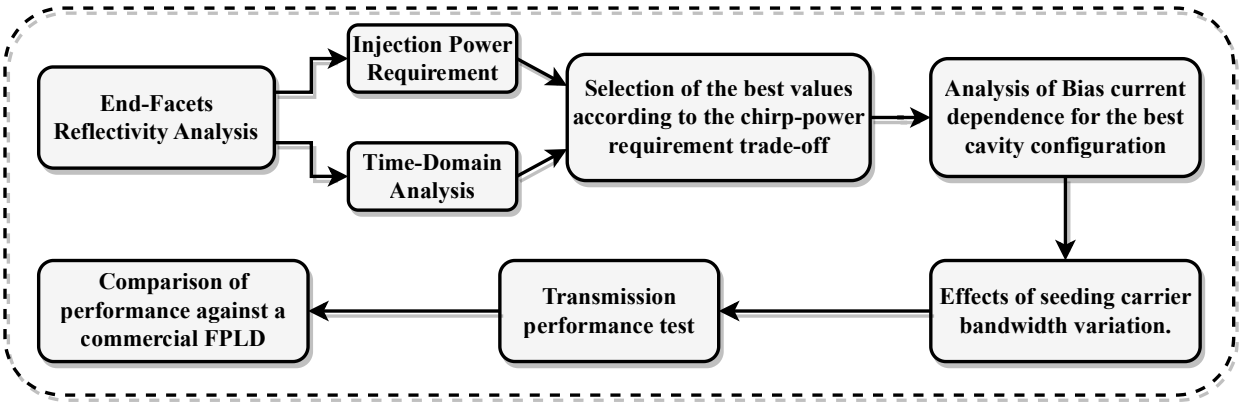

Figure 3.1. Simulation schedule.

The details of each step in the simulation scheme are described as follows:

3.2.1 Simulation scenario for analyzing the impact of reflectivity on the colorless transmitter performance

The first simulation scenario is shown in the figure Figure 3.2. This simulation setup consist of a SuperLuminescent diode (SLED) as a broadband source, an Erbium-doper Fiber Amplifier (EDFA) adjusted to amplify the optical signal from the SLED up to 22 dB, a Standard Single Mode Fiber (SSMF) with a length according to PON standards: 25 km, a Variable Optical Attenuator (VOA) that controls the power of the injection carrier to be between 0.04 and 1.5 mW, a 25 GHz Optical BandPass Filter (OBPF) used for slicing the SLED spectrum into narrower bandwidth optical carriers, and finally a FPLD designed to support longitudinal modes with 100 GHz spacing. Moreover, according to NG2-PON standards, WDM-based access networks are expected to support between 4 and 8 optical. Therefore, all performance measurements were made for two different longitudinal modes: (1) a central mode, where the laser presents its maximum gain, and (2) the side mode shifted by 400 GHz regarding the central longitudinal mode. In this way, considering the spectrum symmetry regarding the central mode, we ensure the operation of the colorless transmitter with at least 9 optical carriers.

The idea of this simulation setup is introducing variations in the reflectivity of the cavity's end-facets. Initially, variations between 32 and 95% are proposed for the cavity back-facet R_2. These reflectivity values are due to the fact that the main idea is that the power of the injected carrier is high, which can be achieved by reflecting most of the power in the back facet. Thus, to analyze whether the back-facet reflectivity affects the injection power requirement and the SMSR, and what is the dependency between them, several fixed values for the reflectivity of the cavity's front-facet were considered: 1 %, 10 % and 30%.

Consequently, after analyzing the back-facet of the cavity and determining what is a suitable value to maintain a low power requirement, the reflectivity of this mirror will be set to that value. Then, the reflectivity of the front-facet of the cavity will be varied between 1% and 90%. These variations are introduced to determine suitable reflectivity values to ensure the lowest possible injection power requirement for a target SMSR (30 dB in our case).

Furthermore, using the same simulation scenario, we analyze how many optical carriers it is possible to tune using a low power requirement (300 μm), and how the optical carrier

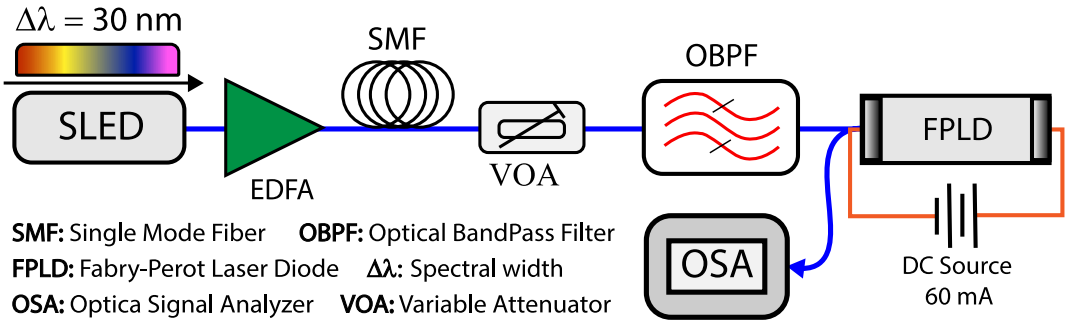

Figure 3.2. Simulation scenario for the cavity reflectivity analysis.

bandwidth affects the injection power required to achieve a 30 dB SMSR. In the latter case, seeding carriers with 3-dB bandwidths $\Delta\omega_{ic}$ of 12.5 GHz, 25 GHz and 50 GHz (typical values for commercially available DEMUX) are considered.

Due to the WDM-based networks operate in a spectral region further away from the optical fiber's zero of dispersion (normally the dispersion in this region is of 16 ps/nm·km), the transmission performance is negatively affected by dispersive phenomena. Consequently, since the broadband source seeding the FPLD emission wavelength is a SLED, which operates using an Amplified Spontaneous Emission (ASE) process, it is necessary to analyze the time-depending frequency variations (or chirp) that this type of source induces in the FPLD-based colorless transmitter.

Here, for this time-domain analysis, it is proposed the same simulation scenario shown in the figure Figure 3.2. This is due to the coherence of the laser and therefore the time domain fluctuation of the emission frequency, it is directly proportional to the reflectivity of the cavity mirrors. As a consequence, analyzing the fluctuation of the laser emission frequency over time for several reflectivity values in the end-facets reflectivity (mainly in the frontal one), it is necessary in order to determine a good trade-off between the power requirement and the transmission performance, that is strongly affected by the pulse broadening causes by the source chirp [15, 54].

3.2.2 Proposed WDM-PON System to analyze the colorless transmitter performance

The figure Figure 3.3 shows the WDM-PON architecture in the upstream channel proposed to evaluate the FPLD performance as a colorless transmitter. The Broad Band Source (BBS) that would be used for the external wavelength tuning process in the ONU's transmitters is located at the Central Office (CO). This BBS consists of a SLED amplified by an EDFA pumped with a 1480 nm laser diode. The resulting amplified light of 30 nm is transmitted unmodulated over an SMF with a length up to 120 km. At the ONU side, the incoming signal is spectrally sliced by MUX/DEMUX. Then, the narrowband optical carrier at the MUX/DEMUX output is injected into the designed FPLD. Then, the external seeding FPLD is directly modulated by a Non-Return to Zero (NRZ) signal using a 60 mA bias current. Finally, we compare the transmission performance of this colorless transmitter regarding external modulated Distributed FeedBack (DFB)) laser using the same power and 3-dB bandwidth conditions.

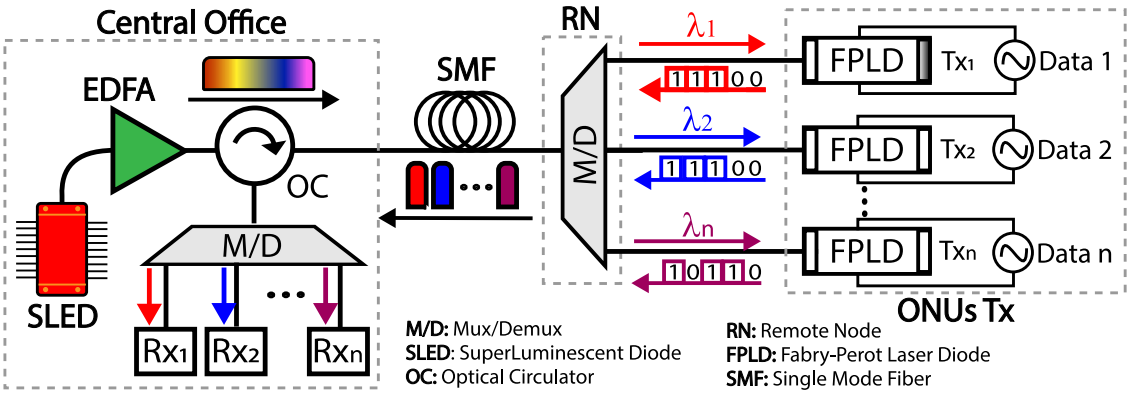

Figure 3.3. Transmission test scenario.

Chapter 4

Performance results of the colorless transmitter based on a FPLD

This chapter shows the results of the reflectivity analysis performed for an FPLD designed to support longitudinal modes spaced 100 GHZ, how these reflectivity values affect the power requirement to achieve an SMSR of at least 30 dB, their impact on coherence of the colorless source and therefore and its chirp. Also, for the best values of the end-facet reflectivity selected using as criteria the trade-off between injection power requirement and chirp, it is performed an analysis of how the bandwidth of optical seeding carrier affects power requirement for a target SMSR. Finally, the transmission performance of the designed colorless source is tested in a WDM-PON system with distances up to 100 km. Additionally. it is analyzed how many optical carriers can be obtained using seeding carrier with 300 μW optical power.

4.1 Colorless transmitter design

The 4.1a shows the optical spectrum of an unseeded FPLD designed to support 100 GHz longitudinal modes and a central emission wavelength in 1552.525 nm (center of c band for optical communications according to ITU-TG.694.1 recomendations) obtained using the simulation software VPIPhotonics Design Suite©. In this case, the optical power spectrum for a Fabry-Perot cavity with a reflectivity configuration 10/90 and 20 mA bias current is observed. On the other hand, to compare the shape of the optical spectrum of the designed FPLD, the optical spectrum of commercial available bulk type FPLD[1]with end-facets reflectivities of 32 % biased at 20 mA is showed in 4.1b. For both cases, the resolution of the Optical Spectrum Analyzer (OSA) was set 0.05 nm in order to have equivalent power measurements (power measurement in an OSA are sensitive to the device frequency resolution)

It is possible to note that the spacing between longitudinal modes of the commercial FPLD does not satisfy the standards for WDM optical networks, i.e., channels spaced a multiple of 12.5 GHz (1.4 nm is equivalent to 174 GHz). Additionally, as expected, although a gain spectrum of the designed FPLD was considered to have parabolic shape with a 3-dB bandwidth of 100 nm (Similar to InGaAsP with hole concentration around 1×10^{18} [31]), a real device no present a well-defined gain shape, therefore modes around the central emission wavelength can exhibit similar peak gains and powers.

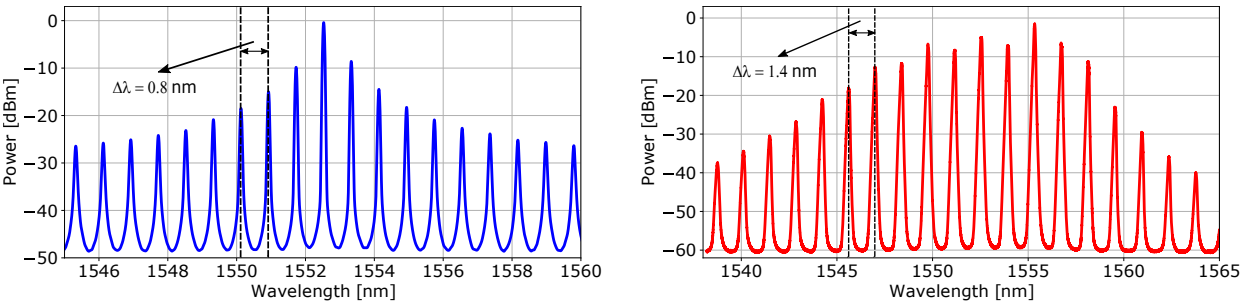

Figure 4.1. FPLD spectrum. a) FPLD designed to support 100 GHz spaced longitudinal modes nm. b) Market available FPLD.

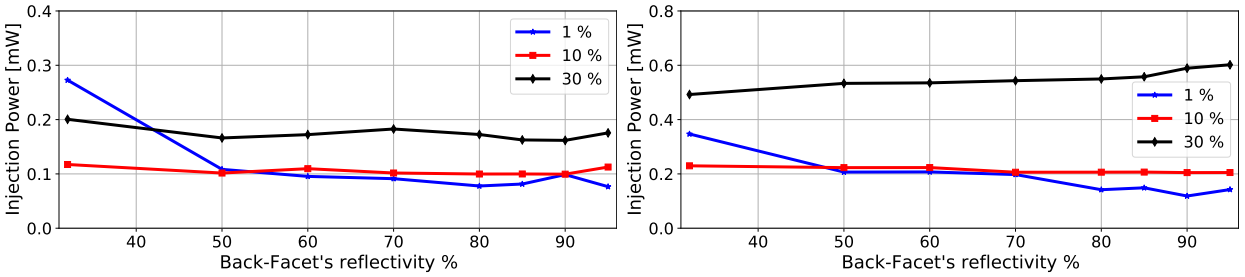

Figure 4.2. Injection power requirement to achieve a SMSR of 30 dB. a) 1552.525 nm (central). b) 1550.125 nm (Side Mode).

4.2 End-Facets reflectivity

First, we analyze how the reflectivity of the back-facet R_2affects the injection power required to achieve 30 dB SMSR. [15] Due to we need to obtain the highest possible power in the cavity, high reflectivity values are necessary to improve the feedback process. Thus, we considered reflectivities for the back-facet in a range between 32 %, that is typical for a FPLD without external mirrors (only cleaved facets, and 95%. Moreover, for each back-facet case, reflectivities of 1, 10 and 30 % are considered for the front-facet.

The Figure 4.2 show the injection power requirement in mW unit that is necessary for achieving a SMSR above to 30 dB of both the central mode (1552.525 nm) and a side mode shifted 400 GHz regarding the central mode (1550.125 nm). The results show that the power requirement to achieve a SMSR of 30 dB no present a considerable dependency regarding back-facet reflectivity (at least for these high values). However, although configurations with 32 % reflectivity on the cavity back-facet achieve a 30 dB SMSR at 300 μW of power in most cases, the injection power requirements increase slightly due to the decrease in feedback gain. If the feedback gain decreases, the injected carrier should have more power so that the power of the tuned mode exceeds the power of the spontaneous emission.

Additionally, in the Figure 4.3 and the Figure 4.4 show that for injection powers higher than 1.2 mW a saturation point is reached for both longitudinal modes, and that for these

[1]Data sheet available in: http://www.oemarket.com

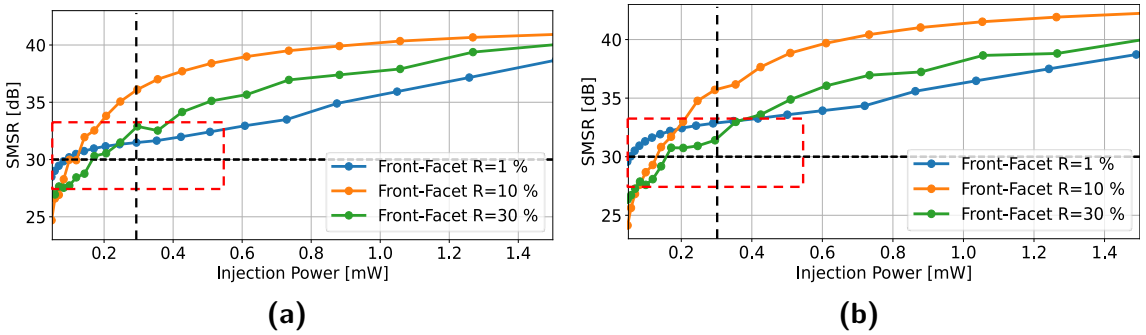

Figure 4.3. SMSR vs Injection power. Central Mode. R_2: a) 90 %. b) 95 %

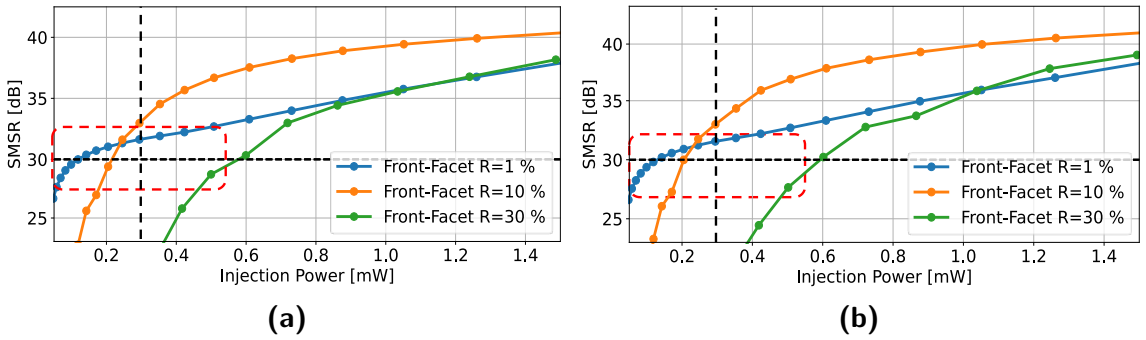

Figure 4.4. SMSR vs Injection power. 400 GHz shifted Side Mode. R_2: a) 90 %. b) 95 %

regions the SMSR presents considerable variations (up to 6 dB) depending on the reflectivity of the cavity back-facet. This behavior is due to the fact that for these end-facets configurations, low injection powers (< 300 μW) are not enough to saturate the cavity gain, so the peak power ratio between the longitudinal modes is maintained, even for different gain values. However, for high injection power, mainly in the case of the central mode where the gain of the active medium is higher, it is possible to find differences in the SMSR for different values of back side reflectivity. This behavior is due to the fact that reflectivity directly affects photon density in the cavity, and therefore at what point the saturation gain is reached. Thus, if gain saturation is not achieved due to low reflectivities implying low feedback gain, the SMSR can keep growing.

Then, since the performance of the FPLD-based colorless source in terms of the SMSR is not significantly affected by the reflectivity values in the cavity's back-facet, we consider using a fixed reflectivity value of 90 %, in order to study how the front-facet reflectivity affects source performance in terms of the injection power requirement and the chirp. Choosing a high reflectivity value guarantees a higher amplification in the cavity, and therefore a higher power output. Moreover, at this point it is necessary to clarify that for a laser operating far from the saturation region, the optical power of the central mode will be directly proportional to the bias current. In consequence, in the case where a side mode is seeded externally, the higher the bias current, the lower the SMSR. Thus, in order to choose an appropriate value for the bias current, it is first necessary to find the laser threshold current. The Fig 4.5a shown the output power as a function of the bias current of a cavity with reflectivities of 1%, 10 % and 30 % in the front facet, and 90% in the back-facet. It is clear that in all cases, the threshold current is above 20 mA, and that the higher the reflectivity of the front-facet,

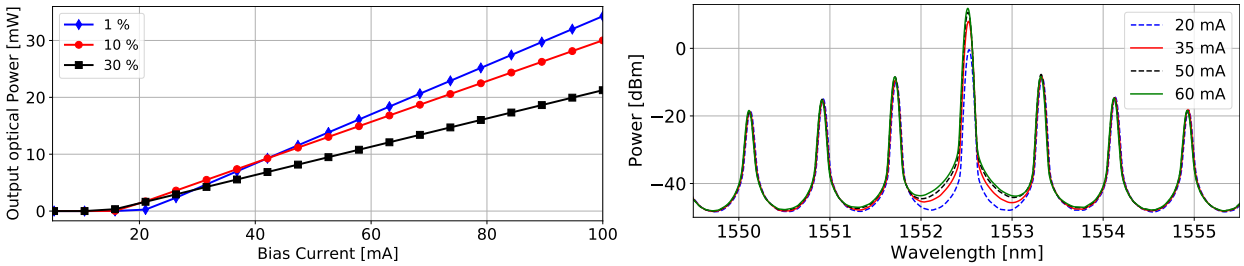

(a) Bias Current vs Optical Output Power **(b)** Colorless transmitter power spectrum

Figure 4.5. Simulations of the designed colorless transmitter. Power characterization.

the lower the value of the threshold current.

Furthermore, the figure 4.5b shows the power spectrum for different values of the bias current of a cavity with a 10/90 % reflectivity configuration. In this case, it is clear that the power of the central mode increases as a function of the bias current, so choosing a value around 20 mA could be considered a suitable option o get a target SMRS. However, operating close to the threshold current is not a recommended for a direct modulation scheme, due to the chirp induced by abrupt changes in carrier density. Thus, to determine the injection power requirement in all cavity's reflectivity configurations, we propose a bias current of 60 mA. This will establish a bias current limit below which, if a certain injection power is guaranteed, the colorless source will guarantee at least 30 dB SMSR.

The 4.6a and the 4.6b shows the SMSR vs injection power of both the central mode a side mode, respectively, for different reflectivity values of the cavity front facet R_1. As we expected, the measurements shows a strong dependency of the power requirement and the reflectivity of the front-facet. In general, the lower the reflectivity value, the lower the power requirement to obtain a SMSR above to 30 dB. For the case of the central mode, even its gain is higher than the 400 GHz shifted side mode, for reflectivities below 50 % relatively-low injection powers (less than 1 mW) are not enough to achieve 30 dB SMSR. However, as can be noticed in the Fig. 4.6b, the performance of the side modes is more affected more than in central mode when the reflectivity of the front-facet is increased. This is because the cavity feedback increases proportionally to the reflectivity of the end-facets, at the point of gain saturation, photon emission will predominate in the spectral regions where the material has higher gain. Therefore, the injection power required for a target SMSR will also increase. Thus, due to the main idea is to achieve 30 dB SMSR using the lowest possible

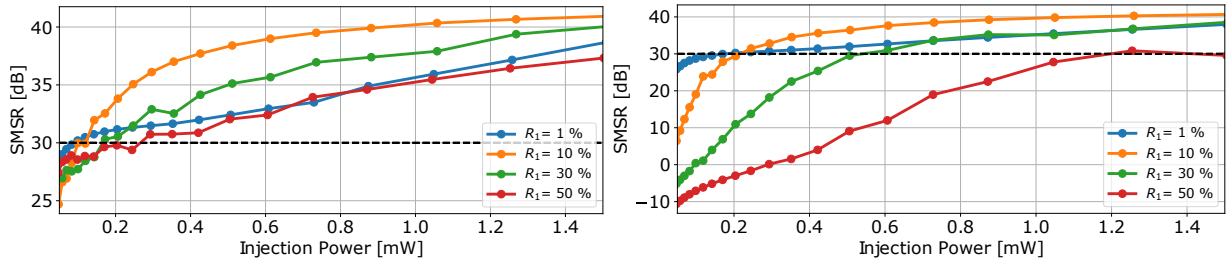

(a) Central Mode **(b)** 400 GHz Shifted Mode

Figure 4.6. SMSR vs. Injection Power

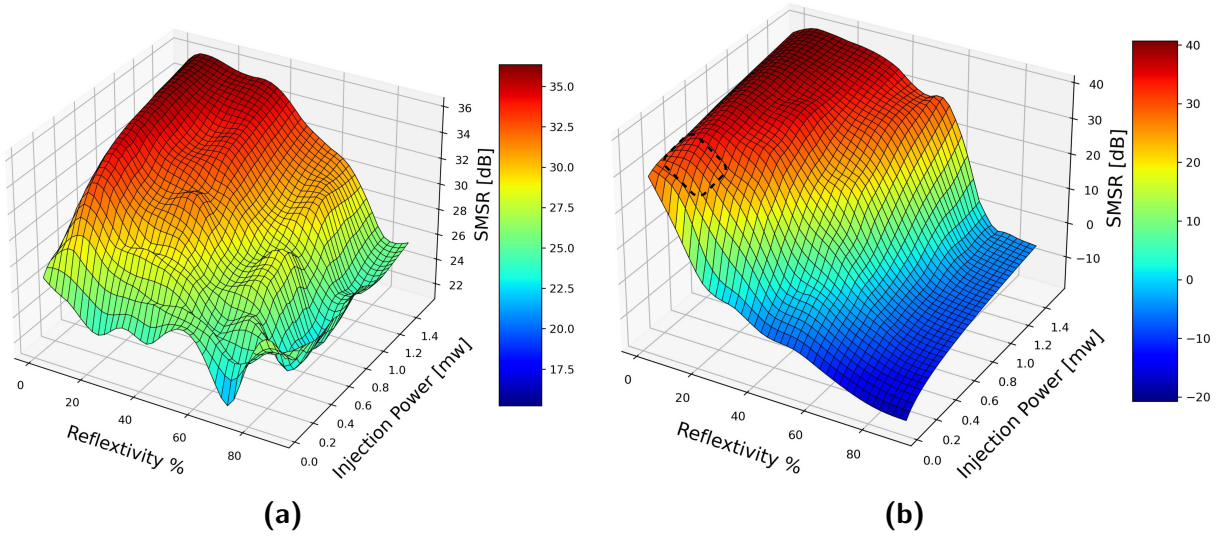

Figure 4.7. SMSR Vs. Inject Power Vs. Reflectivity. a) Central mode. b) Side Mode.

injection power (below 300 μW), only reflectivities between 1 % and 30 % are useful for the FPLD-based colorless transmitter.

Consequently, observing the Figure 4.7 that shows a three-dimensional graph: SMSR Vs. injection power Vs. reflectivity for both tuned longitudinal modes, it is possible to confirm that the side modes impose the reflectivity conditions for the front-facet of the cavity. According to that, only values within the small region represented by the dashed black square satisfy the low power requirement mentioned above: less than 300 μW.

4.3 Time-Domain Analysis

Due to the WDM-based networks operate in a spectral region further away from the optical fiber's zero of dispersion (typically the dispersion in this region is of 16 ps/nm·km), the transmission performance is negatively affected by dispersive phenomena. Consequently, since the broadband source seeding the FPLD emission wavelength is a SLED, which operates using an Amplified Spontaneous Emission (ASE) process, it is necessary to analyze the chirp that this type of source induces in the FPLD-based colorless transmitter.

The Fig. Figure 4.8 shows the chirp of the FPLD externally tuned using the ASE carrier with a 3-dB bandwidth of 12.5 GHz and an optical power of 300 μW. For these measurements, reflectivities of 85, 90 and 95 % were used for the back-facet and of 1, 10 and 30 % for the front-facet. In all cases, to better visualize the results, the average emission frequency was subtracted from the data obtained. In this way, it is possible to visualize by how much the emission frequency fluctuates with respect to its expected value. Thus, it was possible to observe that the maximum frequency fluctuations around 65 GHz in the cases with 10 % and 30 % reflectivity. Other hand, for the case of 1 % the maximum frequency fluctuations exceed 100 GHz.

Furthermore, the probability density distribution obtained from the data histogram of each reflectivity case is shown below to notice how the noise of the FPLD is distributed around the tuned longitudinal mode. The results show that frequency variations over time

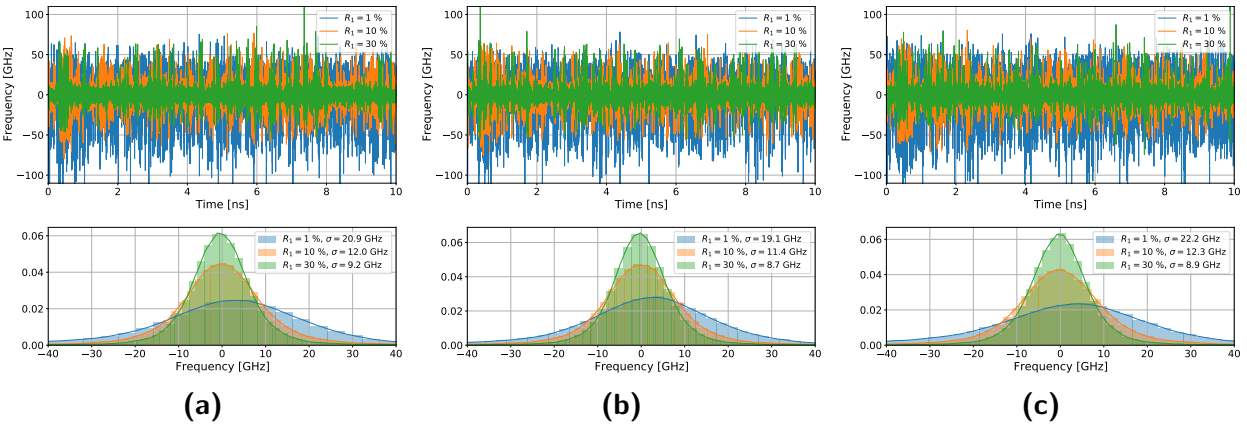

Figure 4.8. Frequency vs time. End-Facet reflectivity : a) 85 %. b) 90 %. c) 95 %.

are not significantly affected when the reflectivity of the cavity's back-facet is above of 85%. This can be observed by measuring the standard deviation of the distribution function of each case. The difference in the standard deviation of the frequency does not differ by more than 1 GHz among the 3 cases. Nevertheless, as the front-facet reflectivity change, the chirp's standard deviation considerably changes regarding its mean value, showing a behavior inversely proportional to the reflectivity. This behavior is expected, since the intensity of the feedback process in the cavity is directly proportional to the reflectivity, which improves the coherence of the laser and reduces frequency variations over time caused by the ASE noise of the own optical carrier.

According to both results, the spectral and time-domain analysis, reflectivity values of 10 % and 90 % in the front face and the end face, respectively, can be considered as the better. This choice was made taking into account that even a 1 % reflectivity presents the lowest injection power requirement (mainly when a side mode is considered), its chirp is bigger than the other cases, and due to the optical fiber's dispersion behavior the chirp will penalize the transmission performance. Furthermore, taking into account the carrier's depletion induced by the modification of photon density, the use of a 10/90 configuration allows to obtain an emission spectrum centered around of 1552.525 nm (center of the optical communications C-band) if the confinement factor is set in 0.4, i.e, the thickness of the cavity should be around 190 nm. The width of the region was set to 2.6 um so that the confinement factor and the transverse mode confinement factor are equivalent[31].

4.4 Carrier bandwidth analysis and number of available modes

We also evaluate the performance of this FPLD-based colorless transmitter for different 3-dB linewidths $\Delta\omega_{ic}$ of the optical carrier used to seed the FPLD emission wavelength: 12.5 GHz, 25 GHz and 50 GHz. The figure Figure 4.9 shows the SMSR measurements as a function of injected optical power for the different $\Delta\omega_{ic}$ values, and for two optical channels: 1552.525 nm (Central mode) and 1550.125 nm (400 GHz shifted side mode). These measurements show that the cavity performance in terms of the SMSR decreases inversely proportional as a function of the carrier bandwidth and the distance of the tuned mode from the center mode. This behavior is explained in the Fig. Figure 4.10, that shows the optical spectra

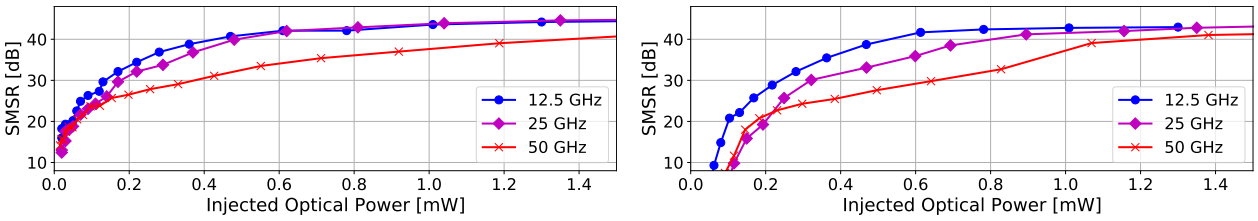

(a) Channel 1: 1552.525 nm (Central Mode) **(b)** Channel 2 1550.125 nm (Side Mode)

Figure 4.9. SMSR vs. Injected power for two different channels.

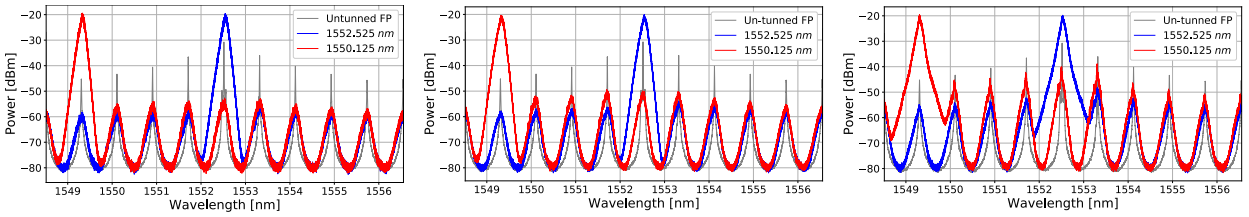

(a) $\omega_{ic} = 12.5$ GHz **(b)** $\omega_{ic} = 25$ GHz **(c)** $\omega_{ic} = 50$ GHz

Figure 4.10. FPLD 2-channel spectrum for different ω_{ic}

of the FPLD after be tuned for each $\Delta\omega_{ic}$ using an injection power of 300 μW. It can be noticed that due to the gain spectrum of the untuned FPLD (gray lines) is not uniform for all wavelengths. As the spectral width of the seeding carrier increases, the lateral modes of the tuned mode begin to receive a greater optical power, so they will be amplified by the cavity according to the gain of the material (which is a frequency-dependent function). This behavior is mainly observed when is used a wide spectral width optical carrier ($\omega_{ic} = 50$ GHz), to tune a longitudinal mode away from the central mode of the FPLD, such as the case of channel 1550.125 nm (red line). In this case, optical carrier 3-dB bandwidth exceeds in more than 30 GHz the 3-dB bandwidth of the longitudinal mode, which is around of 18 GHz (measured with a 0.05 nm OSA). Since for the spectral region where the center mode is located, the gain is the highest, for a low injection powers the longitudinal modes around the gain peak could be amplified if the spontaneous emission is higher than the effective injected power, increasing its optical power and decreasing the SMSR.

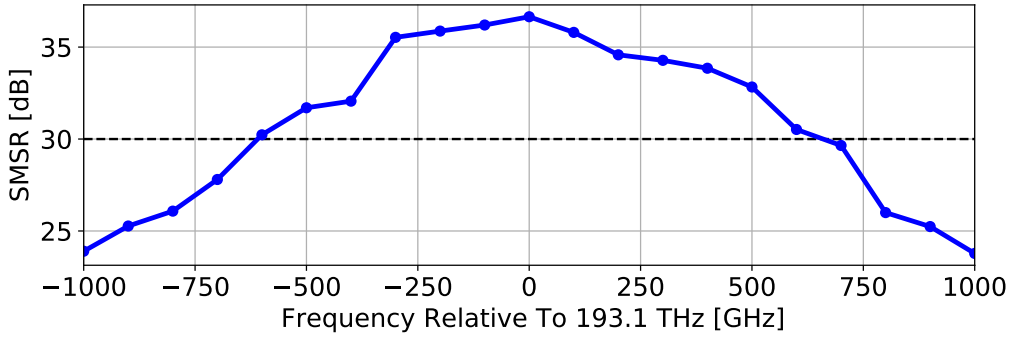

Figure 4.11. SMSR vs Spectrum shift with respect to 193.1 THz (1552.525 nm) using a seeding carrier with 300 um optical power and 25 GHz 3 dB bandwidth.

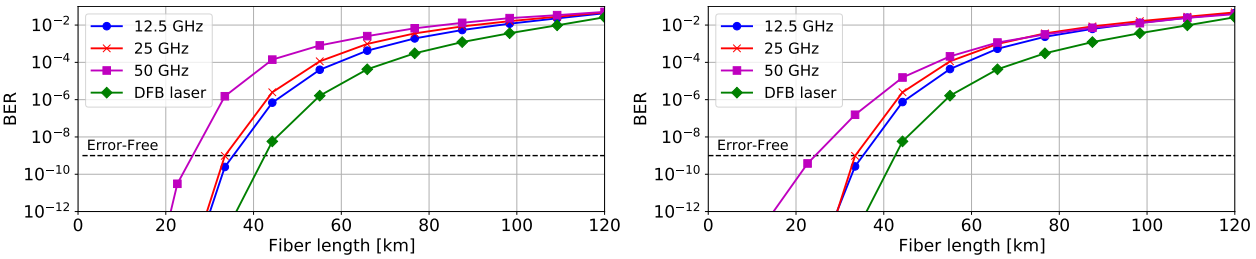

(a) 1552.525 nm (Central mode). **(b)** 1550.125 nm (Side mode)

Figure 4.12. BER vs length for seeding carriers with different 3-dB bandwidths.

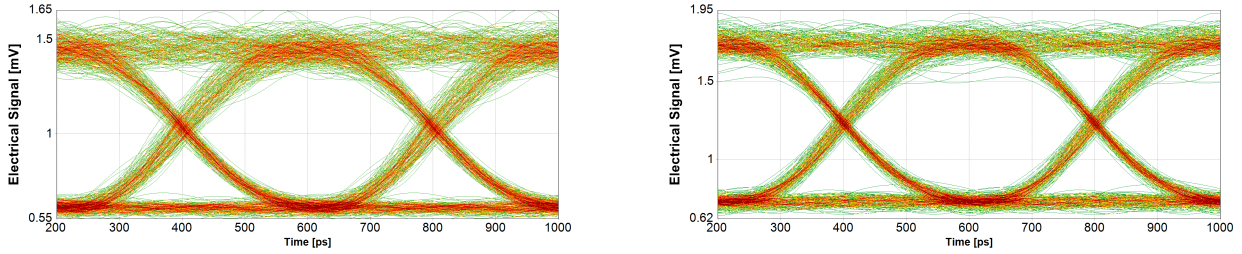

(a) 1552.525 nm (Central mode). **(b)** 1550.125 nm (Side mode)

Figure 4.13. Eye diagram for 20 km transmission length.

Finally, to know the number of modes available in this FPLD configuration, the same scenario shown in Figure Figure 3.2 was used: a FPLD biased with a current of 60 mA, and optical seeding carrier with 300 μW power and 3-dB bandwidth of 25 GHz. Then, using an OBPF, the frequency of the seeding carrier was shifted with respect to the central mode (193.1 THz) using 100 GHz steps (the channel spacing considered in this system). Thus, as shown in Figure Figure 4.11, 13 longitudinal modes can be tuned using a seeding carrier with an optical power of 300 μw, which is sufficient to fulfil standard recommended optical carrier numbers for WDM-PON systems.

4.5 Transmission performance

This section shows the transmission performances of the designed colorless transmitter based on a FPLD. In this performance analysis, the bias current was set in 60 mA according to the reflectivity analysis showed in the section 4.2. Additionally, to compare the performance with one of the best transmission scenarios, an external modulated Distributed FeedBack (DFB) laser using the same power, 3-dB bandwidth conditions and bias current conditions was deployed in the same WDM-PON system.

The figure Figure 4.12 shows the transmission performance of the FPLD-based colorless transmitter in terms of the BER as a function of the transmission distance, and the figure Figure 4.13 shows eye diagrams where the bandwidth of the seeding carrier is 12.5 GHz, which is the best case for transmission. As expected, the transmission performance shows better results when the FPLD-based transmitter colorless is externally tuned by a narrow bandwidth optical carrier. However, for bandwidths below 25 GHz, the transmission perfor-

mance in terms of the BER does not differ significantly. Additionally, the channel associated to the central mode (1552.525 nm) presents a slightly better performance regarding channel associated to the side mode (1550.125 nm): less than 1 km of distance difference considering the BER threshold for an error-free transmission (10^{-9}). Even so, in eye-patterns shown in the figure Figure 4.13 it can be seen that for 20 km transmissions, the extinction ratios for 1550.125 nm (side mode) and 1552.525 nm (central mode) are 3.73 and 3.78 dB, respectively, which allows to differentiate the symbols of the NRZ modulation without error (BER 10^{-20}).

These results are in accordance with the analysis performed in section 4.4, where the power spectrum and the SMSR for the cases with a 12.5 GHz and 25 GHz seeding carrier are almost equal for both longitudinal modes. However, for the case of the 3-dB bandwidth of 50 GHz, the SMSR is penalized due to the lack of power in the spectral region where resonant cavity allow photon's emission (see the explanation of the formation of longitudinal modes in the chapter 3). Thus, since the same optical power is distributed over a wider spectral region, the power remaining in the same region of the spectrum where the longitudinal mode can exist is less than the total power of the seeding carrier. Therefore, this optical power is not enough to extinguish the side longitudinal modes and maintaining a SMSR of 30 dB. This not only penalizes the overall performance of the network due to the interchannel interference is increasing, but part of the modulated information remains at frequencies different from the tuned mode, and when they are filtered at the remote node by the MUX/DEMUX, it will affect the waveform of the information signal, decreasing the performances in terms of the BER.

Moreover, for the comparative scenario, considering the BER threshold for error-free transmission and an ω_{ic} of 12.5 GHz, the transmission distance penalty of the FPLD-based colorless transmitter regarding the external modulated DFB laser was 7.2 km and 7.8 km for 1552,525 nm and 1550,125 nm, respectively. However, although the transmission distance penalty presents considerable values, the cost of implementing direct modulation on a FPLD is much lower than an externally modulated DFB laser, which makes this device a suitable option for a low-cost WDM-PON system, with at least 9 carriers with different emission wavelengths.

4.6 Performance comparison — Comercial available FPLD

To compare the performance of the designed colorless transmitter and a FPLD such the normally available in the market in terms of the SMSR, the injection power requirement and the seeding carrier's bandwidth, in this section is proposed the same simulation scenario described in the section 2.1.2 (see Figure 4.14). Here, a 30 nm SLED with 2mW output power is amplified by a 22 dB gain EDFA and transmitted without modulate over a 20 km SSMF. Then, using a Tunable OBPF, a narrowband optical carrier is obtained and injected in a FPLD. Finally, for controlling the injection power, a Variable Optical Attenuator (VOA) is proposed. Additionally, to analyze the seeding carrier bandwidth impact over the injection power requirement to achieve 30 dB SMSR, an optical carrier with 3-dB bandwidth of 12.5, 25 and 50 GHz was used.

To simulate the FPLD, it is proposed the same photonic TLM described in the section 2.2.1 that is implemented by the software VPI photonics Design Suite©. However, in this

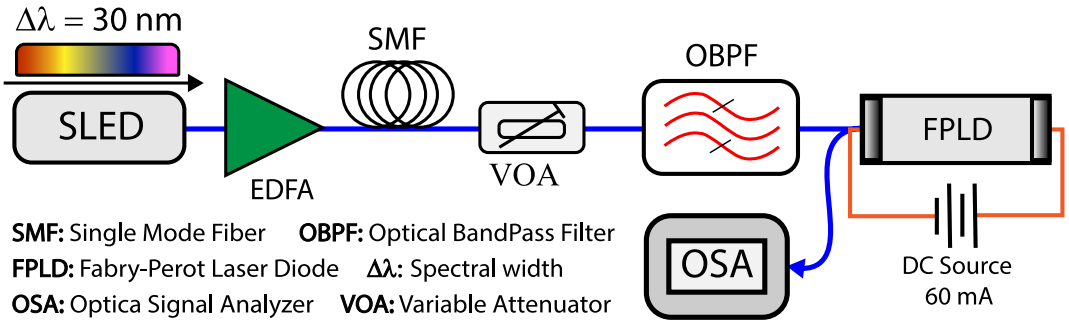

Figure 4.14. Simulation scenario proposed to analyze the market available FPLD.

case, the cavity's length, the cavity's volume, longitudinal modes spacing, and the end facets reflectivity need to be customized.

Consequently, to calculate the cavity length, we can use as reference the FPLD shown in 4.1b: A Fabry-Perot laser fabricated with $In_xGa_{1-x}As_yP_{1-y}$ lattice matched to InP, and with a longitudinal mode spacing of 1.4 nm. Thus, assuming the same fraction of x and y regarding the designed colorless transmitter (y=0.9 and x/y = 0.45), and therefore a group index n_g of 3.7 for a central emission wavelength λ of 1552 nm, it is possible to use the equation 2.5 to determine that the cavity length should be 236.66 μm length. Finally, in the case of a low-cost semiconductor laser such as the FPLD, external mirrors are not required as the two cleaved laser facets act as mirrors, which is enough to feedback the active medium and operate the laser regime. Therefore, the end facets reflectivity for this commercial available FPLD can be calculated as $R = \left(\frac{n-1}{n+1}\right)^2$ [15]. Where n is the refractive index of the gain medium, typically 3.6 for this arsenide fraction, resulting in end-facets reflectivity of 32 %. Furthermore, if we consider that only the fundamental modes propagate, both transverse and longitudinal, according to the equations 2.11 and 2.16, the thickness and width of the active region should be around 200 nm and 2.6 nm, respectively, resulting in a confinement factor of 0.3. Finally, for simulating the gain profile of the spontaneous emission, it is considered a parabolic shape with a 3-dB bandwidth around 100 nm (Similar to InGaAsP with hole concentration around 1×10^{18} [31])

The 4.15a shows the power characterization for the simulated commercial available FPLD. On the left side is shown the output optical power as a function of the bias current. In this case, it is possible to observe a typical curve of Bias Current vs Optical Output Power for a FPLD, which usually presents a threshold current around 12 mA[2]. Other way, the Figure 4.15b shows the power spectrum measurement for different values of the bias current, obtained from an OSA setting to have optical resolution of 0.05 nm. As expected, the shape of the spectrum is slightly different from that shown in Figure 4.1b. This is because the real devices do not present a gain profile with a perfectly defined shape (like a parabolic profile). However, the spacing between longitudinal modes and the dependency of the output power and the optical gain regarding the bias current fit the real devices quite well.

Furthermore, the Figure 4.16 show SMSR as a function of the power of the seeding optical carrier for different 3-dB bandwidths: 12.5, 25 and 50 GHz. Here, it is possible to observe that the performance of the laser source, in terms of SMSR and the injection power requirement is strongly dependent on the bandwidth of the seeding carrier; if the carrier 3-dB

[2]Data sheets for a 1550 nm Fabry-Parot Laser are available in: https://www.rpmclasers.com/product

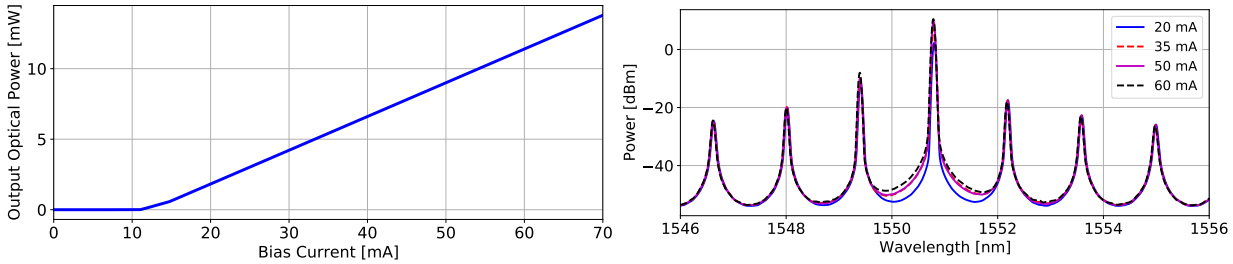

(a) Bias Current vs Optical Output Power **(b)** Power spectrum for different bias current.

Figure 4.15. Simulation of a Market available FPLD. Power Characterization.

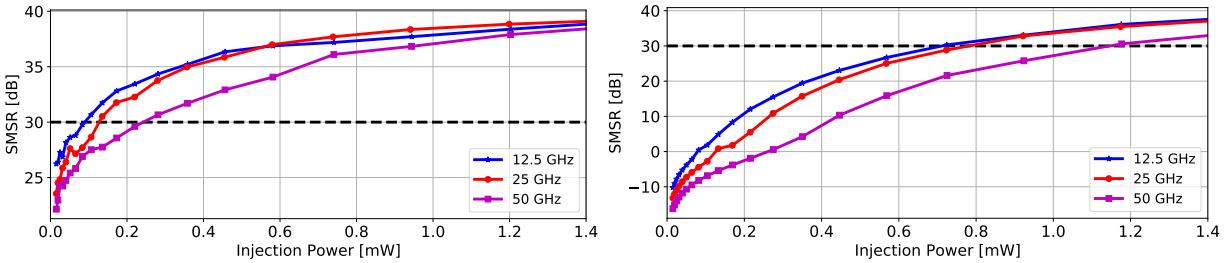

(a) Central Mode **(b)** 700 GHz Shifted Mode

Figure 4.16. SMSR vs. Injection Power for a commercial available FPLD. 1.4 nm spacing for longitudinal modes and 32% for both en facets.

bandwidth is larger than 3-dB bandwidth of the target longitudinal mode around 17 GHz in this case, SMSR is penalized due to decreasing in the effective injection power (see section 4.4). As expected for a reflectivity of 32%, the injection power required to achieve a 30 dB SMSR is higher than 600 μW for a longitudinal mode shifted 4 modes with respect to the central mode, i.e., around 700 GHz shifted. Moreover, we can expect that the bandwidth of a single longitudinal mode increases proportionally to the spacing between longitudinal modes (see equation 2.7. However, due to the cavity length is shorter in this case, the total loss decreases with respect to the designed colorless transmitter, so the *finesse* value is increased and the linewidth for a single mode remains a similar value (only 1 GHz difference).

In comparison with the designed colorless transmitter, in all cases, the commercial FPLD presents a higher power requirement. This behavior can be explained taking into the material gain bandwidth, that it is the same for both cases. Thus, because the fourth mode with respect to the central one is moving away from the commercial FPLD case, and the material gain decreases following a parabolic shape, it is necessary to use a higher injection power to compensate the low gain of the cavity in this region. Thus, since the fourth mode with relation to the central one is farther away for the commercial FPLD than for the colorless transmitter, and the gain of the material decreases following a parabolic shape, it is necessary to use a higher injection power to compensate for the low gain of the cavity in this region. Therefore, a commercially available Fabry-Perot laser is not a suitable option to deploy a colorless network, not only because the mode spacing does not conform to WDM network standards, but also because the power requirements are very high: in the best case, it is about 40 percent of the average power allowed to transmit information.

On the other hand, The Figure 4.17 shows the chirp and its distribution function for a

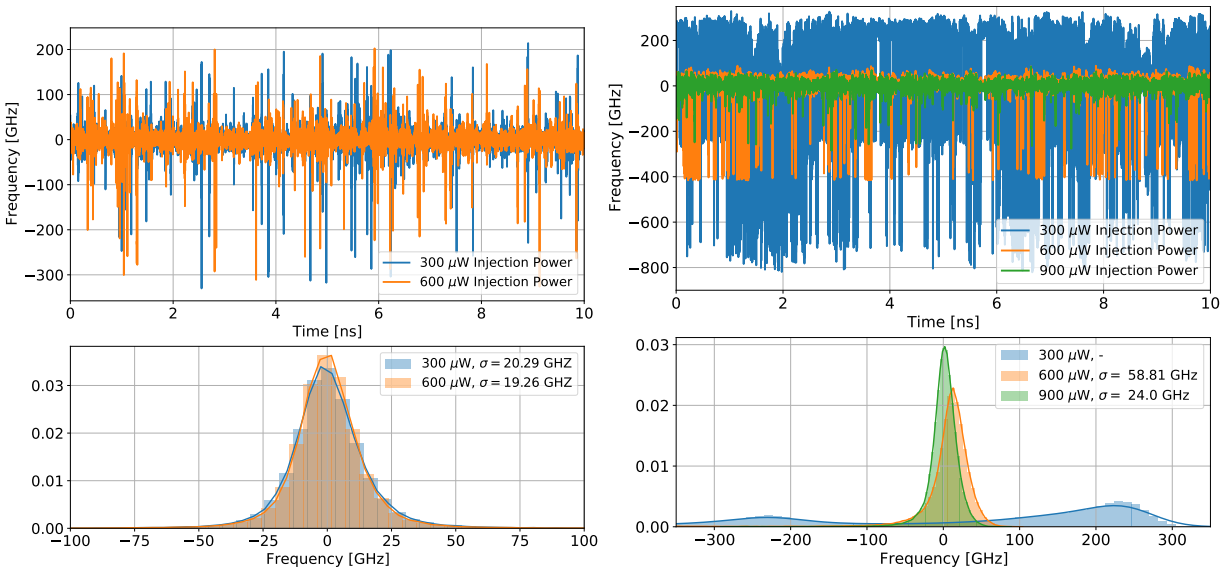

(a) central Mode **(b)** Side Mode

Figure 4.17. Chirp of an external seeding FPLD using optical carrier with different powers. Relative to the tuned mode emission frequency

FPLD seeded by external ASE-carriers. This frequency variations over time were analyzed for carriers with different power values between 300 μW and 900 μW. In general, it was found that the standard deviation of the frequency is around 20 GHz for the central mode (where 200 μW is enough to reach 30 dB SMSR) as shown in figure 4.17a, while the lateral mode is above 24 GHz as is showed in the Figure 4.17b.

The behavior of the chirp for the side mode can be explained observing the Figure 4.18, that shows the power spectra for the external seeding FPLD in two different longitudinal modes, and several injection powers. In this case, it can be noted that for an injection power of 300 μW the SMSR is low: around 12 dB, therefore the frequency variations of the longitudinal modes around the central mode have a significant on the total laser power, so the frequency variations are not only around the tuned mode, are distributed in those modes. Due to that, the instantaneous frequency presents outliers around the emission frequency of the tuned longitudinal mode, and the smaller the SMSR the larger the frequency outliers, and

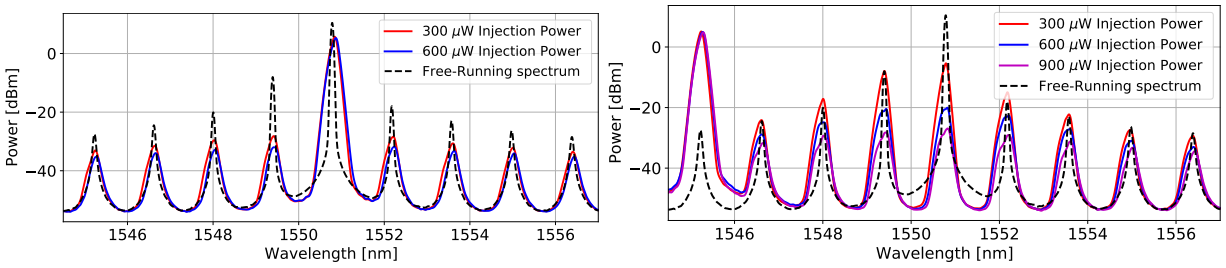

(a) Central Mode **(b)** 700 GHz Side Mode

Figure 4.18. Power spectrum of an external seeding FPLD using optical carrier with different powers

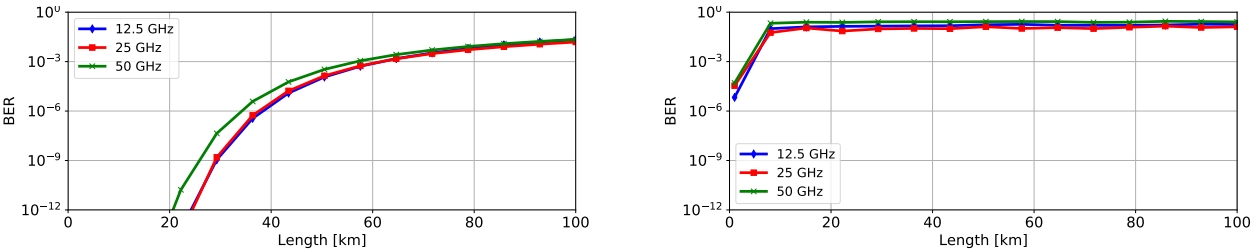

(a) Central mode **(b)** 700 GHz Side Mode

Figure 4.19. BER vs length for seeding carriers with different 3-dB bandwidths.

therefore the larger the standard deviation of the frequency (see figure 4.17b). However, if the seeding carrier power is sufficient to reach 30 dB SMSR, these outliers tend to disappear, resulting in a frequency distribution with a normal appearance, centered on the emission frequency of the tuned mode and with a standard deviation below 24 GHz (comparable to a longitudinal mode bandwidth).

Additionally, the standard deviation of the chirp for a FPLD with a reflectivity of 32 % on both sides of the cavity, is generally higher than for the designed colorless transmitter (10/90 configuration). This is because the reflectivity of the back-facet of the commercial FPLD is relatively small compared to that of the colorless transmitter, which decreases the intensity of the feedback in the cavity and negatively affects the ratio between stimulated emission and spontaneous emission (loss of coherence).

Finally, for the transmission test, we considered an injection power of 300 μW, in order to compare the transmission performance in the same power conditions with respect to the case of the designed colorless transmitter. Thus, the Figure 4.19 shows the transmission performance results in terms of the BER as function of the transmission distance, for a commercial FPLD seeded using ASE optical carriers with different 3-dB bandwidth: 12.5, 25 and 50 GHz. In this case, 2 optical channels were also considered, the channel corresponding to the central mode, and the channel shifted 4 modes away from the central one (700 GHz shifted in this case).The results show that, for the central mode, it was possible to achieve error-free transmission for distances greater than 20 km, even for the 50 GHz seeding carrier. This behavior is expected because the injection power required to achieve a 30 dB SMSR is less than 300 μW in the case of the central mode. Therefore, for the central mode it is possible to consider that a transmission is performed using a narrowband carrier whose performance is less affected by phenomena as the fiber dispersion, mode hopping and loss of information when filtering the carrier at the remote node.

On the other hand, according to the 4.18b, 300 μW of power is not enough to achieve 30 dB SMSR in the case of the lateral mode. Because of this, for the channel corresponding to the side mode shifted 700 GHz with respect to the center mode, a transmission with a single carrier source cannot be considered. Since the information travels in multiple wavelengths over the fiber, dispersive phenomena, mode hopping and channel interference will deteriorate the transmission performance, causing that an error-free transmission is not possible in any case above 20 km.

Chapter 5

Proposal of a Pulsed laser as a seeding source for colorless WDM-PON systems based on external wavelength seeding

In this chapter, we present the design and the experimental implementation of ultrashort pulsed laser based on optical fiber and nanomaterials as a viable option for obtaining broad optical sources usable as seeding sources in colorless network. Thus, we show the design and implementation of a pulsed source using fiber optics and graphene, including optical, frequency and spectral stability characterization. We also show a simulation interface based on VPI software, which uses the experimental data of the source spectrum to generate a multi-wavelength source with applications in WDM systems. Consequently, this multi-carrier source can be used to seed a wavelength in a colorless transmitter based on an FPLD, or it can be used in a colorless system that performs wavelength carrier reuse.

5.1 Motivation and context

Wavelength-Division-Multiplexing (WDM) techniques over Passive-Optical-Networks (PON) is an advanced access network technology that provides a scalable and secure point-to-point wavelength link with highly valued conditions to handle the continuous growth in bandwidth demand and 5G fronthaul deployment. [20]. However, the application of WDM techniques over PON has been under discussion for several years due to its high implementation cost, mainly due to the lack of low cost optical sources and the use of fixed wavelength assignment for optical transmitters at the user side (which increases inventory and deployment costs) [60]. To overcome these problems, the use of colorless transmitters, which act as tunable wavelength lasers controlled by an external mechanism generally located at the Central Office, has been proposed. Most of the low cost colorless approaches are usually based on an Amplified Spontaneous Emission (ASE) BroadBand optical Sources (BBS) that are spectrally sliced to obtain narrow-band optical carriers [18, 24, 27, 29, 61]. However, being colorless transmitters a feasible solution for low-cost access networks, the spectral optimization is an issue to be further explored. Thus, a useful approach among the spectrum BBS-based

colorless techniques is to use the same optical carrier for DownStream (DS) and UpStream (US), in a communication scheme known as carrier re-use or carrier re-modulation [18, 24]. Nevertheless, this approach involves the use of an ASE source as optical transmitters in the DS link, whose performance is penalized due to the low-coherence of ASE-sources [27].

On the other hand, other well-known optical comb generation techniques, such as those based on Mach-Zenhder modulators, guarantee a better coherence regarding the spectrum slicing ASE source. However, these techniques do not generate optical carriers in a range greater than 12 nm, and usually require a cascade or loop configuration to achieve this spectral width, which implies an increase in the complexity and cost of the transmitter device [62, 63]. Thus, to improve the performance of optical communications based on spectrum sliced BBS, the implementation of comb generators such as Ultra-Short Pulse Lasers (USPL) based on passive mode-locking techniques has been considered, mainly due to their high spectral stability, wide spectrum and high coherence [64–66].

Some of the most popular approaches for passive mode-locking techniques for generating ultra-short pulses in a laser-cavity are the Non-linear Polarization Rotation (NPR) and the Semiconductor Saturable Absorbing Mirrors (SESAM). However, the Saturable Absorbers (SA) based on 2D nanomaterials in conjunction with fiber-based lasers, have been considered a promising solution for applications in optical communications systems, not only because they make possible to build lower-cost optical sources with a high compatibility in fiber-based optical systems, but also allow to improve the mode-locking instabilities caused by the NPR, or to avoid fixed both wavelength and pulse repetition rate as in the SESAM case. Hence, in terms of the nano-material choice for SA design, the characteristics of graphene, such as fast recovery time, high modulation depth, low fluence and wide absorption spectrum, make this material a suitable choice [67, 68]. Besides, the fabrication process of a graphene-based saturable absorber is relatively simple, and does not require special care as black phosphorus, which can easily become oxidized [69, 70].

5.2 Ultra-short Pulsed Laser design and experimental characterization

In this section we show the experimental setup used to generate ultra-short pulses in the spectral region around 1558.6 nm, a performance characterization of the proposed graphene-based SA, and an analysis of the spectral behavior of the USPL.

5.2.1 USPL experimental setup

The experimental setup proposed for the USPL is shown in the Fig Figure 5.1. This configuration make it possible to generate ultra-short pulses by introducing a graphene-based SA and Polarization Controller (PC) into an Erbium-Doped Fiber Laser (EDFL) cavity. This laser has a ring-shaped cavity with 33.82 fs/nm of accumulated dispersion, and a total length of 4.86 m (including PC's fiber length). It consists of: a 980 nm pump laser diode with an output optical power of 80 mW, a 980/1550 nm WDM device in co-propagating configuration, an erbium-doped fiber with a length of 1 m and an absorption coefficient of -33.8 dB/m as the gain medium, an optical isolator with 30 dB isolation, and an optical coupler 70/30, 70 % to the feedback process and the remainder 30 % at the laser output.

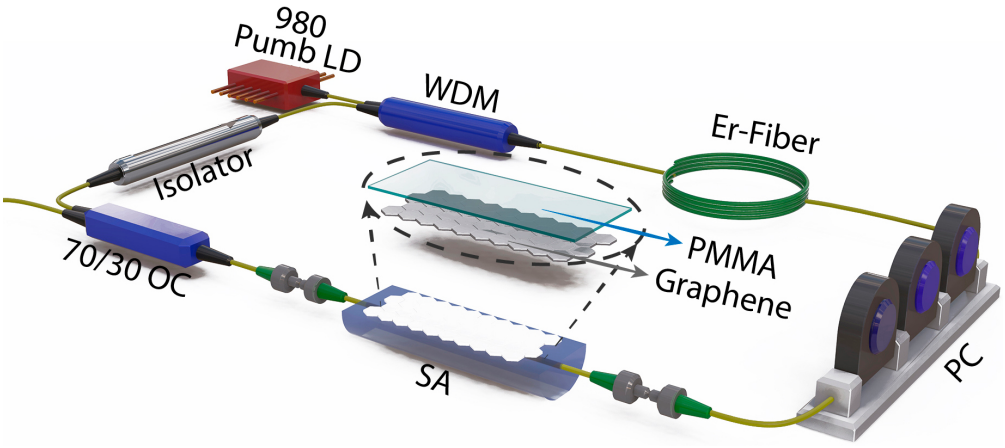

Figure 5.1. USPL Experimental setup.

The average optical power of this source, working in pulsed regimen, was around of 2 mW [71].

On the other hand, the proposed SA consists of a 13 mm mono-layer graphene length fabricated by Chemical Vapor Deposition (CVD) process, deposited on the surface of a single mode fiber (SMF) side-polished (D-shaped fiber-See Fig Figure 5.2a) approximately to 1 μm regarding the fiber core. The monolayer graphene was transferred from cooper to a D-shaped optical fiber via wet transfer, using a PMMA layer of 300 nm thickness. Fig Figure 5.2a and Fig Figure 5.2b show front and top view images of D-shaped fiber with graphene deposited, taken by an optical microscope using 20X objective lens. This configuration allows to obtain SAs with relative extinction ratios up to 98%. The high value of the extinction rate contribute to the generation of ultra-short pulse [72].

For analyzing the deposited graphene quality along the fiber surface area, Raman spectroscopy was proposed. In the Fig Figure 5.2c, it is shown the Raman spectrum in a point of the transferred monolayer graphene, shown as a red square in the Fig Figure 5.2b. Thus, we performed a Raman mapping of the IG/I2D intensity ratio between the G and 2D bands from a 20 μm × 20 μm coverage area on the polished side of the D-shaped optical fiber. In this mapping, 95% of monolayer graphene is observed on image analysis. This percentage is identified in Fig. Figure 5.2d by blue color, where the intensity ratio is $0.25 < \text{IG/I2D} \leq 0.5$. The other areas are composed by bilayer (yellow color) and multilayer graphene (red to brown tones), which is typical of the CVD graphene growth process [72–78]. Additionally, the Raman spectrum of monolayer graphene onto D shaped optical fiber shows the –D peak. This peak indicates that there is a disorder in the graphene structure caused by the sp_2 to sp_3 local transmutation of the graphene carbon atoms, due to the interaction between the functional groups of the PMMA structure and the graphene lattice [74–78]. In addition, in the graphene process growth CVD there are some regions polycrystalline, these regions generate defects in the graphene crystal structure. Hence, to measure the level of defects on graphene, a Raman mapping of the ID/IG Intensity ratio between D and G bands in an area of 25 × 25μm was performed. The Fig Figure 5.2e shows that 80 % of monolayer Graphene has a low level of defects, which can be identified by blue color in the mapping, where the intensity ratio is $0.1 \leq \text{ID/IG} \leq 0.3$ [74–78]. The low level of defects in graphene is very important because the mobility and optical absorption is highly dependent on defects of the

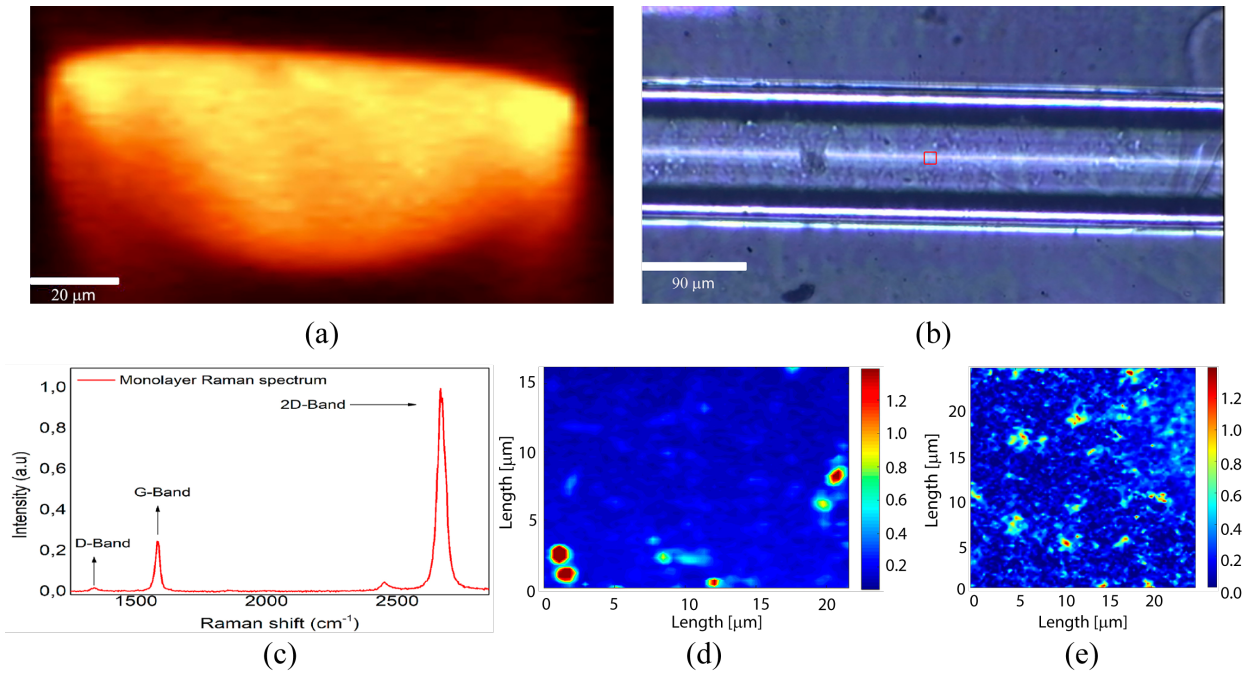

Figure 5.2. SA Optical characterization. a) D-Shaped Fiber Front View. b) D-Shaped Fiber top view. c) Raman spectrum in a point of the monolayer. d)Raman mapping of the IG/I2D intensity ratio transferred graphene. e) Raman mapping of the ID/ IG intensity ratio in a 25 x 25 μm in the transferred graphene.

crystalline structure. In our case, due to monolayer graphene has low defects, there is an increase in the number of electronic transitions at low intensities which consequently occupies a greater number of electronic states in the material and facilitates the Pauli blocking effect [79]. Therefore, the graphene becomes more efficient as a SA in the ultrashort pulse generation.

5.2.2 Spectral Characterization

This subsection shows the experimental measurements of the USPL necessaries to deploy the simulation interface and analyze the multi-wavelength source performance in a WDM-PON system. The time-domain measurement was carried out with a 10 GHz photo-diode connected to a 4-GHz sampling oscilloscope, and the spectral measures were made with an optical spectrum analyzer (OSA) of 0.05 nm resolution using a 99/1 beam splitter.

The Fig. Figure 5.3a shows the EDFL spectrum before to introduce the SA, and as it is expected for a laser working in a Continuous Wave (CW) regime, the EDFL present a relatively narrow Full Width at Half Maximum (FWHM) of 0.22 nm. Thus, as shown in Fig. Figure 5.3b, when the EDFL is connected to a PIN photo-diode, it presents a time-constant response which ensures that without SA, the EDFL works in CW regime.

Now, the optical power spectrum after introducing the SA in the EDFL cavity is shown in the Fig Figure 5.4a. In this case, we selected a polarization state that allows the formation of only one pulse per round in the EDFL ring-cavity. As expected, and according to the Fourier transform analysis, when the laser works in the pulsed regime its spectrum is broadened, obtaining a 3-dB bandwidth (or Full Width at Half Maximum — FWHM) up to 21.8 nm

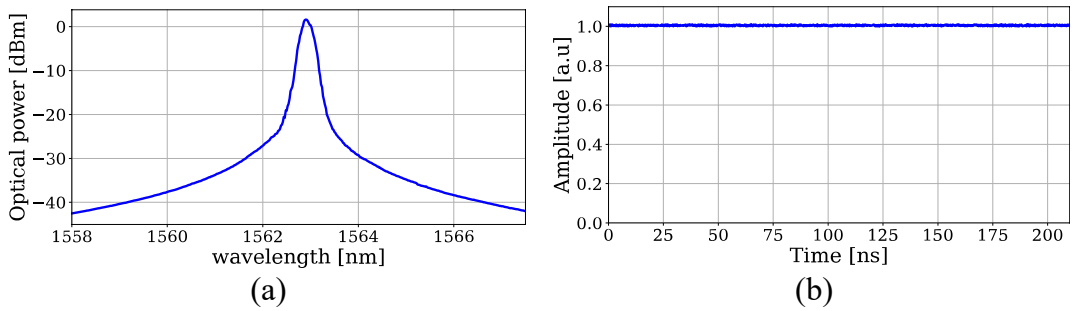

Figure 5.3. EDFL characterization. a) Optical Power spectrum, FWHM = 0.22 nm. b) Temporal waveform.

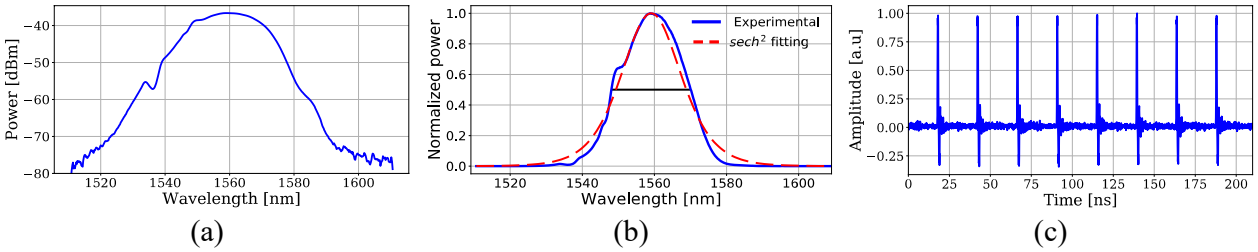

Figure 5.4. USPL characterization. (a) Power spectrum (best case), $\lambda_c = 1558.8$ nm. b) Linear-scale normalized spectrum, FWHM = 21.8 nm. c) USPL Temporal waveform $f =$ 41.18 MHz.

for an optimum polarization state. It is necessary to emphasize that in comparison with previous implementations, this configuration allows to obtain an ultra-short pulsed laser with 3-dB bandwidth at least 11 nm larger [72]. Subsequently, in the Fig Figure 5.4b is showed the same power spectrum in linear-scale (blue line) together with a $sech^2$ fitting function (red line) according to soliton formed in the cavity. The results show a Pearson correlation coefficient r of 99.32 % and a mean square error (MSE) of 0.1986 % with respect to the ideal fitting function. This characterization allows calculating an approximation of the pulse duration time by using the time-bandwidth product limit for a $sech^2$ pulse-shape: $\Delta t \Delta \nu \leq 0.315$. Hence, we obtain that an estimation of the pulse duration time for the case in which the 3-dB linewidth was 21.8 nm, is $\Delta t = 117$ fs. Finally, in the Fig. Figure 5.4c is shown a temporal measure for the USPL after the 10-GHz PIN photo diode detection. In this figure is evidenced the pulsed performance of the optical source, obtaining a fundamental Pulse Repetition Rate (only one pulse per round) $f =$ of 41.18 MHz, according to expect round-trip time for a cavity with 4.86 m length.

5.2.3 Stability analysis

The spectral stability over the time, in terms of transmitted power, wavelength and 3-dB bandwidth, is a fundamental requirement to be fulfilled in WDM-PON systems because of the following: (1) if the power fluctuations are very high, the power of the transmitted signal may be insufficient to reach the minimum receiver sensitivity to achieve a target BER (such as 10^{-9}). (2) If the emitted frequency fluctuates in a value comparable to the channel spacing, it can result in carrier hopping. This carrier hopping decreases the transmission performance

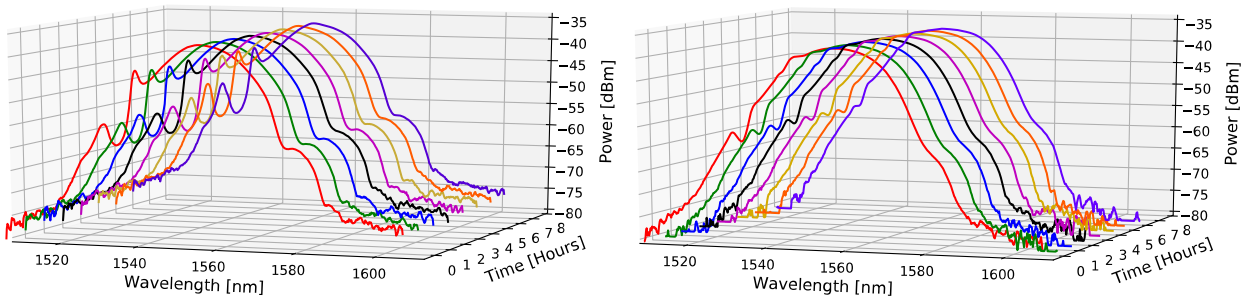

Figure 5.5. Spectral stability measures. a) Polarization state 1. b) Polarization state 2.

due to optical crosstalk. (3) The 3-dB bandwidth controls the number of optical carriers available in the WDM system, which need to be a well-defined number. If the number of carriers is reduced by these bandwidth fluctuations, the total system capacity will decrease as well.

Table 1: Statistical measurements of the USPL's spectrum using 2 different polarization states

	P_{peak} $[\mu W]$	FWHM [nm]	λ_{peak} [nm]	$\overline{r}$
μ	24.52	15.9	1557.7	0.9996
σ	0.46	0.25	0.2	0.0002
σ*	0.49	0.28	0.25	NA

(a) Polarization state 1

	P_{peak} $[\mu W]$	FWHM [nm]	λ_{peak} [nm]	$\overline{r}$
μ	22	21.6	1558.6	0.9988
σ	0.35	0.14	0.31	0.0007
σ*	0.42	0.33	0.42	NA

(b) Polarization state 2

Fig Figure 5.5a and Fig. Figure 5.5b shows a 3D representation of the power spectrum measurements of the USPL taken at one-hour time intervals for 2 different polarization states. In order to measure the spectrum variations over the time, three parameters: peak power P_{Peak}, FWHM, and peak wavelength λ_{peak} were measured and statistically analyzed. The Table 5.1a and the Table 5.1b show the mean μ, standard deviation regarding the mean value σ, and the standard deviation regarding the first spectral measure σ^*. Additionally, in order to compare the mean spectrum shape regarding the initial spectrum, the Pearson correlation coefficient r was calculated. In both cases, the variations with respect to an average spectrum and to the initial measurement were at least 50 times smaller than the mean value of the peak power. In the case of Pearson correlation, the mean Pearson coefficient $\overline{r}$ for polarization states was approximately 1, with a p-value of 0. These results show that the peak power, the FWHM, λ_{peak}, and spectrum shape were considerably stable even for different states of polarization.

5.3 Transmission performance analysis

To analyze the behavior of the USPL as a multi-wavelength source in a WDM-PON system, it is necessary to define several fundamental factors according to this type of optical network: (1) channel spacing, (2) transmission distance, (3) transmission rate, (4) optical carrier power, and (5) the optical carrier bandwidth.

According to the standard ITU-T G.989.2 (NG2 — PON), which regulates WDM-based passive optical networks (PON), these WDM-PON networks are expected to have lengths between 20 and 40 km, symmetrical channels with bit rates up to 10 Gbps per lambda (between 4 and 8 wavelengths depending on the duplexing technique), and a channel spacing equal to a multiple of 6.25 GHz [6]. Then, the power of the optical carrier must be sufficient to achieve a minimum sensitivity value in the optical receivers, and the bandwidth of the transmitted signal should be adequate to not generate interchannel interference. Thereby, to get an idea of power requirements in real scenarios, we follow the ITU-T G.989.2 recommendation. We considered the minimum transmission power: 0 dBm, which is proposed for an optical distribution network class N1 (Maximum optical loss below 29 dB). On the other hand, the condition of the optical carrier bandwidth can be guaranteed due to the optical comb behavior of the pulsed laser spectrum, in which the resulting optical combs do not overlap between them (regardless of spacing). However, for a direct modulation, a rate of 10 Gbps Nyquist pulses are needed to be considered with channel spacing of 12.5 GHz, otherwise the bandwidth of the modulated signal will exceed the channel spacing generating interchannel interference.

Due to the USPL presents a time-domain periodic waveform, its spectrum presents a comb-shape with comb-lines separated from each other an amount equal to its repetition rate (according to the Fourier analysis) [80]. Therefore, in order to have a CW carrier suitable to be externally modulated in an On-Off Keying (OOK) format, it is necessary to guarantee only one comb-line per channel, and for this the USPL repetition rate must be tuned to match a channel spacing value according to ITU-T G.694.1. Experimentally, it is possible to tune the pulsed laser's repetition rate in the order of GHz using an external mechanism such as a phase modulator. For example, configuration hybrid mode-locked erbium fiber laser with a 40 GHz phase modulator and graphene on D-shaped optical as SA was reported [81]. However, since the pulse width does not change substantially when an external modulator is introduced into the laser's cavity (even for different modulation rates) [82], in our simulation interface this pulse repetition rate control system consists of repeating the optical pulse, obtained from the experimental data, with a frequency equal to the channel spacing.

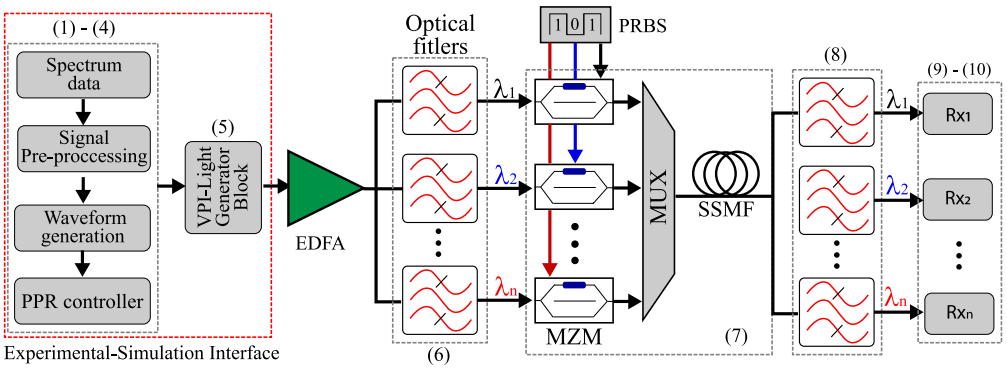

Figure 5.6. WDM-PON simulation setup.

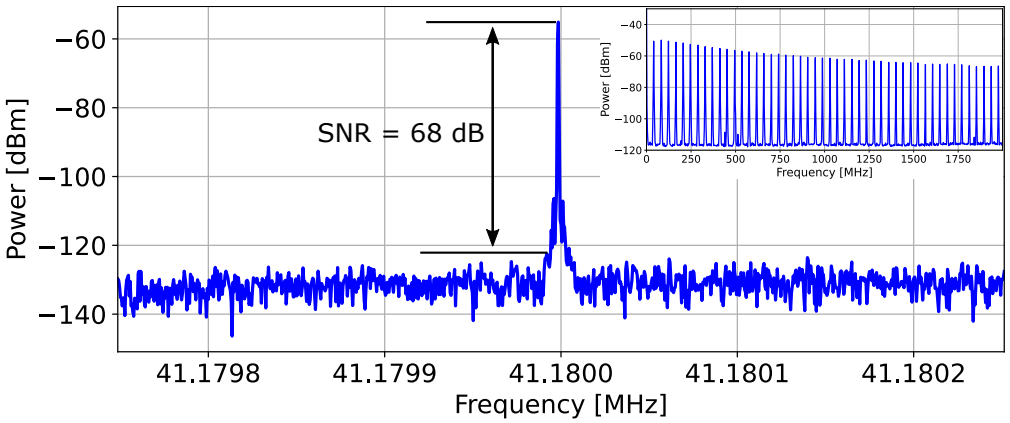

Figure 5.7. RF spectrum for the USPL using polarization state that allows an optical 3-dB bandwidth of 21.6 nm.

5.3.1 Simulation setup

Fig. Figure 5.6 shows the simulation setup proposed to implement the multi-wavelength source based on the experimental measurements of the pulsed laser spectrum, and numerically analyze its performance in a WDM-PON system. Each step of this simulation process is described as follows: (1-2) Pre-processing of the experimental optical spectrum, including normalization and up-sampling the power spectrum, which allows control of the laser power scale and the spectral resolution, respectively. The mean optical power was tuned to 2 mw (see section 5.2.1) and the up-sampling was performed to analyze the optical spectra in comb form, even for a repetition rate of the order of MHz (about 6×10^5 samples for an 80 nm window). (3) Application of the inverse Fourier transform over the pre-processed spectrum in order to obtain the time domain waveform of a single optical pulse (using Matlab). Additionally, the pulse duration time for the temporal shape was validated using the time-bandwidth product limit for a $Sech^2$ pulse shape (see section 5.2.2). (4) To obtain a comb-shape spectrum with comb-lines spaced according to ITU-T G.694.1 was emulating a 12.5 GHz pulse repetition rate. (5) Loading the resultant periodic waveform in the software VPItransmissionMaker^{TM}. At this stage, it is necessary to take into account the pulsed laser noise. For this purpose, we experimentally measured the radio frequency (RF) noise using a PIN photodiode and an RF spectrum analyzer, obtaining the spectrum shown in Figure 5.7 which exhibited an electrical signal-to-noise ratio (SNR) of 68 dB in fundamental mode, typical value in this type of sources [64] (6) Amplification and spectral separation of each comb-line using an EDFA and a 12.5-GHz-spacing optical DEMUX with a 3-dB bandwidth of 6.25 GHz, respectively. For the amplification stage, the optical gain was tuned for achieving at least 1 mW power for each filtered comb-line. (7) Transmission evaluation at 2.5 and 10 Gbps using external modulation over a Standard Single Mode optical Fiber (SSMF) with distances up to 60 km. This external modulation is applied over each filtered comb-line using Mach-Zehnder Modulators (MZM) driven by square root Nyquist pulses in Non-Return-to-Zero (NRZ) format and 2 different bit rates: 2.5 and 10 Gbps. (8) Demultiplexing the optical signal, (9) optical-to-electrical conversion using a PIN PhotoDiode (PD), and finally (10) demodulation and Bit Error Rate (BER) estimation.

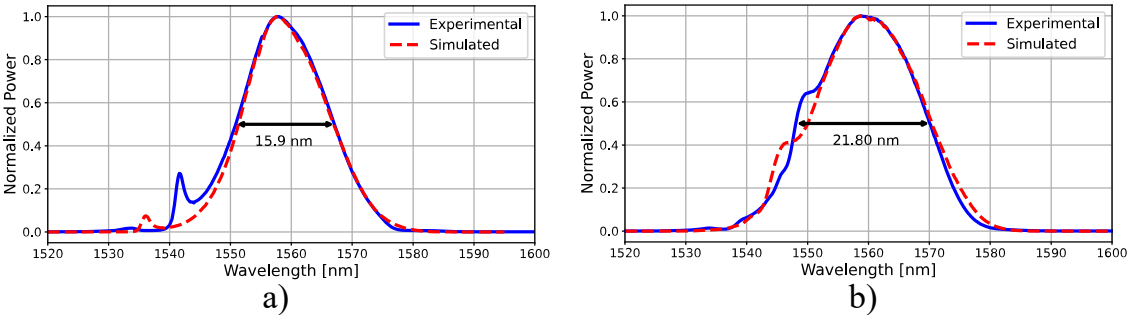

Figure 5.8. Simulated spectrum Vs Experimental. 3-dB bandwidth: a) 16.38 nm. b) 21.8 nm.

5.3.2 Results and discussions

In this section, the simulated transmission performance of the multi-wavelength source, based on a spectrum sliced USPL, is analyzed.

The Fig Figure 5.8 shows a comparison between the experimental power spectrum, and the power spectrum obtained using the simulation setup proposed in the section 5.3 (Up to stage 6). It can be appreciated that there are some differences in both spectra, which is due to the fact that the inverse Fourier transform is applied over the power optical spectrum of the signal. This means, according to the Fourier analysis properties, that the result of the inverse Fourier transform is actually the autocorrelation function of the pulse, not its time-domain waveform. However, being a $sech^2$ waveform, the auto-correlation function and the time waveform have the same shape, with small differences in those regions of the spectrum where there are distortions due to the periodic losses in the cavity (dispersive waves). However, considering the spectrum shape for a spectral a 3-dB spectral width, it can be observed that them do not present considerable differences: ≤ 0.8 nm. This means that the pulse's shape, its duration time, and the number of optical carriers obtained from the simulation-interface do not present considerable differences regarding the experimental ones, and therefore the USPL's performance as multi-wavelength source can be numerically analyzed as a good real case approximation.

For the transmission performance test, it was considering a single carrier (resulting after the spectrum slicing stage) with an emission wavelength of 1558.6 nm, and in order to compare its transmission performance regarding an ideal case, an external modulated laser

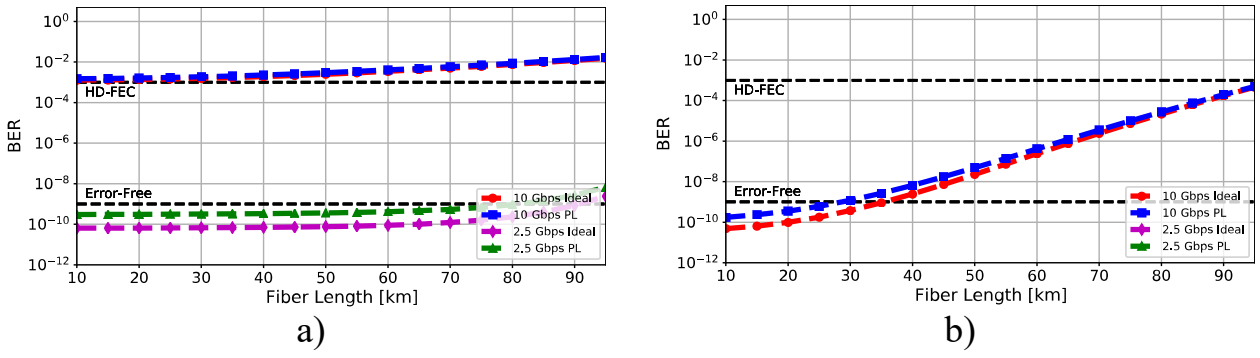

Figure 5.9. BER vs Length. a) 12 dB OSNR. b) 18 dB OSNR.

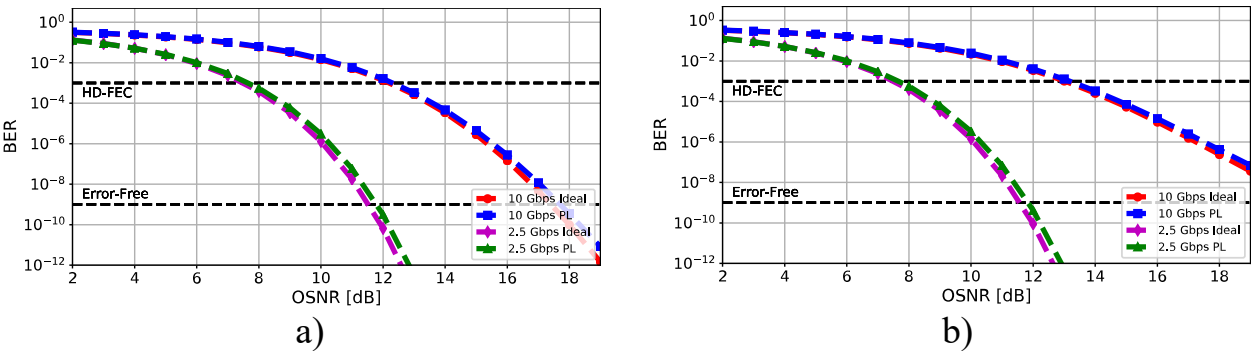

Figure 5.10. BER vs OSNR. a) 20 km fiber length. b) 60 km fiber length.

with the same power, bandwidth a bit rate conditions were simulated. The Fig Figure 5.9a and the Fig Figure 5.9b show the results of the transmission performance in terms of the BER as a function of the fiber length for two different Optical Signal to Noise Ratio (OSNR): 12 dB and 18 dB. As expected for an optical carrier with a 3-dB bandwidth less than 100 MHz and a bit rate of 2.5 Gbps, an error-free transmission over a distance range of 20 to 60 km is always possible, even for relatively low OSNR values: 12 dB, whereas for 10 Gbps a successful transmission is not achieved with this OSNR value. Moreover, in the case of a bit rate of 10 Gbps and 18 dB OSNR, it was possible to achieve error-free transmissions for distances of less than 30 km, which is within the coverage range imposed by the WDM-PON standards. Additionally, it was also possible to observe that penalty of distance of multi-wavelength source in comparison with the ideal laser was less than 6 km.

On the other hand, the Fig Figure 5.10a and the Fig Figure 5.10b shows the performance transmission results in terms of BER as a function of the OSNR. In these curves, it can be evidenced the transmission performance difference between both optical sources: the ideal laser and USPL-based multi-wavelength source, for 2 fixed transmission distances: 20 km and 60 km, and 2 different bit rates: 2.5 and 10 Gbps. For all cases, it was found that for the HD-FEC BER threshold (3.8×10^{-3}) the performance difference is negligible, and that considering the error-free BER threshold (10^{-9}) the OSNR penalty is less than 0.5 dB, even for the 10 Gbps case.

The transmission performance difference between both sources can be explained by considering the waveform of the optical carrier resulting after the spectrum slicing stage. Since the optical MUX/DEMUX used to filter each comb-line of the USPL allows a fraction of

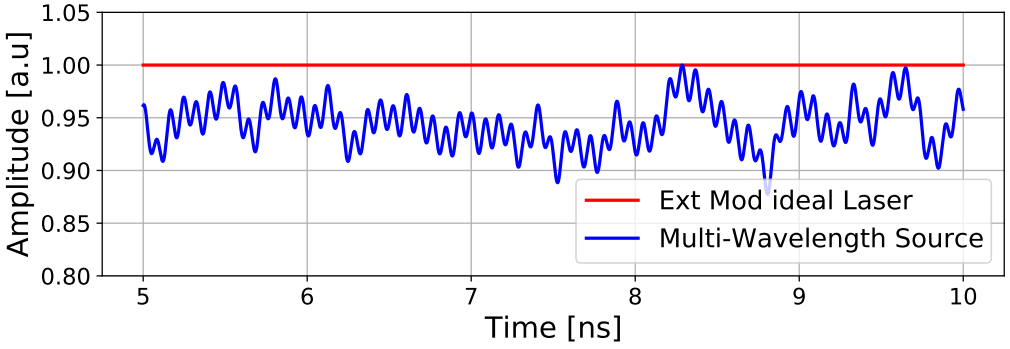

Figure 5.11. Time-domain wave form (simulation).

the spectral components to pass from the adjacent channels, the resulting waveform for each carrier is not completely CW, but maintains a ripple around a DC level, as shown in figure Figure 5.11. This ripple is greater at the USPL-based multi-wavelength source than at the ideal laser, so the noise and distortions in the modulated data are greater as well, which negatively affects the transmission performance.

Chapter 6

Conclusions and Future Work

6.1 Conclusions

An optical colorless transmitter based on an InGaAsP Fabry-Perot Laser Diode was designed to support longitudinal modes spaced according to the ITU-T G.694.1 recommendation for WDM-PON systems: Multiples of 12.5 GHz. In this case, it was proposed a colorless transmitter with longitudinal modes spaced at 100 GHz.This way, the commercial available Mux/Demux can be used to both separate or join the optical channels, and spectrally slice the ASE broad band source used for seeding the FPLD emission wavelength

Since this colorless transmitter approach proposes an architecture that uses a spectral sliced ASE-carrier to seed the laser emission wavelength (the carrier is injected in the FPLD), a cavity with the low-reflective configuration in the frontal facet is necessary to decrease the power requirement to achieve a SMSR above 30 dB. However, while decreasing the reflectivity of the cavity front reduces the injection power requirement for an SMSR target, it also reduces the coherence, and therefore increases the chirp of the optical source.

Thus, after analyzing the impact of reflectivity on the required injection power and source chirp, it was determined that with a 10/90 reflectivity configuration (front-facet/back-facet) it is possible to obtain good trade-off between the power requirement to achieve 30 dB SMSR and the source chirp. The result shows that to achieve an SMSR of 30 dB, injection powers of less than 300 μW are required, which represents only 10% of the average power established for transmitting in WDM links. On the other hand, with this configuration the frequency variance over time remains below 12 GHz, which is less than the 3-dB bandwidth for a single longitudinal mode. In addition, in terms of SMSR and injection power requirement, the performance of the colorless transmitter showed a dependence on bandwidth of the seeding carrier. Thereby, if the 3 dB bandwidth of the seeding optics exceeds the 3 dB bandwidth of a single longitudinal mode by more than 10 GHz, the injection power requirement is increased to achieve a 30 dB SMSR. This behavior is explained by considering the mode formation in a resonant cavity: The boundary conditions of a resonant cavity impose that only the frequencies corresponding to the round-trip phase shift can exhibit gain because of the feedback. If the seeding carrier has frequency components that do not match this condition, they will not be amplified and will not contribute to the formation of the mode.

In the transmission performance test for the colorless transmitter based on this low-reflective FPLD, it was possible to achieve error-free transmissions (BER of the order of 10^{-9}) for fiber lengths up to 36 km, using a direct NRZ modulation at 2.5 Gbps. Besides,

a transmission performance comparison between an external modulated DFB laser with a 3-dB bandwidth of 16 GHz, and the narrowest wavelength seeding carrier (12.5 GHz) showed a distance penalty of 7.2 km and 7.8 km for the transmission case using the central mode and the 400 GHz shifted side mode, respectively. Consequently, even if in the worst case (seeding carriers with a 3-dB bandwidth of 50 GHz) it is possible to have distance penalties of up to 17 km with respect to the externally modulated DFB, the cost of implementing a direct modulation scheme is much lower than that of an externally modulated scheme (more than 2 digits). In addition, DFBs are generally more expensive than FPLDs, which are the simplest transmitters available, therefore, the implementation of this FPLD-based colorless transmitter in a low-cost WDM PON system could have a good trade-off.

In addition, if seeding carriers with bandwidths below 25 GHz, and power of at least 200 μW are considered, it is possible to obtain at least 8 optical carriers spaced 100 GHz apart, which is the minimum stipulated by the NG2-PON standard. However, it should be noted that to guarantee this behavior, it is necessary that the bias current is less than 60 mA. In fact, decreasing the bias current can increase the number of available carriers, since it reduces the center mode gain and reduces the power requirements for 30 dB SMSR.

Besides, the performance of the transmission was compared to an FPLD such as are currently available on the market. As expected, the spacing between longitudinal modes does not necessarily match the standardized channels for WDM networks. Furthermore, because these devices do not normally use reflective films at the ends of the cavity (which is why they are so inexpensive), the reflectivity is typically on the order of 32 %. This implies that the power requirement to achieve a target SMSR is larger with respect to the designed colorless transmission: more than 700 μW in the worst case, which is unfeasible considering that it is comparable to the mean transmission power standardized for WDM networks.

On the other hand, regarding USPL as a possible seeding source in a colorless system with or without carrier reuse, we demonstrated that it is possible to obtain multi-wavelength source in a spectral region of 21.8 nm, which allows up to 50 optical carriers when considering a channel spacing of 100 GHz. In contradistinction to MZM-based configurations, which generate optical carriers only in a spectral range around 12 nm [71]. Moreover, we probed that it is possible to perform error-free transmission over 20 km using NRZ modulation at 2.5 GHz, and 10 Gbps it is possible under the FEC limits. Thus, these results proved that it is possible to use this source in a colorless system with carrier re-use even at high transmission speed. Finally, the fabrication process of EDFL and the graphene-based SA is relatively simple, and does not need the special care required by various materials such as black phosphorus, which can easily become oxidized in an uncontrolled environment.

6.2 Future Work

The modulation bandwidth of an FP laser is typically in the order of 2.5 GHz, so transmitting at 10 Gbps (expected value per carrier in NG-PON2) is not an option if an OOK modulation format is used. Thus, to meet the transmission rate recommended by the ITU-T standards, it is necessary to analyze a simple multilevel modulation format that is based on direct detection, such as M-PAM.

Generally, in low-cost Fabry-Perot lasers, no external mirrors are required, since the two split facets of the laser act as mirrors, obtaining a reflectivity of 32 % in both final

facets. However, the cavity configuration we propose requires modifying these reflectivity values. Therefore, it is necessary to study which fabrication methods allow modifying these reflectivity values without compromising the cost-benefit ratio of the colorless source. At this point it should be taken into account that although the reflectivity of the rear facet of the cavity can reach a reflectivity of 32 %, according to our analysis it is advisable to use a 10/90 % configuration. However, it is worthwhile to perform an experimental implementation of the colorless WDM network, using the designed FPLD laser, to learn the limitations of the system and its performance in a real scenario.

Finally, it is necessary to compare the performance of the designed colorless transmitter when tuned using the proposed sources: the SLED and the USPL-based multi-wavelength, in order to analyze how the coherence of the seeding sources affects the transmission performance of the colorless transmitter.

Chapter 7

Publications

- Jhon A. Lopera, J. J. Granada, A. M. Cardenas and J. D. Zapata, "Ultrashort Pulse Generation in EDFL Cavities using Graphene as Saturable Absorber for applications in optical communications systems," IEEE Colombian Conference on Communications and Computing (COLCOM), Barranquilla, Colombia, 2019

- Jhon A. Lopera, K. Arroyave and J. D. Zapata, "Repetition rate and spectral performance for short EDFL cavities using a D-shaped fiber/graphene saturable absorber", IEEE Colombian Conference on Communications and Computing (COLCOM), Barranquilla, Colombia, 2019

- Jhon A. Lopera, A. M. Cárdenas, G. A. Quintero, J. D. Zapata, and J. J. Granada Torres, "Low-reflective Fabry-Perot Laser Diode Cavity as a Colorless Source on a WDM-PON System," in OSA Advanced Photonics Congress (AP) 2020(IPR, NP, NOMA, Networks, PVLED, PSC, SPPCom, SOF), L. Caspani, A. Tauke-Pedretti, F. Leo, and B. Yang, eds., OSA Technical Digest (Optical Society of America, 2020), paper NeTu2B.3

- Jhon A. Lopera, Karen Arroyave, Ana M. Cárdenas, Jhon J. Granada Torres and Juan D. Zapata, "Graphene-based multi-wavelength source for WDM-PON", OSA FiO+LS, Fiber Optics and Optical Communications Photonics, AnOSA virtual meeting, 2020

- Escobar Pérez, A., Arroyave Giraldo, K., Lopera Cortés, J. A., and Granada Torres, J. J. (2021). Mitigation of Nonlinear Effects using Machine Learning, in Coherent Optical Access Networks. INGE CUC, 17(2).https://doi.org/10.17981/ingecuc.17.2.2021.02

- Jhon A. Lopera, Karen Arroyave, Ana M. Cardenas, Jhon J. Granada Torres, Juan D. Zapata, "Wavelength division multiplexing-passive optical network using a graphene-based ultrashort pulsed fiber laser," Opt. Eng. 60(9)096104 (20 September 2021), https://doi.org/10.1117/1.OE.60.9.096104

- Karen A. Giraldo, J. A. L. Cortés, J. J. G. Torres, and J. D. Z. Caro, "Optical Combs Generation using a Graphene-based Source in comparison with MZM Configurations," in Frontiers in Optics + Laser Science 2021, C. Mazzali, T. (T.-C.) Poon, R. Averitt, and R. Kaindl, eds., Technical Digest Series (Optica Publishing Group, 2021), paper JTu1A.79

- Jhon A. Lopera, A. M. Cárdenas, J. J. Granada Torres and J Zapata, "Design of a colorless transmitter based on a low-resonant Fabry–Perot Laser for applications in WDM-PON". Optik, 2022, p. 168523

Acronyms

ASE Amplified Spontaneous Emitting.

BBS Broad Band Source.

CO Central Office.

DEMUX Demultiplexer.

DFB Distributed Feedback.

DS Downstream.

EAM ElectroAbsorption modulator.

EDFA Erbium-Doped Fiber Amplifier.

EDFL Erbium-Doped Fiber Laser.

FPLD Fabry-Perot Laser Diode.

GVD Group Velocity Dispersion.

InGaAsP Indium gallium Arsenide phosphide.

MUX Multiplexer.

MZM Mach-Zehnder Modulators.

NRZ Non-return to Zero.

OBPF Optical Bandpass Filter.

OLT Optical Line Terminal.

ONU Optical Network Unit.

OSA Optical Spectrum Analyzer.

PMD Polarization Mode Dispersion.

PON Passive Optical Network.

RN Remote Node.

RSOA Reflective Semiconductor Optical Amplifier.

SLED Super Luminescent diode.

SMF Single Mode Fiber.

SMSR SIde Mode Suppresion Ratio.

SSMF Standard Single Mode Fiber.

TDM Time-Division-Multiplexin.

TLD Tunable Laser Diode.

TLLM Transmission-Line Laser Model.

TLM Transmission-Line Model.

US Upstream.

USPL Ultra Short Pulsed Lasers.

VOA Variable Optical Attenuator.

WMD Wavelength Division Multiplexing.

List of Figures

Bibliography

[1] M. Romagnoli, V. Sorianello, M. Midrio, F. H. Koppens, C. Huyghebaert, D. Neumaier, P. Galli, W. Templ, A. D'Errico, and A. C. Ferrari, "Graphene-based integrated photonics for next-generation datacom and telecom," *Nature Reviews Materials*, vol. 3, no. 10, pp. 392–414, 2018.

[2] U. Cisco, "Cisco annual internet report (2018–2023) white paper," 2020.

[3] Q. T. Nguyen, G. Girault, O. Vaudel, L. Bramerie, P. Besnard, A. Shen, G.-H. Duan, C. Kazmierski, S. Lobo, M. Joindot *et al.*, "Colorless components for wdm-based optical access networks," 2008.

[4] N. N. Cikan and M. Aksoy, "A review of self-seeded rsoa based on wdm pon," *Canadian Journal of Electrical and Computer Engineering*, vol. 42, no. 1, pp. 2–9, 2019.

[5] S. Rajalakshmi, A. Srivastava, and A. Pandey, "Analysis of tdm and wdm pon using different coding schemes for extended reach," *IJCSNS*, vol. 11, no. 7, p. 171, 2011.

[6] J. S. Wey, "The outlook for pon standardization: a tutorial," *Journal of Lightwave Technology*, vol. 38, no. 1, pp. 31–42, 2020.

[7] M. Kumari, R. Sharma, and A. Sheetal, "Passive optical network evolution to next generation passive optical network: A review," in *2018 6th Edition of International Conference on Wireless Networks & Embedded Systems (WECON)*. IEEE, 2018, pp. 102–107.

[8] ITU-T, "Gigabit-capable passive optical networks (GPON)," International Telecommunication Union (ITU), Geneva, Recommendation G.984.x, 2012.

[9] ——, "10-gigabit-capable passive optical network (XG-PON) systems," International Telecommunication Union (ITU), Geneva, Recommendation G.987.x, 2016.

[10] ——, "10-gigabit-capable symmetric passive optical network (XGS-PON) systems," International Telecommunication Union (ITU), Geneva, Recommendation G.9807.1 Amendment 1, 2017.

[11] A. Mishra and P. Mishra, "Optical communication with time division multiplexing (otdm) and hybrid wdm/otdm pon," *system*, vol. 3, p. 4, 2014.

[12] S. Pradhan, B. Patnaik, and R. Panigrahy, "Hybrid multiplexing (otdm/wdm) technique for fiber optic communication," in *2018 IEEE 5th International Conference on Engineering Technologies and Applied Sciences (ICETAS)*. IEEE, 2018, pp. 1–5.

[13] Z. Zhang, Y. Chen, S. Cai, B. Zhang, M. Zhang, and X. Chen, "Colorless-light and tunable-light-source schemes for twdm and wdm pons," *IEEE Communications Magazine*, vol. 56, no. 8, pp. 120–128, 2018.

[14] M. M. Bruno and S. Kumar, "Performance analysis of otdm using pon in direct and external modulation."

[15] G. P. Agrawal, *Fiber-optic communication systems*. John Wiley & Sons, 2012, vol. 222.

[16] D. Hood and E. Trojer, *Gigabit-capable passive optical networks*. Wiley Online Library, 2012.

[17] B. E. Saleh and M. C. Teich, *Fundamentals of photonics*. john Wiley & sons, 2019.

[18] N. N. Cikan and M. Aksoy, "Data erasure analysis of fpld based on remodulation bidirectional pon system," *Journal of Modern Optics*, vol. 67, no. 2, pp. 139–145, 2020.

[19] Z. Zhang, Y. Chen, S. Cai, B. Zhang, M. Zhang, and X. Chen, "Colorless-light and tunable-light-source schemes for twdm and wdm pons," *IEEE Communications Magazine*, vol. 56, no. 8, pp. 120–128, 2018.

[20] N. N. Cikan and M. Aksoy, "A review of self-seeded rsoa based on wdm pon," *Canadian Journal of Electrical and Computer Engineering*, vol. 42, no. 1, pp. 2–9, 2019.

[21] C. Wagner, J. Zou, M. Ortsiefer, C. Greus, C. Neumeyr, K. Grobe, M. Eiselt, S. Paul, J. Cesar, F. Küppers *et al.*, "Full c-band tunable mems-vcsel for next generation g. metro mobile front-and backhauling," in *2017 Optical Fiber Communications Conference and Exhibition (OFC)*. IEEE, 2017, pp. 1–3.

[22] P. Parolari, A. Gatto, and P. Boffi, "Long wavelength vcsels exploitation for low-cost and low-power consumption metro and access networks," in *2018 20th International Conference on Transparent Optical Networks (ICTON)*. IEEE, 2018, pp. 1–4.

[23] M. M. H. Adib, J. N. Kemal, C. Füllner, M. S. Mahmud, A. Ramdane, C. Koos, W. Freude, and S. Randel, "Colorless coherent passive optical network using a frequency comb local oscillator," in *2019 Optical Fiber Communications Conference and Exhibition (OFC)*. IEEE, 2019, pp. 1–3.

[24] W. Zhan, P. Zhou, Y. Zeng, M. Mukaikubo, T. Tanemura, and Y. Nakano, "Optimization of modulation-canceling reflective semiconductor optical amplifier for colorless wdm transmitter applications," *Journal of Lightwave Technology*, vol. 35, no. 2, pp. 274–279, 2016.

[25] D. R. Celino, U. R. Duarte, and M. A. Romero, "Improved self-seeding and carrier remodulation performance for wdm-pon by means of double rsoa erasure," *Optics Communications*, vol. 459, p. 125018, 2020.

[26] P. K. Choudhury, "Enhanced noise tolerance for 10 gb/s bi-directional cross-wavelength reuse colorless wdm-pon by using spectrally shaped ofdm signals," *Optical Fiber Technology*, vol. 42, pp. 6–10, 2018.

[27] H.-W. Hung, Y.-L. Lee, C.-W. Sung, C.-H. Hsu, and S.-L. Lee, "10-gb/s bidirectional wdm-pon transmission using spectrum-sliced ase light sources," *Journal of the Chinese Institute of Engineers*, vol. 40, no. 1, pp. 93–99, 2017.

[28] C. Zuo, X. Li, Y. Xia, X. Dai, and L. Wang, "Horn-waveguide rsoa-eam as a colorless emitting source with reduced crosstalk," *Journal of Lightwave Technology*, vol. 36, no. 24, pp. 5942–5948, 2018.

[29] M. T. A. Khan, E. Alkhazraji, A. M. Ragheb, H. Fathallah, K. Qureshi, S. Alshebeili, and M. Khan, "100 gb/s single channel transmission using injection-locked 1621 nm quantum-dash laser," *IEEE Photonics Technology Letters*, vol. 29, no. 6, pp. 543–546, 2017.

[30] M. Deng, R. Giddings, C.-T. Tsai, G.-R. Lin, and J. Tang, "Colorless wrc-fplds subject to gain-saturated rsoa feedback for wdm-pons," *IEEE Photonics Technology Letters*, vol. 30, no. 1, pp. 43–46, 2017.

[31] G. P. Agrawal and N. K. Dutta, *Semiconductor lasers*. Springer Science & Business Media, 2013.

[32] C. Buczek, R. Freiberg, and M. Skolnick, "Laser injection locking," *Proceedings of the IEEE*, vol. 61, no. 10, pp. 1411–1431, 1973.

[33] N. P. Barnes and J. C. Barnes, "Injection seeding. i. theory," *IEEE Journal of Quantum Electronics*, vol. 29, no. 10, pp. 2670–2683, 1993.

[34] A. J. Lowery, "New dynamic semiconductor laser model based on the transmission-line modelling method," *IEE Proceedings J (Optoelectronics)*, vol. 134, no. 5, pp. 281–289, 1987.

[35] A. Emsia, Q. T. Le, R. E. Guendogdu, M. Malekizandi, E. I. de Betou, M. Olson, J. Keck, R. Herber, K. Rienecker, M. Fricke *et al.*, "Cost-efficient upstream transmitter using injection locked fabry-perot laser diodes for multi-gbit/s wdm-pon," in *Photonic Networks; 17. ITG-Symposium; Proceedings of.* VDE, 2016, pp. 1–8.

[36] M. Deng, R. Giddings, C.-T. Tsai, G.-R. Lin, and J. Tang, "Colorless wrc-fplds subject to gain-saturated rsoa feedback for wdm-pons," *IEEE Photonics Technology Letters*, vol. 30, no. 1, pp. 43–46, 2017.

[37] Y.-C. Su, Y.-C. Chi, H.-Y. Chen, and G.-R. Lin, "Data erasing and rewriting capabilities of a colorless fpld based carrier-reusing transmitter," *IEEE Photonics Journal*, vol. 7, no. 3, pp. 1–12, 2015.

[38] A. J. Lowery, "New dynamic semiconductor laser model based on the transmission-line modelling method," *IEE Proceedings J (Optoelectronics)*, vol. 134, no. 5, pp. 281–289, 1987.

[39] P. B. Johns and R. L. Beurle, "Numerical solution of 2-dimensional scattering problems using a transmission-line matrix," in *Proceedings of the Institution of Electrical Engineers*, vol. 118, no. 9. IET, 1971, pp. 1203–1208.

[40] W. J. Hoefer, "The transmission-line matrix method-theory and applications," *IEEE Transactions on Microwave Theory and Techniques*, vol. 33, no. 10, pp. 882–893, 1985.

[41] A. J. Lowery, P. C. Gurney, X.-H. Wang, L. Nguyen, Y. C. Chan, and M. Premaratne, "Time-domain simulation of photonic devices, circuits, and systems," in *Physics and Simulation of Optoelectronic Devices IV*, vol. 2693. International Society for Optics and Photonics, 1996, pp. 624–635.

[42] A. J. Lowery, "Transmission-line modelling of semiconductor lasers: The transmission-line laser model," *International Journal of Numerical Modelling: Electronic Networks, Devices and Fields*, vol. 2, no. 4, pp. 249–265, 1989.

[43] A. Lowery, "Transmission-line laser modelling of semiconductor laser amplified optical communications systems," *IEE Proceedings J (Optoelectronics)*, vol. 139, no. 3, pp. 180–188, 1992.

[44] ——, "Amplified spontaneous emission in semiconductor laser amplifiers: Validity of the transmission-line laser model," *IEE Proceedings J-Optoelectronics*, vol. 137, no. 4, pp. 241–247, 1990.

[45] A. J. Lowery, "A two-port bilateral model for semiconductor lasers," *IEEE journal of quantum electronics*, vol. 28, no. 1, pp. 82–92, 1992.

[46] Z. Ahmed, L. Zhai, A. J. Lowery, N. Onodera, and R. S. Tucker, "Locking bandwidth of actively mode-locked semiconductor lasers," *IEEE journal of quantum electronics*, vol. 29, no. 6, pp. 1714–1721, 1993.

[47] A. Lowery and D. Hewitt, "Large-signal dynamic model for gain-coupled dfb lasers based on the transmission-line laser model," *Electronics Letters*, vol. 28, no. 21, pp. 1959–1960, 1992.

[48] VPIphotonics, *VPIcomponentMaker™ Photonic Circuits - User's manual*. VPIphotonics GmbH, 2019.

[49] K. Kurokawa, "Power waves and the scattering matrix," *IEEE transactions on microwave theory and techniques*, vol. 13, no. 2, pp. 194–202, 1965.

[50] Y.-P. Xi, W.-P. Huang, and X. Li, "High-order split-step schemes for time-dependent coupled-wave equations," *IEEE journal of quantum electronics*, vol. 43, no. 5, pp. 419–425, 2007.

[51] K. Petermann, *Laser diode modulation and noise*. Springer Science & Business Media, 1991, vol. 3.

[52] C. Henry, "Theory of spontaneous emission noise in open resonators and its application to lasers and optical amplifiers," *Journal of lightwave technology*, vol. 4, no. 3, pp. 288–297, 1986.

[53] S. F. Mingaleev and K. Busch, "Scattering matrix approach to large-scale photonic crystal circuits," *Optics letters*, vol. 28, no. 8, pp. 619–621, 2003.

[54] G. P. Agrawal, "Nonlinear fiber optics," in *Nonlinear Science at the Dawn of the 21st Century*. Springer, 2000, pp. 195–211.

[55] M. Rumi and J. W. Perry, "Two-photon absorption: an overview of measurements and principles," *Advances in Optics and Photonics*, vol. 2, no. 4, pp. 451–518, 2010.

[56] A. J. Lowery, A. Keating, and C. N. Murtonen, "Modeling the static and dynamic behavior of quarter-wave-shifted dfb lasers," *IEEE journal of quantum electronics*, vol. 28, no. 9, pp. 1874–1883, 1992.

[57] A. J. Lowery and D. Novak, "Performance comparison of gain-coupled and index-coupled dfb semiconductor lasers," *IEEE journal of quantum electronics*, vol. 30, no. 9, pp. 2051–2063, 1994.

[58] L. Zhai, A. Lowery, Z. Ahmed *et al.*, "Detuning characteristics of mode-locked semiconductor lasers with a chirped fibre-grating external cavity," in *18th Australian Conference on Optical Fibre Technology (ACOFT-18'93): Proceedings*. Institution of Radio and Electronics Engineers Australia, 1993, p. 193.

[59] M. Premaratne and A. J. Lowery, "Analytical characterization of soa-based optical pulse delay discriminator," *Journal of lightwave technology*, vol. 23, no. 9, p. 2778, 2005.

[60] D. J. Shin, Y. Keh, J. Kwon, E. Lee, J. Lee, M. Park, J. Park, Y. Oh, S. Kim, I. Yun *et al.*, "Low-cost wdm-pon with colorless bidirectional transceivers," *Journal of Lightwave Technology*, vol. 24, no. 1, p. 158, 2006.

[61] J. A. Lopera, A. M. Cárdenas, G. A. Quintero, J. D. Zapata, and J. J. G. Torres, "Low-reflective fabry-perot laser diode cavity as a colorless source on a wdm-pon system," in *Photonic Networks and Devices*. Optical Society of America, 2020, pp. NeTu2B–3.

[62] S. Ullah, R. Ullah, A. Khan, H. A. Khalid, Q. Zhang, Q. Tian, F. Khan, and X. Xin, "Optical multi-wavelength source for single feeder fiber using suppressed carrier in high capacity lr-wdm-pon," *IEEE access*, vol. 6, pp. 70 674–70 684, 2018.

[63] A. Rosado, A. Pérez-Serrano, J. M. G. Tijero, Á. Valle, L. Pesquera, and I. Esquivias, "Enhanced optical frequency comb generation by pulsed gain-switching of optically injected semiconductor lasers," *Optics express*, vol. 27, no. 6, pp. 9155–9163, 2019.

[64] D. Steinberg, J. D. Zapata, E. A. T. de Souza, and L. A. Saito, "Mechanically exfoliated graphite onto d-shaped optical fiber for femtosecond mode-locked erbium-doped fiber laser," *Journal of Lightwave Technology*, vol. 36, no. 10, pp. 1868–1874, 2018.

[65] J. D. Zapata, L. Saito, A. M. Cárdenas, and E. T. de Souza, "Sub-150 fs mode-locked erbium doped fiber laser based on monolayer graphene on a d-shaped optical fiber," in *CLEO: QELS_Fundamental Science*. Optical Society of America, 2016, pp. JTu5A–71.

[66] J. A. Lopera, K. Arroyave, A. M. Cárdenas, J. J. G. Torres, and J. D. Zapata, "Graphene-based multi-wavelength source for wdm-pon," in *Laser Science*. Optical Society of America, 2020, pp. JTh4B–4.

[67] H. G. Rosa, D. Steinberg, J. D. Zapata, L. A. Saito, A. M. Cárdenas, J. C. Gomes, and E. A. T. De Souza, "Raman mapping characterization of all-fiber cvd monolayer graphene saturable absorbers for erbium-doped fiber laser mode locking," *Journal of Lightwave Technology*, vol. 33, no. 19, pp. 4118–4123, 2015.

[68] G. Sobon, J. Sotor, I. Pasternak, K. Grodecki, P. Paletko, W. Strupinski, Z. Jankiewicz, and K. M. Abramski, "Er-doped fiber laser mode-locked by cvd-graphene saturable absorber," *Journal of lightwave technology*, vol. 30, no. 17, pp. 2770–2775, 2012.

[69] L. Li, Y. Wang, and X. Wang, "Ultrafast pulse generation with black phosphorus solution saturable absorber," *Laser Physics*, vol. 27, no. 8, p. 085104, 2017.

[70] R. M. Gerosa, D. Steinberg, D. A. Nagaoka, J. D. Zapata, S. H. Domingues, E. A. T. de Souza, and L. A. Saito, "Liquid phase exfoliated black phosphorus and reduced graphene oxide polymer-based saturable absorbers fabrication using the droplet method for mode-locking applications," *Optics & Laser Technology*, vol. 106, pp. 107–112, 2018.

[71] J. A. Lopera, K. Arroyave, A. M. Cardenas, J. J. G. Torres, and J. D. Zapata, "Wavelength division multiplexing-passive optical network using a graphene-based ultrashort pulsed fiber laser," *Optical Engineering*, vol. 60, no. 9, pp. 1 – 12, 2021. [Online]. Available: https://doi.org/10.1117/1.OE.60.9.096104

[72] J. Zapata, D. Steinberg, L. A. Saito, R. De Oliveira, A. Cárdenas, and E. T. De Souza, "Efficient graphene saturable absorbers on d-shaped optical fiber for ultrashort pulse generation," *Scientific reports*, vol. 6, p. 20644, 2016.

[73] L. Malard, M. A. Pimenta, G. Dresselhaus, and M. Dresselhaus, "Raman spectroscopy in graphene," *Physics reports*, vol. 473, no. 5-6, pp. 51–87, 2009.

[74] M. Pimenta, G. Dresselhaus, M. S. Dresselhaus, L. Cancado, A. Jorio, and R. Saito, "Studying disorder in graphite-based systems by raman spectroscopy," *Physical chemistry chemical physics*, vol. 9, no. 11, pp. 1276–1290, 2007.

[75] M. J. Matthews, M. A. Pimenta, G. Dresselhaus, M. Dresselhaus, and M. Endo, "Origin of dispersive effects of the raman d band in carbon materials," *Physical Review B*, vol. 59, no. 10, p. R6585, 1999.

[76] A. C. Ferrari, J. C. Meyer, V. Scardaci, C. Casiraghi, M. Lazzeri, F. Mauri, S. Piscanec, D. Jiang, K. S. Novoselov, S. Roth *et al.*, "Raman spectrum of graphene and graphene layers," *Physical review letters*, vol. 97, no. 18, p. 187401, 2006.

[77] A. C. Ferrari, "Raman spectroscopy of graphene and graphite: Disorder, electron–phonon coupling, doping and nonadiabatic effects," *Solid state communications*, vol. 143, no. 1-2, pp. 47–57, 2007.

[78] N. Villa, J. D. Zapata, and D. Ramirez, "Paraffin wax assisted chemical vapor deposited graphene transfer method," *Thin Solid Films*, vol. 721, p. 138556, 2021.

[79] F. Zhang, S. Han, Y. Liu, Z. Wang, and X. Xu, "Dependence of the saturable absorption of graphene upon excitation photon energy," *Applied Physics Letters*, vol. 106, no. 9, p. 091102, 2015.

[80] U. Keller, "Recent developments in compact ultrafast lasers," *Nature*, vol. 424, no. 6950, pp. 831–838, 2003.

[81] E. J. Aiub, E. A. T. de Souza, and L. A. Saito, "Hybrid mode-locked erbium fiber laser with a 40 ghz phase modulator and graphene saturable absorber," in *Frontiers in Optics*. Optical Society of America, 2018, pp. FTu4B–3.

[82] E. Boncristiano, L. Saito, and E. De Souza, "396 fs pulse from an asynchronous mode-locked erbium fiber laser with 2.5 12 ghz repetition rate," *Microwave and Optical Technology Letters*, vol. 50, no. 11, pp. 2994–2996, 2008.